Laser Induced Electron Emission

By

JAMES HARVEY BECHTEL

A dissertation submitted in partial fulfillment
of the requirements for the degree of
Doctor of Philosophy (Physics)
in The University of Michigan
1973

Doctoral Committee:

Professor Peter A. Franken, Chairman
Professor G. W. Ford
Professor W. A. Hiltner
Associate Professor John F. Ward
Professor Gabriel Weinreich

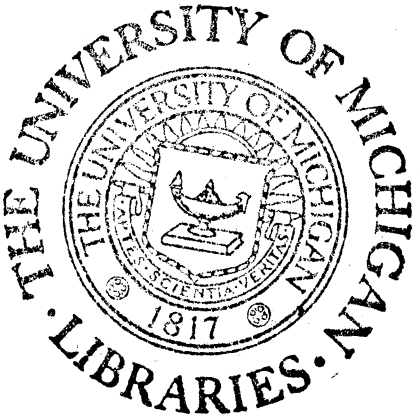
THE UNIVERSITY OF MICHIGAN
LIBRARIES
THE UNIVERSITY OF MICHIGAN
1817

ABSTRACT

LASER INDUCED ELECTRON EMISSION

by

James Harvey Bechtel

Chairman: Peter A. Franken

Laser induced electron emission from tungsten, molybdenum, and platinum has been observed using Q-switched ruby lasers. Experimental results from tungsten indicated that processes other than thermionic emission occur at irradiances of tens of megawatts per square centimeter and pulse durations of tens of nanoseconds. For these laser irradiances and pulse durations the emitted electron pulses had maximum currents in the range of .1 to 100 milliamperes, and this maximum current was delayed approximately 5 nanoseconds with respect to the maximum incident laser irradiance. This measured time delay is consistent with a thermal origin for the electron emission process; however, the relation between the emitted current and the incident laser irradiance was substantially less nonlinear than that predicted by the Richardson-Dushman equation.

Theoretical models for expected temperature changes

of laser irradiated materials were then developed using several different functional forms for both the spatial and temporal distribution of the incident laser irradiance. These results were applied to laser induced thermionic emission and to two other electron emission processes which we have called one-photon assisted thermionic emission and two-photon assisted thermionic emission. The mechanism for these photon assisted processes is as follows: the incident laser pulse acts not only as a heat source but also as a photon source. The heating effect pushes the Fermi tail of the electron distribution closer to the vacuum level, and electrons in the tail of this distribution may then be ejected from the metal by either a one-photon or a two-photon process.

The experimental results from tungsten and molybdenum rods are consistent with the theory of the two-photon assisted thermionic emission effect. In addition, results have also been obtained from tungsten ribbon cathodes, the initial temperature of which could be varied by changing the current in the ribbon. In this case, however, when the maximum emitted current is compared to the initial cathode temperature for constant laser irradiance, the results are more consistent with thermionic emission than with the two-photon assisted thermionic emission process. This difference is as yet unexplained.

LASER INDUCED ELECTRON EMISSION

by
James Harvey Bechtel

A dissertation submitted in partial fulfillment
of the requirements for the degree of
Doctor of Philosophy
(Physics)
in The University of Michigan
1973

Doctoral Committee:

Professor Peter A. Franken, Chairman
Professor G. W. Ford
Professor W. A. Hiltner
Associate Professor John F. Ward
Professor Gabriel Weinreich

It is the great beauty of our science that advancement in it, whether in a degree great or small, instead of exhausting the subject of research, opens the doors to further and more abundant knowledge, overflowing with beauty and utility.

Michael Faraday

ACKNOWLEDGMENTS

It is a pleasure to thank those people who have contributed to the research documented in this dissertation. I wish to thank William D. Hall of the Environmental Research Institute of Michigan for helping me with the initial phases of the research, and I wish to thank Irving Bigio and Kang-Ming Leung for much help with the use of the lasers at the University of Michigan. Gene Robinson and Otto Wagner of the Electron Physics Laboratory, University of Michigan provided much technical assistance with the construction of the vacuum tubes. Joe Jenney and C. R. Giuliano of the Hughes Research Laboratories kindly provided their laboratory facilities for my use, and Jerry Rickel of that laboratory assisted in the taking of data.

Several useful discussions with R.W. Terhune and A.W. Overhauser of the Ford Scientific Laboratories are greatfully acknowledged.

I wish to thank all of the members of my doctoral committee for their interest in this work. In particular I should thank John Ward for the use of the lasers and for his many useful suggestions. Finally, Peter Franken provided the guidance and inspiration that I needed during this project.

This research was supported in part by the National Science Foundation and CFC Products Inc.

TABLE OF CONTENTS

LIST OF TABLES

LIST OF ILLUSTRATIONS

FIGURE Page

FIGURE Page

LIST OF APPENDICES

CHAPTER I

INTRODUCTION

Early in 1963 it was discovered that burst mode lasers could produce substantial electron emission from an irradiated target. At nearly the same time Lichtman and Ready[1], Honig and Woolston[2], Verber and Adelman[3], and Giori, MacKenzie, and McKinney[4] reported electron emission from a variety of solids including tungsten, carbon, thoriated tungsten and tantalum using a focused laser beam. All of these authors concluded from their experiments that the electron emission could be explained as thermionic emission from the laser heated surface. Unfortunately the complicated temporal structure of the relaxation oscillations in the burst mode laser made it nearly impossible to make a detailed study of the emission process.

In 1965 Ready[5] reported laser induced electron emission produced by Q-switched ruby laser pulses with a peak irradiance in the range of 10-25 megawatts per square centimeter and approximately 50 nanoseconds (full-width-at-half-maximum) time duration. He concluded that the observed electron emission could be explained in terms of thermionic emission effects, and data was reported from tungsten, thoriated tungsten, and platinum target material. However, his laser was not single transverse mode, and the observed current was somewhat greater than that predicted by theory.

In other experiments lasers have been used to study electron emission which was inferred to be other than thermionic. Teich and Wolga[6] used a pulsed GaAs laser to study two-photon photoemission from sodium. Their measurements indicated that the observed current density was proportional to the square of the incident laser power per unit area. Other measurements by Logothetis and Hartman[7] have been conducted to study both two-photon and three-photon photoemission from gold, stainless steel, CsI, and KCl. Using laser irradiances of less than 1 megawatt per square centimeter they have observed electron current densities proportional to the square and the cube of the incident irradiance for two-photon and three-photon photoemission respectively.

At laser irradiances of greater than 100 megawatts per square centimeter and for pulse durations of the order of tens of nanoseconds most materials are vaporized at the surface. Although we have observed effects associated with irradiances greater than 100 megawatts per square centimeter, the major emphasis of the research reported here is for unfocused laser beams with irradiances of a few tens of megawatts per square centimeter. All of the work was accomplished with Q-switched ruby lasers.

The studies that we have performed on laser induced electron emission actually originated by accident in that we observed a substantial amount of electron emission from a laser irradiated metal surface before we were aware that

others had previously investigated this subject. Moreover, our initial studies were directed at a rather different problem which is discussed in Appendix I. Our initial observation was that the electron emission was a highly nonlinear effect in that a small change in the laser power per unit area produced a very large change in the observed electron current. Subsequently we found that at least some of the data indicated that the electron emission was apparently thermal in origin, but in fact it did not seem to fit the theory of thermionic emission, at least for any "normal" metal. It was this basic contradiction that stimulated our interest in the problem.

In Chapter II the basic experiment is described and the lasers used in the experiment are discussed in some detail. In Chapter III several mechanisms of electron emission are considered and the various ways that a laser can be used to produce electron emission are considered. In Chapter IV the experimental results are presented, and finally in Chapter V the results are discussed in the context of our present understanding.

CHAPTER II

THE EXPERIMENT

The block diagram of the experiment is displayed in Figure 1. The Q-switched ruby laser irradiates a metal cathode and any electron current produced thereby is detected with oscilloscope no. 1. A small portion of the laser beam is monitored by photodiode no. 2 which is calibrated to measure the incident pulse energy. The output of photodiode no. 2 is displayed on oscilloscope no. 2 and photographically recorded on type 410 Polaroid film. Both oscilloscopes are externally triggered by photodiode no. 1.

More details of the circuit are given in Figure 2. A high voltage power supply is used to maintain the anode at a positive potential with respect to the cathode. The laser induced current pulses are detected across a 50 ohm resistor, and a 50 ohm transmission line (RG-58 C/U) is used to transmit the signal to oscilloscope no. 1. The laser pulses were usually of 10-20 nanoseconds duration; consequently, fast oscilloscopes such as the Tektronix 7704 or 7904 were used to observe the laser induced current pulses.

The electron tubes used in the experiments were of two different geometries, as shown in Figure 3. Figure 3a

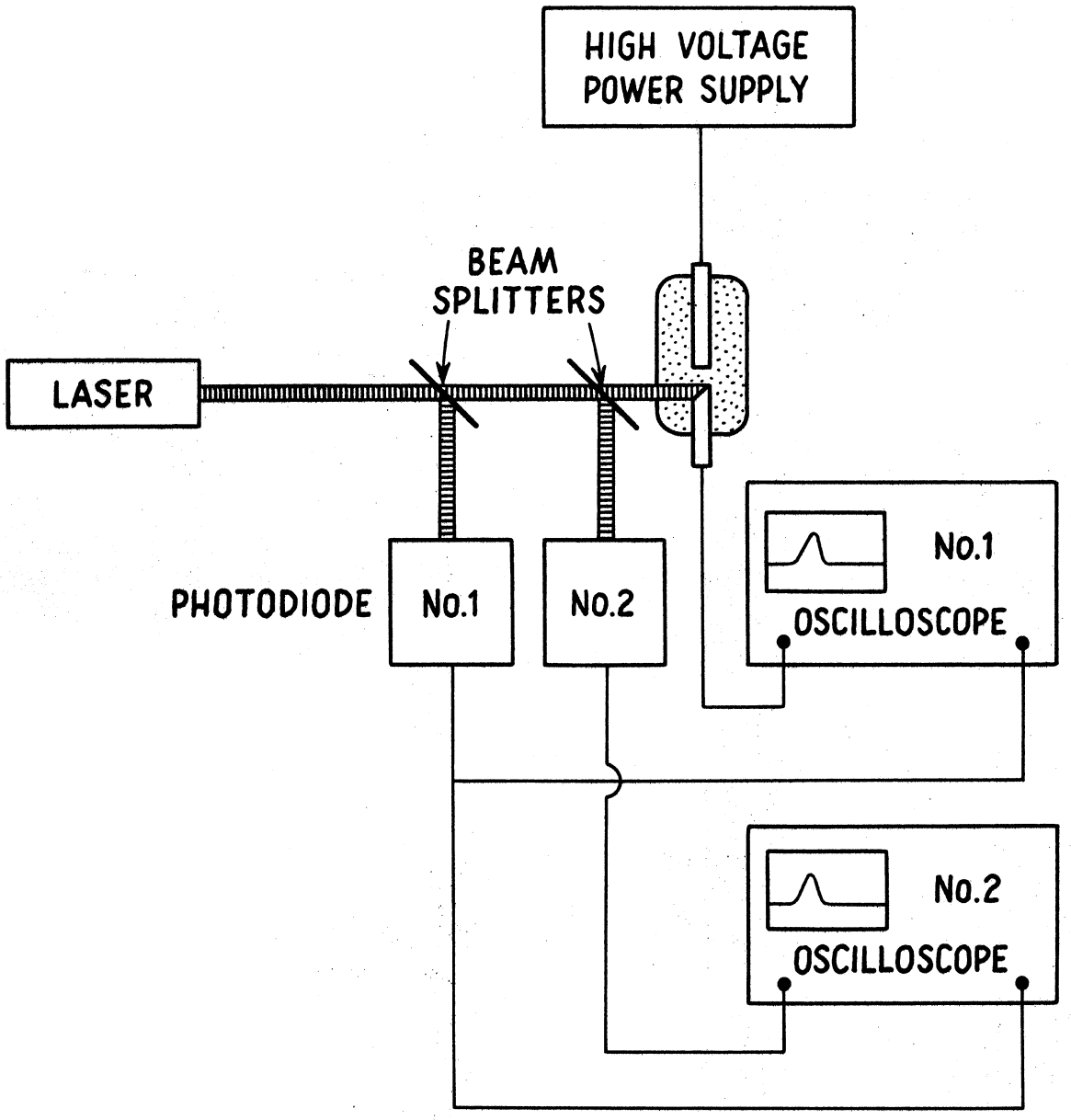

Figure 1. Block Diagram of the Experiment.

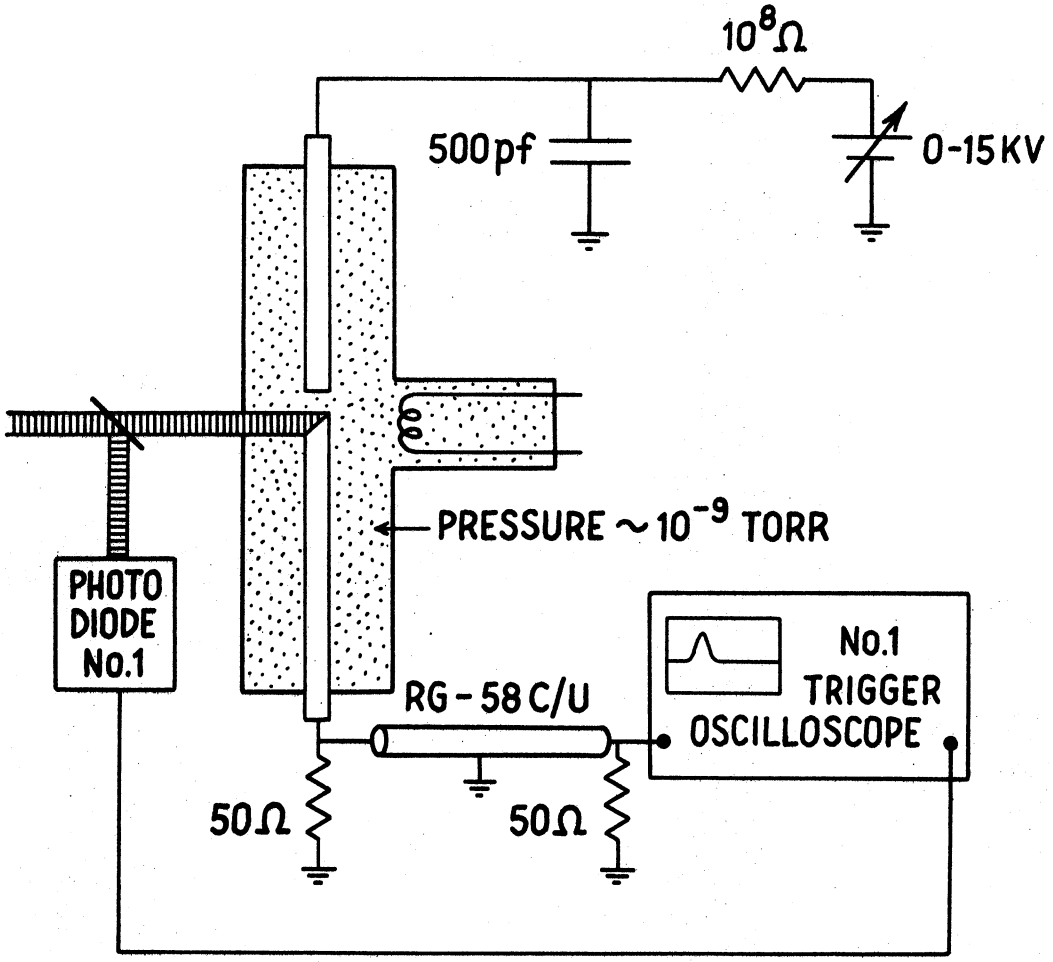

Figure 2. Electrical Circuit for the Detection of Current Pulses.

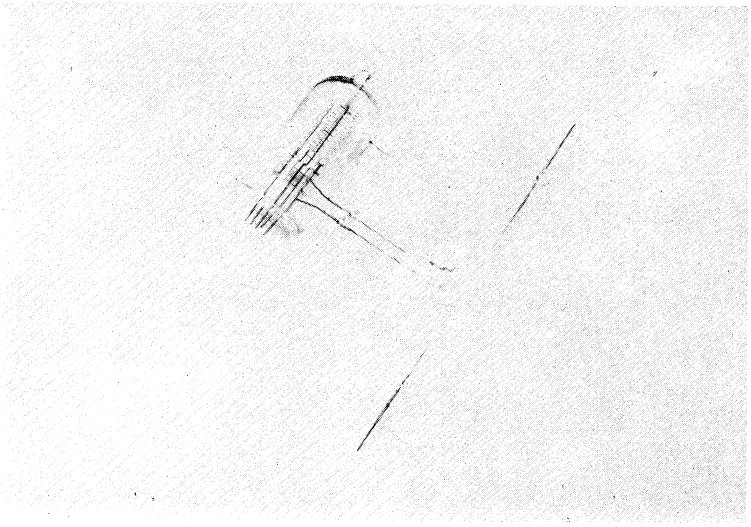

Figure 3a. Vacuum Tube with Field Emission Cathode.

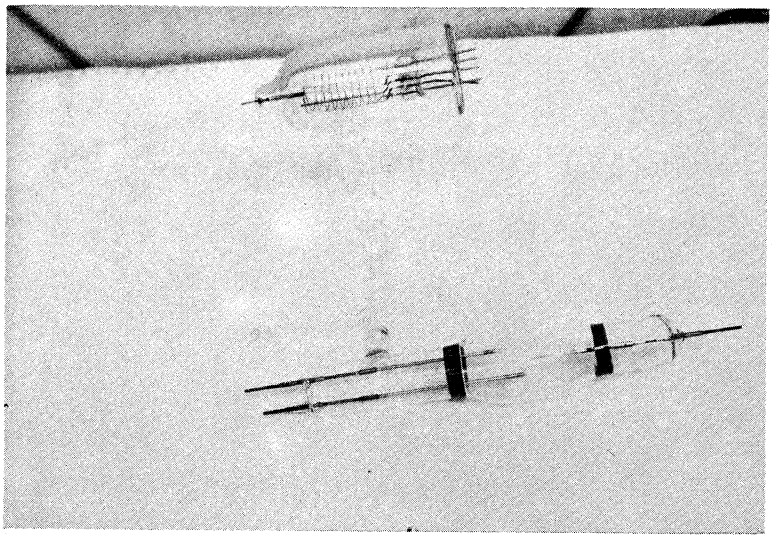

Figure 3b. Vacuum Tube with Ribbon Cathode.

exhibits the tube geometry employed in the first experiments which were characterized by the utilization of a field emission point cathode. The second type of tube as seen in Figure 3b has a tungsten ribbon cathode. The electron tubes were fabricated from borosilicate glasses; both Corning Type 7740 and Corning Type 7052 were used in the tube assembly. Additional graded seals were supplied where needed.

The glass was cleaned in a weak solution of HF followed by a rinse in deionized water and finally a rinse in methanol. The glass was subsequently dried in hot air.

In the field emission tubes the 0.04 inch diameter tungsten rods were vacuum brazed to Kovar using a Au-Ni eutectic alloy, Nioro. The Kovar was found necessary to make reliable glass to metal seals. After the complete assemblage of the tube it was attached to a vacuum pump, evacuated, and baked at 400 C for several days.

To clean the metal electrodes an auxiliary electron gun was installed in the field emission tubes. The gun consisted of a 0.01 inch diameter tungsten filament that could be used to supply an electron beam for bombardment heating of the field emission diode. Filament currents of approximately 6 amperes provided thermionic emission in the 30 milliampere range. A voltage difference of 1500 volts would then provide an electron beam power of 45 watts, which was found adequate to heat the electrodes to red hot temperatures. The scattered radiation from

the filament made it difficult to measure these temperatures with an optical pyrometer, but we estimate that the maximum temperature was about 1200 C. This temperature was maintained at each electrode for approximately 30 minutes. The field emission current-voltage relation was monitored during various stages of the tube processing, and there were no significant changes in the Fowler-Nordheim plots (the theory of field emission is reviewed briefly in Appendix II).

After the metal electrodes had been cleaned by the electron beam bombardment the tubes were tipped off from the vacuum station. The residual pressure was 10^{-8}-10^{-9} torr, and this pressure was monitored with an attached Bayard-Alpert ionization gauge. The ionization gauge used in the experiments was a tungsten filament Veeco Type TG-75P. We observed that this type of ionization gauge has a significantly higher temperature than the more common gauges that have a thoriated iridium filament. This higher temperature provides more pumping action because of the higher probability of molecular dissociation into chemically active gases. We thus used the ionization gauge not only as a monitor of the tube pressure but also as a small vacuum pump.

The ribbon filament electron tubes were fabricated in a similar fashion to the field emission tubes except that no auxiliary electron gun was required. The ribbon was

cleaned by passing approximately 10 amperes of current through it, and the emitted electrons were used for bombardment heating of the anode. After the tube was sealed the pressure again was 10^{-8}-10^{-9} torr. The tungsten ribbons were 0.003 inches thick, and both etched and unetched ribbons were studied. The etch was KOH, the same base that was used to electropolish the field emission cathodes.

The lasers used in the experiment were both ruby devices emitting 6943 Å radiation at room temperature. The experiments performed at the University of Michigan were done with a Korad K-15 system. This laser has a Pockels cell Q-switch and a peak power of approximately 1 megawatt. The laser was found to be nearly single transverse mode in its output. The beam size was determined by scanning a small pinhole across the beam and measuring the relative amount of light transmitted by this pinhole as it traversed the laser beam. The temporal structure of the University of Michigan laser was somewhat complicated. Several longitudinal modes would usually beat, and thus a modulated output was observed. The dominant beat frequency was 200 megahertz, which is just the spectral interval of the Fabry-Perot laser cavity. The laser was attenuated, when appropriate, by passing the beam through various solutions of $CuSO_4$.

The laser used at the Hughes Research Laboratories

was a single transverse mode, single longitudinal mode Q-switched ruby laser. The laser had a peak power of approximately 5 megawatts, and the longitudinal mode selection was obtained by the use of a dye Q-switch and a resonant mode selector. The pulse structure of the laser was found to be highly reproducible with only 1 shot in 20 providing any evidence of more than a single mode. The beam size was measured by a multiple lens technique that has been reported in detail elsewhere[8]. A comparison of the outputs of the lasers at the University of Michigan and at the Hughes Research Laboratories is given in Figure 4. Both photographs are of CRO traces of the output of a fast photodiode (ITT FW-114A) and were obtained with a Tektronix 519 oscilloscope.

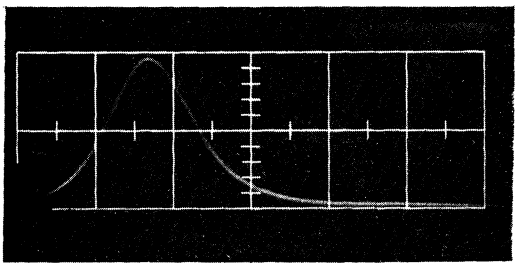

Figure 4a. Photodiode Output of Laser at the Hughes Research Laboratory. 10 ns per division.

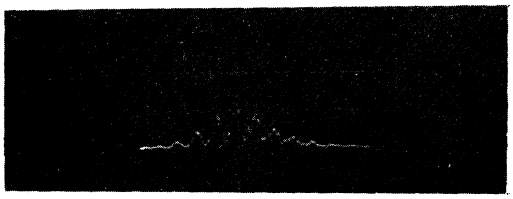

Figure 4b. Photodiode Output of Laser at the University of Michigan. 10 ns per division.

CHAPTER III

LASER HEATING OF MATERIALS AND ELECTRON EMISSION

When a laser irradiates a surface, that surface is heated by the absorbed energy of the incident radiation. The following analysis develops predictions for the temperature changes that would arise from several different sets of assumptions. In this discussion, unless otherwise stated, we assume that the laser emits a pulse of radiation that is of nanosecond duration or longer; picosecond pulses are so rapid that local thermodynamic equilibrium may not be established on the time scale of the pulse duration. We assume, moreover, that the material doesn't change state; that is, at the irradiances of interest here no melting or vaporization occurs. Finally, we initially assume that the optical and the thermal properties of the material are not functions of the temperature of the material. The effect of temperature variation of these parameters will be discussed later.

In general the temperature at a point r in the material and at any time t can be found by solving the classical heat-conduction equation equation

$$\nabla^2 T(\boldsymbol{r},t) - \frac{1}{\varkappa}\frac{\partial T(\boldsymbol{r},t)}{\partial t} = -\frac{G(\boldsymbol{r},t)}{K} \quad (3.1)$$

where $T(\vec{r},t)$ is the temperature, $\varkappa$ is the thermal diffusivity, K is the thermal conductivity, and $G(\vec{r},t)$ is the generation function. The thermal diffusivity is related to the thermal conductivity K, the specific heat C, and the mass density ρ, by the relation

$$\varkappa = \frac{K}{\rho C} \tag{3.2}$$

Before discussing detailed solutions to equation 3.1 we should note that the function $G(\vec{r},t)$ specifies the net amount of heat supplied per unit volume per unit time. For the problem of laser induced temperature changes this term will be determined by the power per unit area incident upon the surface of the material and by the way that the laser radiation is attenuated within the material.

In principle we should also include loss effects such as thermal radiation from the surface. Indeed, on a sufficiently long time scale thermal radiation from a heated surface will become an important effect, but here the major emphasis is on Q-switched laser effects for irradiances of 1-100 MW/cm^2 and for a time scale of a few tens of nanoseconds. In this region reradiation by the surface can be ignored. We parenthetically note that this is quite fortunate because the inclusion of the Stefan-Boltzmann law on the right-hand side of equation 3.1 would make this a nonlinear differential equation.

As an example of a solution to the equation of heat conduction we consider a semi-infinite metal irradiated by

a spatially uniform laser beam the lateral dimensions of which are very large compared to any distances of thermal diffusion. In this case equation 3.1 can be considered as a spatially one-dimensional problem. Thus,

$$\frac{\partial^2 T}{\partial z^2} - \frac{1}{\kappa}\frac{\partial T}{\partial t} = -\frac{G}{K} \tag{3.3}$$

If the laser irradiance is attenuated exponentially in the form $I(z,t)=I(t)(1-R)\exp(-\alpha z)$ where R is the surface reflectivity, and α is the absorption coefficient, then the function $G(z,t)$ is given by

$$G(z,t) = I(t)(1-R)\alpha e^{-\alpha z} \tag{3.4}$$

Specifically we can now consider an incident laser pulse for which $I(t)$ is a square pulse. We thus have

$$\begin{aligned} I(t) &= I_o \qquad & 0 < t < \tau \\ I(t) &= 0 \qquad & 0 > t > \tau \end{aligned} \tag{3.5}$$

Since the zero of temperature is arbitrary, equation 3.3 can be solved with the initial condition $T(z,0)=0$, and the boundary conditions that $T(\infty,t)=0$ and $\frac{dT(0,t)}{dz}=0$. This solution to equation 3.3 has been given by Carslaw and Jaeger[9]. Their solution is:

$$T(z,t) = \frac{2I_o(1-R)}{K}\sqrt{\kappa t}\ \text{ierfc}\left[\frac{z}{2\sqrt{\kappa t}}\right] - \frac{I_o(1-R)}{\alpha K}e^{-\alpha z}$$

$$+ \frac{I_o(1-R)}{2\alpha K}e^{\alpha^2\kappa t-\alpha z}\ \text{erfc}\left[\alpha\sqrt{\kappa t} - \frac{z}{2\sqrt{\kappa t}}\right] \qquad (3.6)$$

$$+ \frac{I_o(1-R)}{2\alpha K}e^{\alpha^2\kappa t+\alpha z}\ \text{erfc}\left[\alpha\sqrt{\kappa t} + \frac{z}{2\sqrt{\kappa t}}\right]$$

$$0 < t < \tau$$

where

$$\text{erfc } x = \frac{2}{\sqrt{\pi}}\int_x^\infty e^{-y^2}dy$$

and

$$\text{ierfc } x = \int_x^\infty \text{erfc } y\ dy = \frac{1}{\sqrt{\pi}}e^{-x^2} - x\ \text{erfc } x$$

At this point it is useful to note that even the simplest spatial and temporal distribution of the incident irradiance leads to a relatively complicated expression, viz., equation 3.6. Fortunately the major interest here is with metals that rapidly attenuate the incident radiation. For a wavelength of 7000 Å the radiation is attenuated by a factor of e in a distance of approximately 10^{-6}cm.[10] For strongly attenuated radiation equation 3.6 may be approximated by taking the limit as $\alpha\to\infty$, which means that the radiation is absorbed right at the surface. The mathematical implication of this approximation is that the boundary value problem is simpler to solve. We thus find that the surface

temperature in the limit as $\alpha \to \infty$ becomes

$$T(z,t) = \frac{2I_o(1-R)\sqrt{\kappa t}}{K} \text{ ierfc}\left[\frac{z}{2\sqrt{\kappa t}}\right] \tag{3.7}$$

$$= \frac{2I_o(1-R)}{K}\left[\sqrt{\frac{\kappa t}{\pi}}\, e^{-z^2/4\kappa t} - \frac{z}{2}\,\text{erfc}\left[\frac{z}{2\sqrt{\kappa t}}\right]\right] \qquad 0 < t < \tau$$

For times t greater than the pulse duration τ the corresponding expression for the temperature is

$$T(z,t) = \frac{2I_o(1-R)\sqrt{\kappa\tau}}{K}\left[\sqrt{\frac{t}{\tau}}\,\text{ierfc}\left[\frac{z}{2\sqrt{\kappa t}}\right] - \left(\frac{t}{\tau}-1\right)^{1/2}\text{ierfc}\left[\frac{z}{2\sqrt{\kappa(t-\tau)}}\right]\right] \tag{3.8}$$

$t > \tau$

For the surface temperature, T(0,t), these expressions reduce to

$$T(0,t) = \frac{2I_o(1-R)}{K}\sqrt{\frac{\kappa t}{\pi}} = \frac{2I_o(1-R)}{\sqrt{K\rho C}}\sqrt{\frac{t}{\pi}} \qquad t \le \tau \tag{3.9}$$

$$T(0,t) = \frac{2I_o(1-R)}{K}\left[\sqrt{\frac{\kappa t}{\pi}} - \sqrt{\frac{\kappa(t-\tau)}{\pi}}\right] \qquad t \ge \tau \tag{3.10}$$

Expressions 3.9 and 3.10 represent the surface temperature as a function of time for an incident temporally square laser pulse. From these expressions one observes that the thermal properties of the material enter into the result

as $\sqrt{K\rho C}$. This factor as a function of the temperature is plotted in Figure 5 for tungsten, molybdenum, and platinum.

When $t=\tau$, $T(0,t)$ reaches a maximum value; therefore, setting $t=\tau$ in equation 3.9 provides a convenient expression for estimating the maximum surface temperature increase for a given pulse duration and irradiance. In Figure 6 the surface temperature increase is plotted against time for incident square pulses of 13 nanoseconds and 20 nanoseconds duration. The irradiance is assumed to be 1 megawatt per square centimeter, and the material constants of tungsten are also assumed. The effect of slight differences in the values of $\sqrt{K\rho C}$ at 300 K initial temperature and 1500 K initial temperature is demonstrated in this graph.

For more complicated temporal and spatial distributions of the incident laser irradiance the solution to equation 3.3 becomes more complicated. A uniform spatial distribution and an arbitrary temporal dependence of the incident irradiance produces an increase in surface temperature given by[11]

$$T(z,t) = \frac{1}{K}\sqrt{\frac{\kappa}{\pi}} \int_{-\infty}^{t} \frac{(1-R)}{(t-u)^{1/2}} \, I(u) \, e^{-z^2/4(t-u)\kappa} \, du \qquad (3.11)$$

This expression can be used to find the temperature rise associated with a spatially uniform but temporally Gaussian

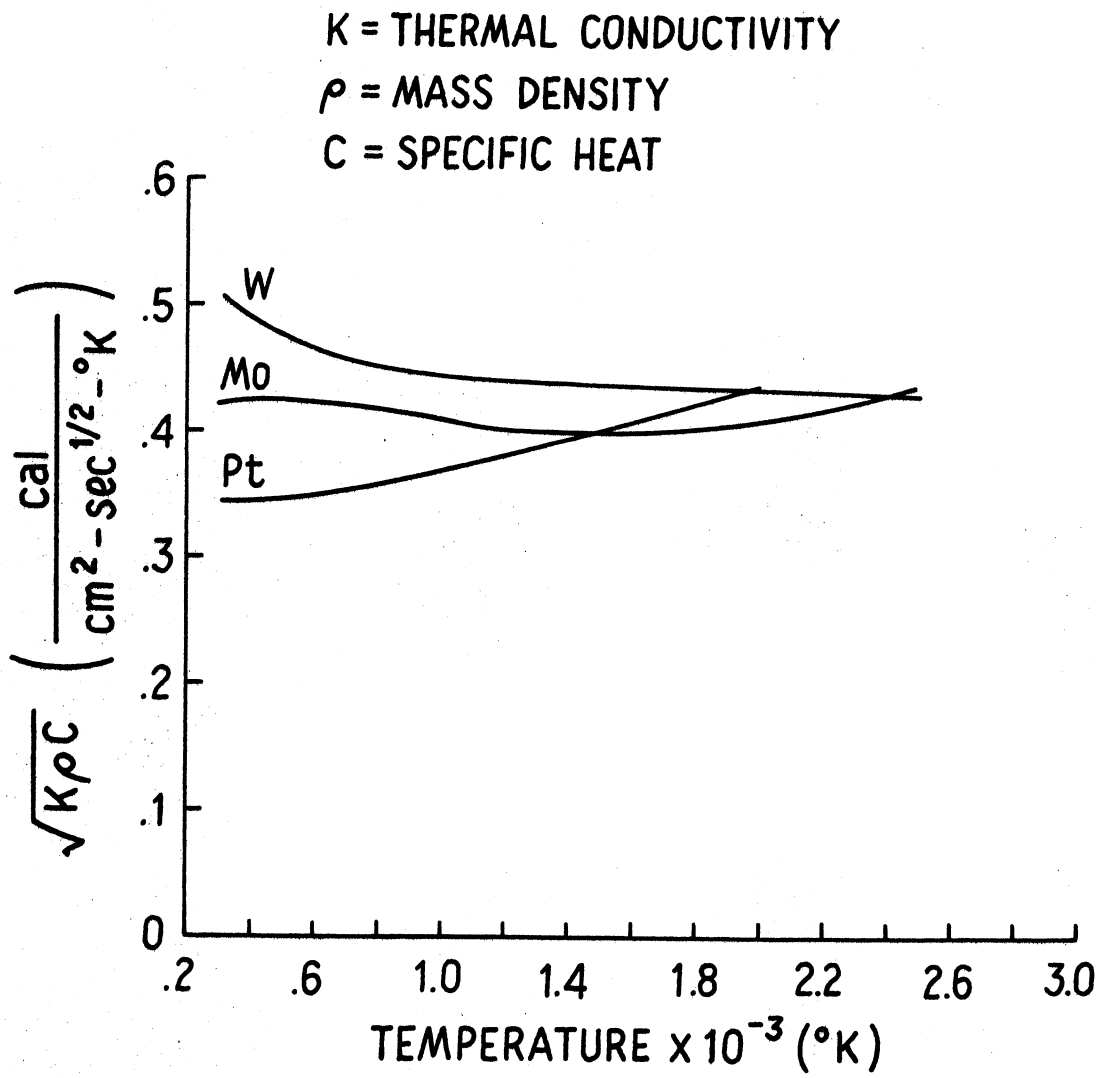

Figure 5. Thermal Parameter $\sqrt{K\rho C}$ for the Metals Tungsten, Molybdenum, and Platinum. (see Reference 12)

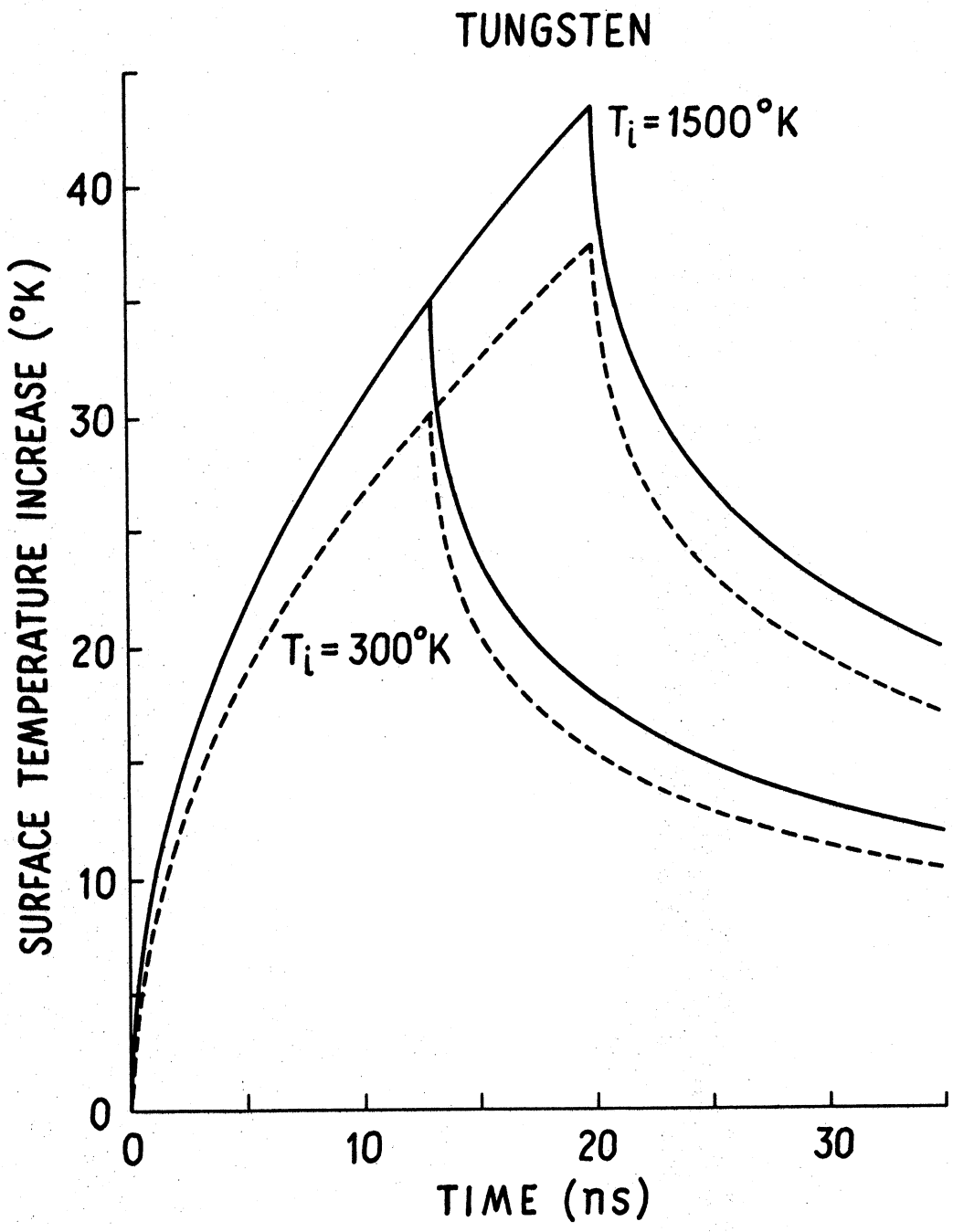

Figure 6. Laser Induced Surface Temperature Rise Produced by Temporally Square Pulses of 13 ns and 20 ns Duration. 1 MW/cm^2 and the reflectivity of tungsten is 0.5

incident laser pulse the irradiance of which is

$$I(t) = I_o e^{-(t/T_g)^2} \tag{3.12}$$

For this type of pulse the total pulse energy ϵ is related to the maximum irradiance I_o and the time T_g by

$$\epsilon = \sqrt{\pi}\, I_o T_g = 1.064\, I_o \tau_{FWHM} \tag{3.13}$$

where the full-width-at-half-maximum τ_{FWHM} is

$$\tau_{FWHM} = 2(\ln 2)^{1/2} T_g = 1.665 T_g \tag{3.14}$$

The temperature rise is thus given by

$$T(z,t) = \frac{1}{K}\sqrt{\frac{\kappa}{\pi}} \int_{-\infty}^{t} \frac{I_o(1-R)}{(t-u)^{1/2}}\; e^{-z^2/4\kappa(t-u) - (u/T_g)^2}\, du \tag{3.15}$$

This integral is not known to be expressible in terms of tabulated functions, but if we restrict ourselves to the surface temperature, this expression becomes

$$T(0,t) = \frac{I_o(1-R)}{\sqrt{K\rho C}}\sqrt{\frac{T_g}{\sqrt{2}}}\; e^{-t^2/2T_g^2}\; D_{-1/2}(-\sqrt{2}\, t/T_g) \tag{3.16}$$

Here the function $D_\nu(x)$ is the Weber parabolic cylinder function. One can, therefore, write the surface temperature as

$$T(0,t) = \frac{I_o(1-R)}{\sqrt{K\rho C}} \sqrt{\frac{T_g}{\sqrt{2}}}\ \eta(t/T_g) \qquad (3.17)$$

The function $\eta(t/T_g)$ is plotted in Figure 7, and this expression is used to compute the surface temperature rise associated with a Gaussian pulse of maximum irradiance of 1 MW/cm^2 on a tungsten surface. The full-width-at-half-maximum of the incident pulse is taken as 13 nanoseconds. The results are displayed in Figure 8. The zero of time corresponds to the maximum irradiance, and as one can see from Figure 8, the maximum in the temperature occurs somewhat more than 4 nanoseconds after the peak in the incident laser irradiance. The time lag of the temperature maximum with respect to the irradiance maximum is given by the approximation

$$t_{lag} \simeq \frac{\tau_{FWHM}}{3}$$

This approximation, although not true in general, is valid for a time scale of 10^{-8} sec.

Consider now the case more relevant to the single transverse mode laser in which the incident pulse has a Gaussian spatial distribution of irradiance. For this type of pulse the incident irradiance is of the form

$$I(r,t) = I_o e^{-(r/d)^2} g(t) \qquad (3.18)$$

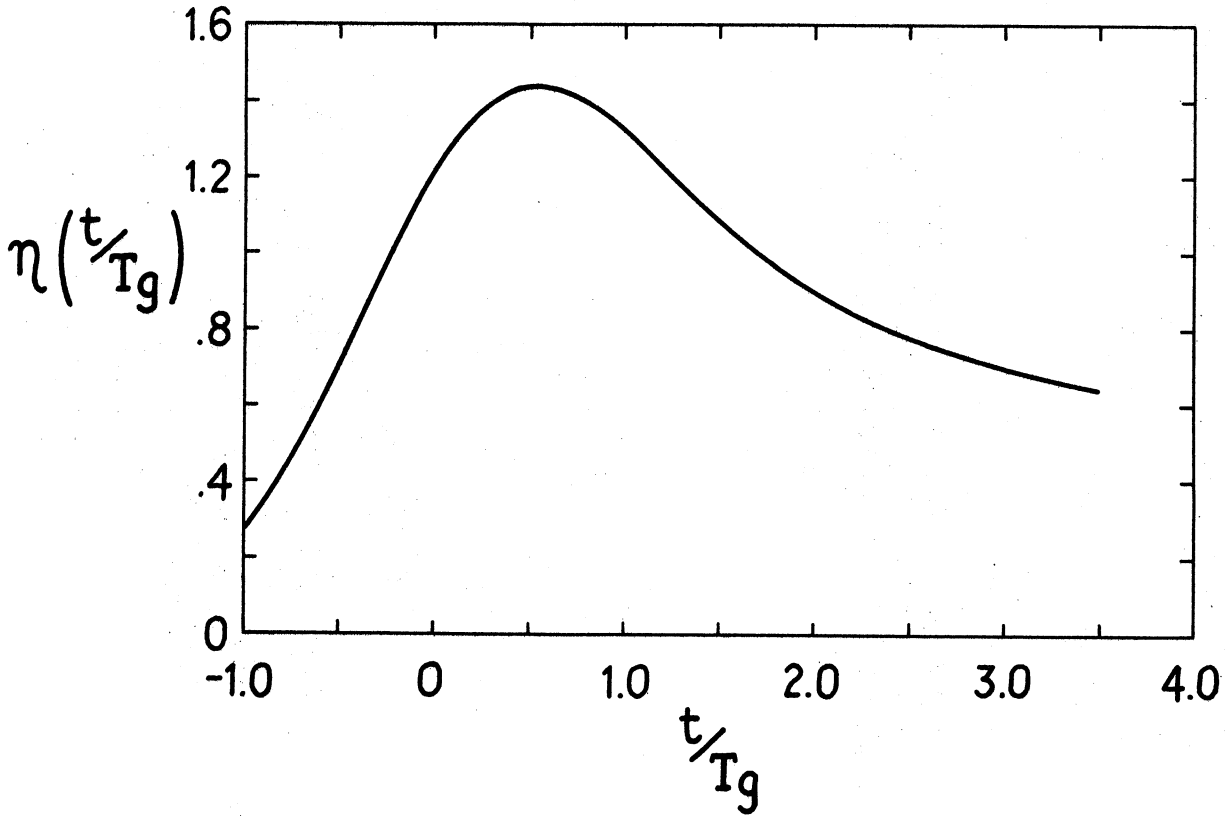

Figure 7. Function $\eta(t/T_g)$ versus t/T_g

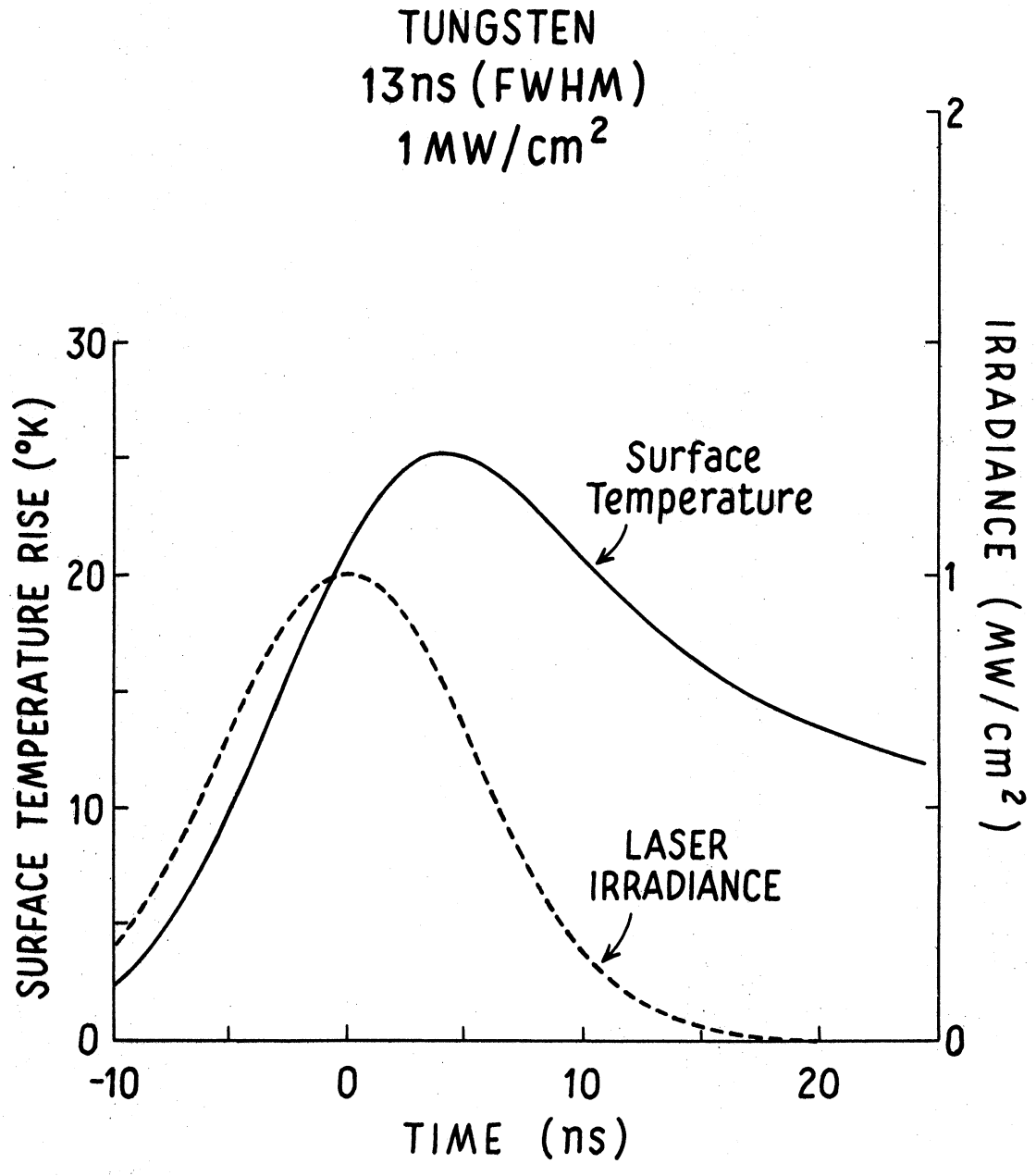

Figure 8. Time Dependence of Surface Temperature Increase and of Laser Irradiance.

where g(t) is a function of unit value at the maximum irradiance. Again we can show that if this energy is absorbed at the surface, then the temperature rise associated with this type of pulse becomes

$$T(r,z,t) = \frac{I_o(1-R)d^2}{\sqrt{\pi}\sqrt{K\rho C}} \int_{-\infty}^{t} \frac{g(t')\, e^{-\frac{z^2}{4\kappa(t-t')} - \frac{r^2}{4\kappa(t-t')+d^2}}}{(t-t')^{1/2}\,(4\kappa(t-t') + d^2)}\, dt' \tag{3.19}$$

For even a simple temporal dependence we must evaluate the integral numerically. If, however, we are interested only in the surface temperature, and we restrict ourselves to times t such that $4\kappa t \ll d^2$, then an approximate expression for the temperature increase produced by the Gaussian laser pulse is

$$T(r,0,t) \simeq \frac{I_o(1-R)e^{-r^2/d^2}}{\sqrt{K\rho C}} \sqrt{\frac{T_g}{\sqrt{2}}}\, e^{-t^2/2T_g^2}\, D_{-1/2}\left(-\sqrt{2}\,\frac{t}{T_g}\right) \tag{3.20}$$

$$\simeq \frac{I_o(1-R)e^{-r^2/d^2}}{\sqrt{K\rho C}} \sqrt{\frac{T_g}{\sqrt{2}}}\, \eta(t/T_g)$$

The restriction $4\kappa t \ll d^2$ simply means that thermal diffusion in the plane of the surface is negligible and can thus be ignored for the time scale of interest.

The values of the thermal constants actually do depend on the temperature. To calculate the maximum surface tem-

perature for a laser pulse such that the change in the temperature is relatively large, we can divide the pulse into many time intervals and compute the expected temperature change for each interval using a value of $\sqrt{K\rho C}$ appropriate to that interval. This has been done for the elements tungsten, molybdenum and platinum; the results are given in Figures 9 and 10. As we see in Figure 9, a 13 nsec (FWHM) laser pulse incident on 300 K tungsten produces a maximum surface temperature of 1500 K if the incident irradiance is 40-45 MW/cm^2.

Having discussed the increase in surface temperature produced by laser pulses, we may now discuss the electron emission associated with such temperature changes. Historically, thermionic emission has been successfully described by the Richardson-Dushman equation

$$J = A_r T^2 e^{-\varphi/kT} \tag{3.21}$$

where J is the current density, φ is the work function of the metal, k is Boltzmann's constant, T is the surface temperature, and A_r is the Richardson constant. For tungsten $A_r \simeq 70$ $A/cm^2/K^2$.

If the laser used to induce the heating is single transverse mode, then the surface temperature at some distance r from the center of the beam is approximately

$$T(r) \simeq T_i + \Delta T e^{-(r/d)^2} \tag{3.22}$$

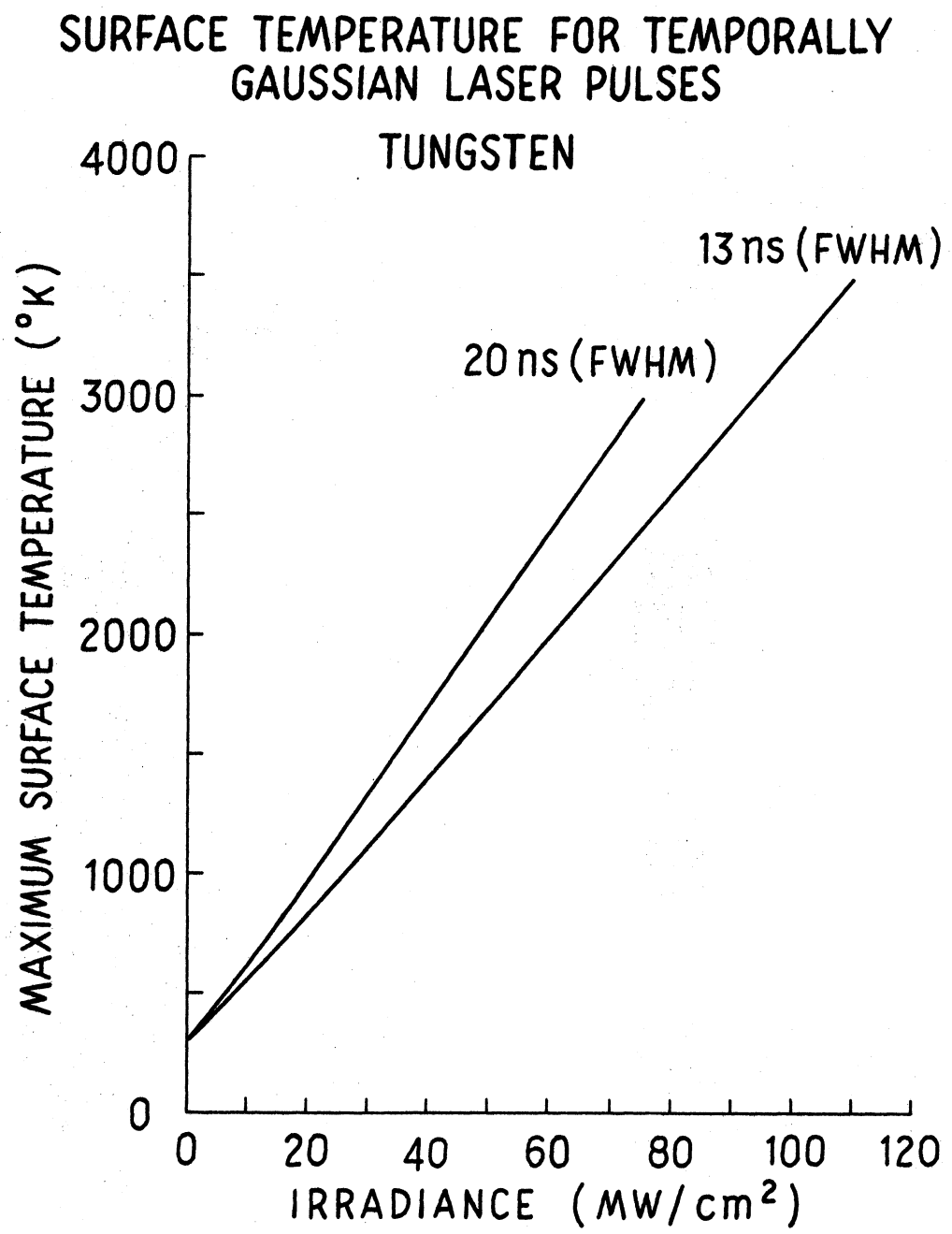

Figure 9. Maximum Surface Temperature Versus Peak Incident Irradiance. Tungsten target with temporally Gaussian incident pulse of duration 20 and 13 ns (FWHM). The reflectivity of tungsten is 0.5

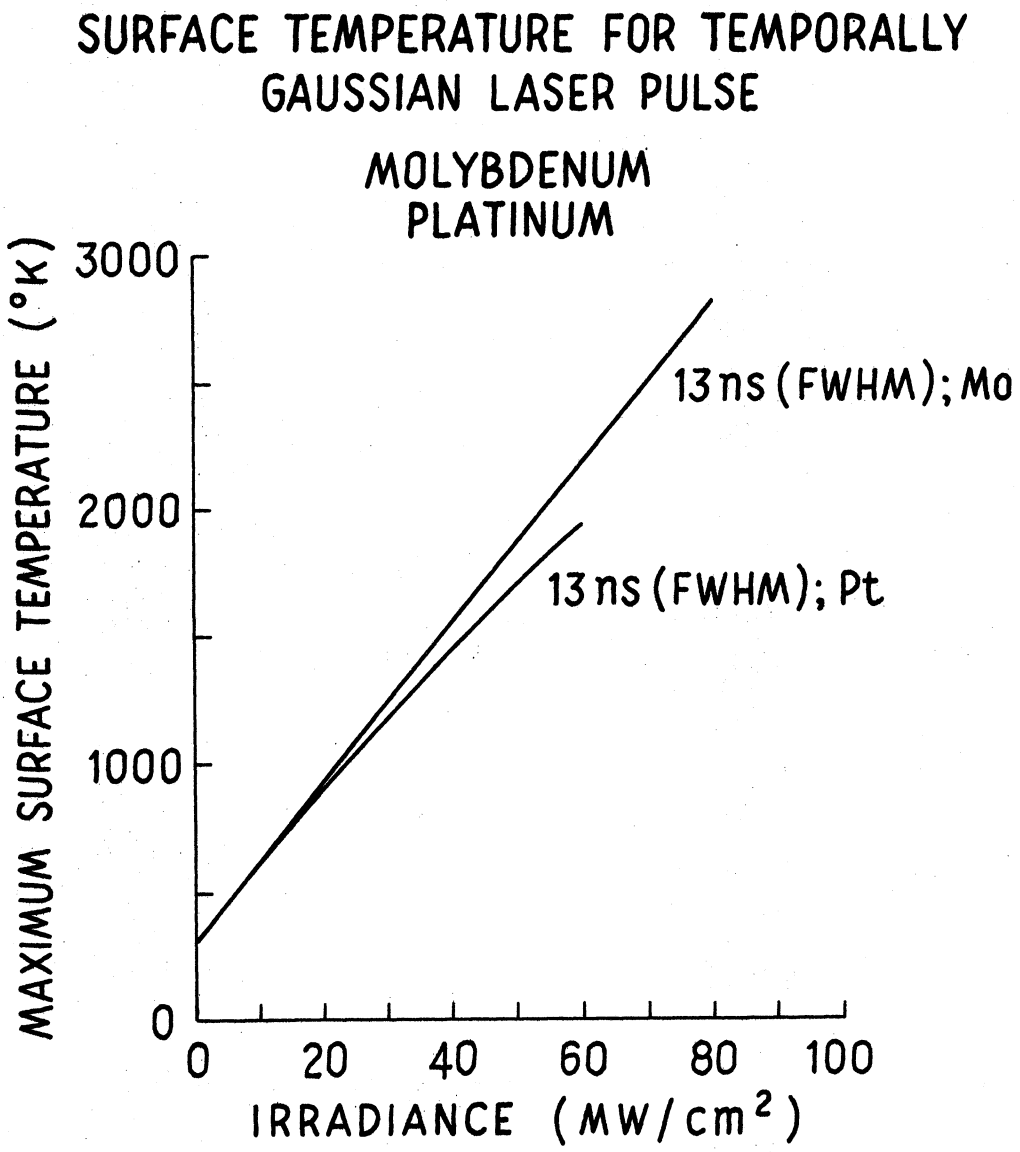

Figure 10. Maximum Surface Temperature Versus Peak Incident Irradiance. Molybdenum and Platinum target with temporally Gaussian incident pulse of duration 13 ns (FWHM). The reflectivity of Mo is 0.5, and the reflectivity of Pt is 0.6.

Here the initial surface temperature is T_i and ΔT is the change in temperature produced by the laser at the center of the beam. It is understood that ΔT is a function of time. In this case the total current may be obtained by integrating the Richardson-Dushman equation over the effective area of the laser beam. This gives

$$i = 2\pi A_r \int_0^d T(r)^2 e^{-\varphi/kT(r)} r \, dr$$

$$= \pi d^2 A_r \left(\frac{\varphi}{k}\right)^2 \sum_{j=0}^{\infty} \left(\frac{kT_i}{\varphi}\right)^j \left[\Gamma\left(j-2, \frac{\varphi}{k(T_i+\Delta T)}\right) - \Gamma\left(j-2, \frac{\varphi}{k(T_i+\Delta T)}\right)\right] \qquad (3.23)$$

where $\Gamma(a,x)$ is the incomplete gamma function defined by

$$\Gamma(a,x) \equiv \int_x^{\infty} t^{a-1} e^{-t} \, dt$$

If kT_i/φ is small compared to unity, and $\varphi/k(T_i + \Delta T)$ is large compared to unity, then this expression for the current may be approximated by taking the asymptotic expansion of the incomplete gamma function. The result is

$$i \simeq \pi d^2 A_r \frac{k}{\varphi}(T_i + T)^3 \, e^{-\varphi/k(T_i+\Delta T)} \qquad (3.24)$$

This expression for the current is proportional to the cube

of the surface temperature instead of the square of the surface temperature because the "effective area" of electron emission is not πd^2 but rather $\pi d^2/(\varphi/k(T_i+\Delta T))$. This result follows directly from the spatially Gaussian dependence of the laser irradiance. The expression $i/\pi d^2$ is plotted in Figure 11 assuming a work function of 4.5 eV and a Richardson constant A_r of 70 $A/cm^2/K^2$.

For lasers exhibiting single transverse and longitudinal modes, the temporal dependence of the irradiance is Gaussian, and thus the current as a function of time is given by :

$$i \simeq \pi d^2 A_r \frac{k}{\varphi}(T_i+\Delta T)^3 \, e^{-\varphi/k(T_i+\Delta T)} \qquad (3.25)$$

$$\Delta T = \frac{I_o(1-R)}{\sqrt{K\rho C}} \sqrt{\frac{T_g}{\sqrt{2}}} \quad \eta(t/T_g)$$

where $\eta(t/T_g)$ is given in Figure 7. Again T_g is related to the full-width-at-half-maximum of the incident laser pulse by $\tau_{FWHM} \simeq 1.665\ T_g$. As we see in Figure 12 the current produced by a 13 nsec (FWHM) laser pulse is delayed with respect to the incident irradiance by slightly more than 4 nsec. Moreover, we see in Figure 12 that the full-width-at-half-maximum of the emitted current is substantially less than the full-width-at-half-maximum of the incident laser pulse. The current pulse for thermionic emission is slightly asymmetric, there being a slight tail to this pulse. In these calculations it is assumed that the

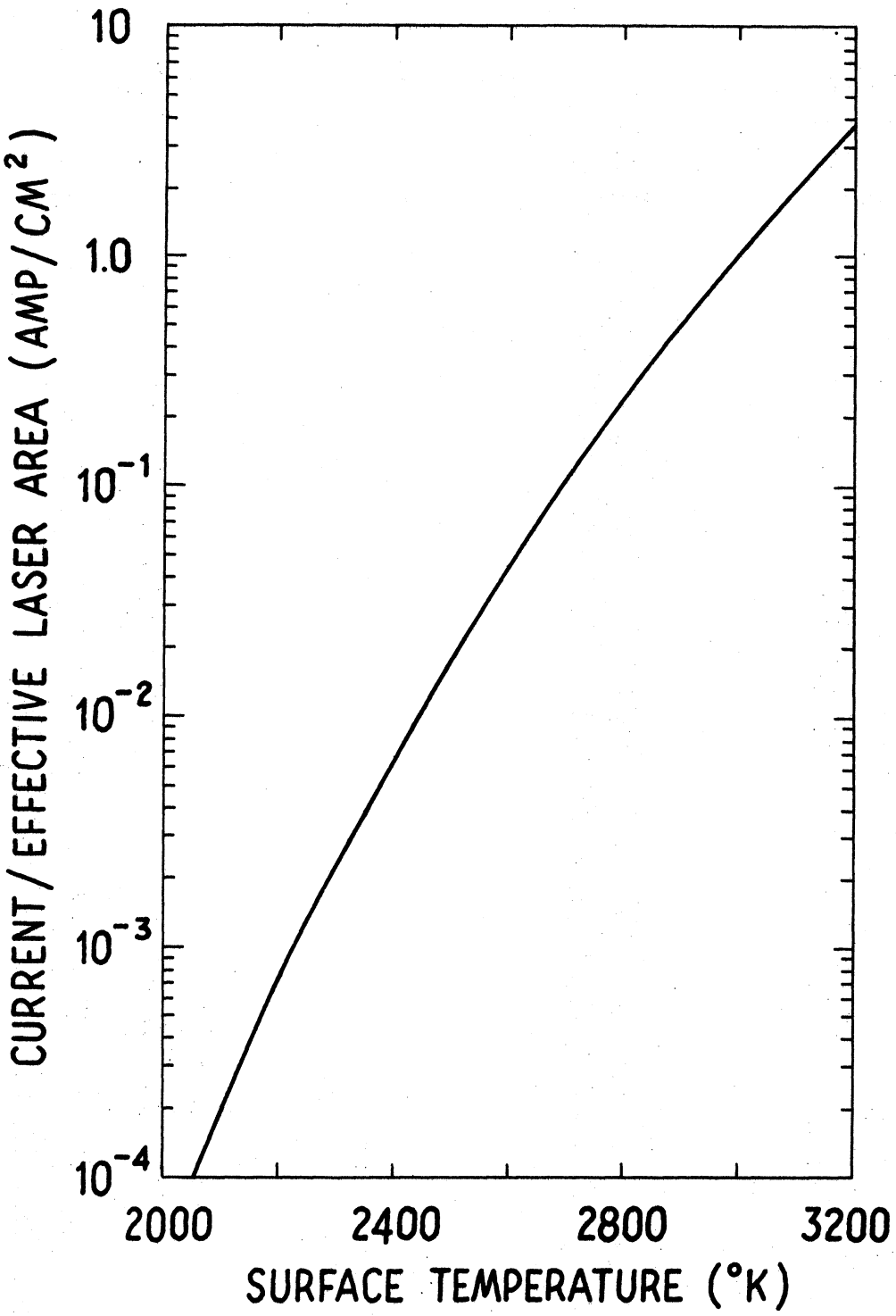

Figure 11. Current per Effective Laser Area (πd^2) Versus Maximum Surface Temperature for a Spatially Gaussian Heated Surface.

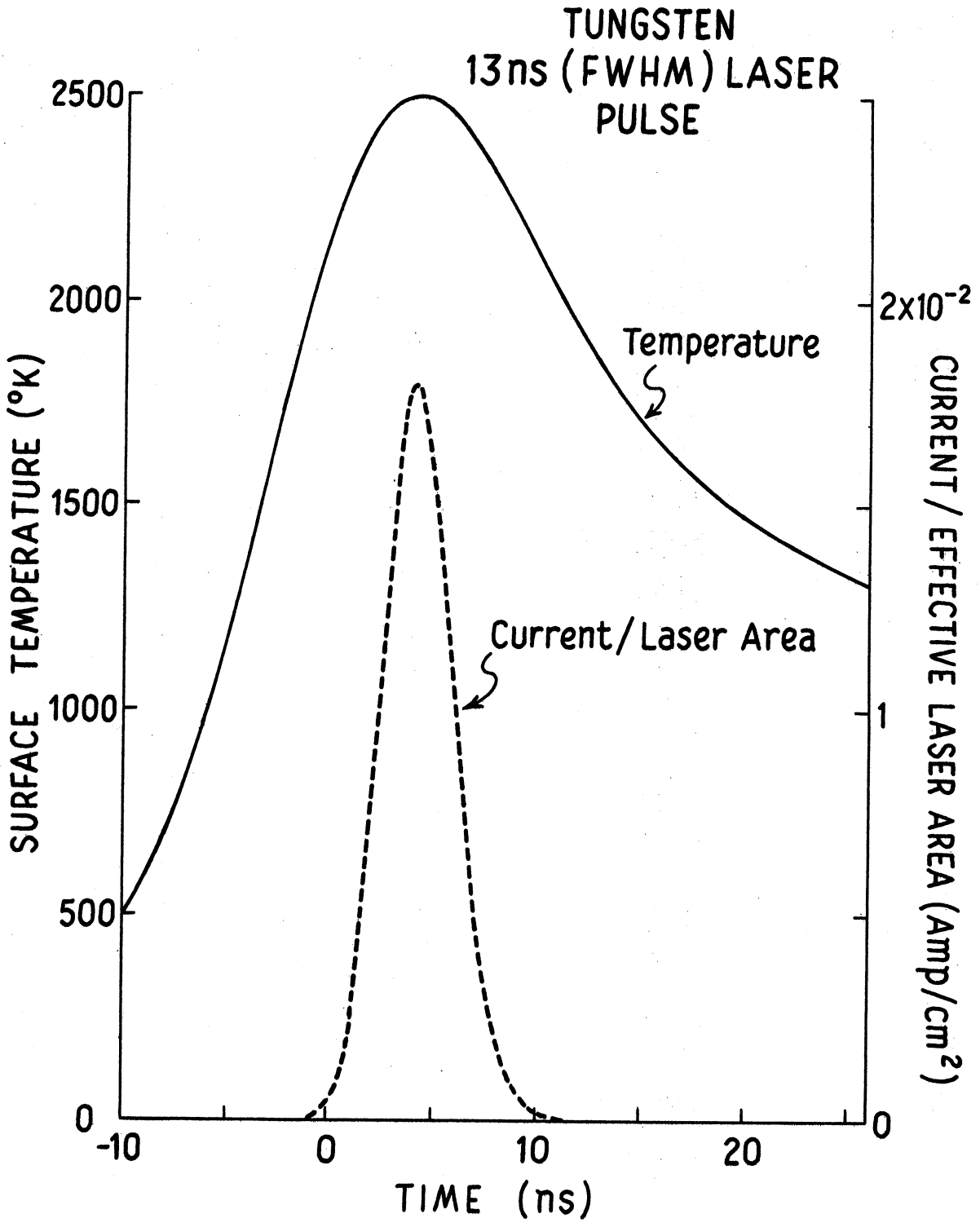

Figure 12. Temporal Dependence of Temperature and Current per Effective Laser Area. The maximum surface temperature is assumed to be 2500 K.

inter-electrode voltage is large enough so that space-charge effects may be neglected.

The maximum current i_{max} depends on the maximum irradiance I_o and the maximum surface temperature increase ΔT_{max} in the following way

$$i_{max} \simeq \pi d^2 A_r \frac{k}{\varphi} (T_i+\Delta T_{max})^3 \, e^{-\varphi/k(T_i+\Delta T_{max})} \qquad (3.26)$$

Here $\Delta T_{max} = \alpha I_o$, where α is some coefficient of proportionality. We can now construct a function that we shall call m, which is defined such that

$$m \equiv \frac{d(\ln i_{max})}{d(\ln I_o)}$$

Using equation 3.26 we find

$$m \simeq \frac{T - T_i}{T} \left[3 + \frac{\varphi}{kT}\right] \qquad (3.27)$$

where $T = T_i + \Delta T_{max}$. Thus T is the maximum surface temperature of the irradiated metal produced by a maximum incident irradiance I_o. The variable m is consequently the slope of a log-log plot of peak current versus peak irradiance. This slope is written implicitly in terms of the temperature T instead of explicitly in terms of the irradiance I_o. If the laser were of uniform spatial irradiance, then the factor 3 would be replaced by a factor 2.

In Figure 13 the slope m is plotted against maximum surface temperature for selected values of the work function. As one can see from this plot, for a work function of 4.5 eV and maximum surface temperature of 2500 K, the slope of a plot of current versus laser power should be nearly 20. In addition the plot should not be a straight line but rather a curve that is steadly decreasing in slope for increasing surface temperature. In Figure 13 the initial surface temperature is assumed to be 300 K.

The slope m* can also be calculated. In this case

$$m^* \equiv \frac{d(\ln i_{max})}{d(\ln T_i)} \simeq \frac{T_i}{T}\left[3 + \frac{\varphi}{kT}\right] \qquad (3.28)$$

Again m* is to be interpreted as the slope of a log-log plot of maximum current versus initial surface temperature at constant laser irradiance. In Figure 14 m* is plotted against T_i for selected values of the surface work function at ΔT_{max} = 1000 K. In Figure 15 m* is plotted against T_i for a work function of 4.5 eV with several different values of ΔT_{max}.

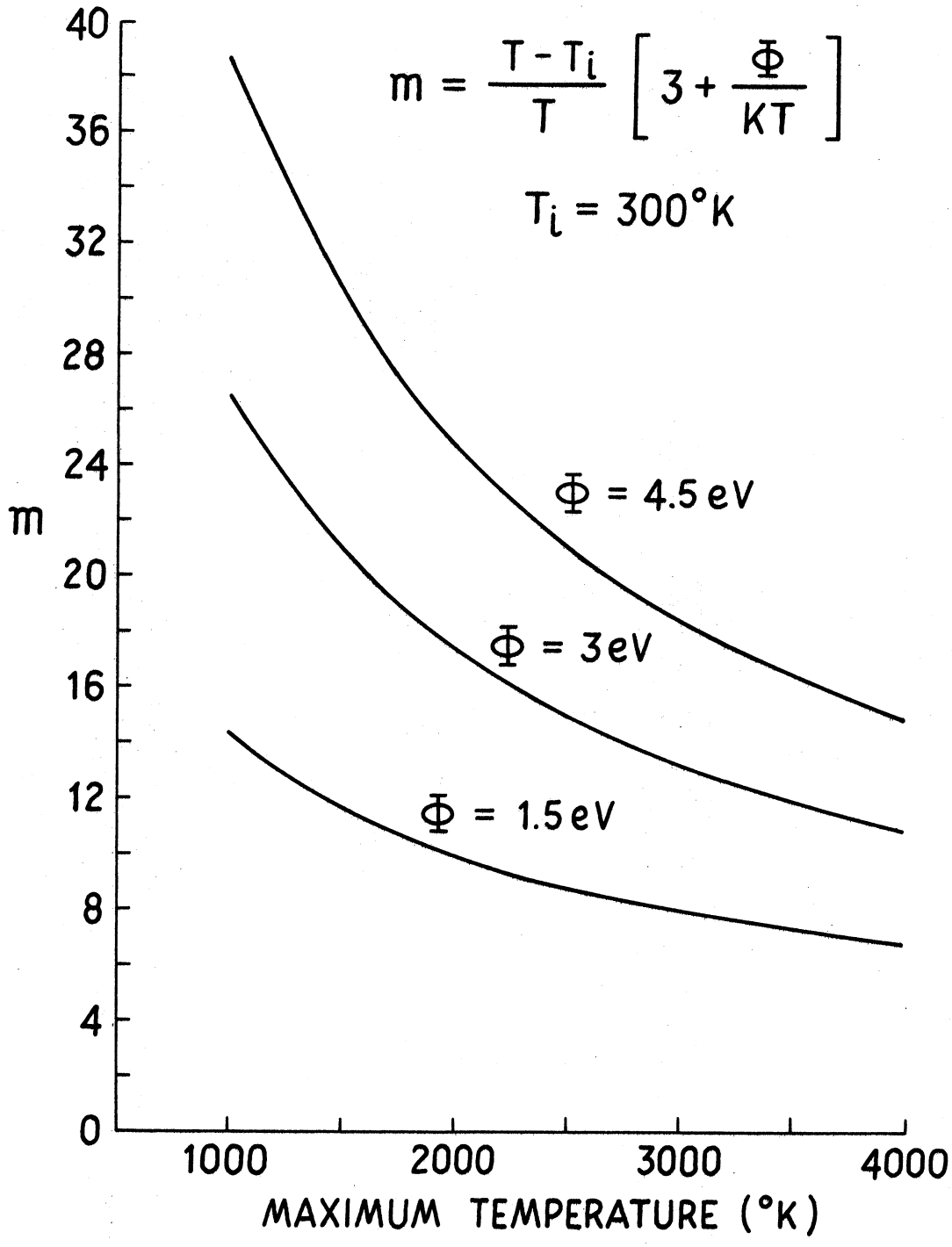

Figure 13. Slope m Plotted Against Maximum Surface Temperature.

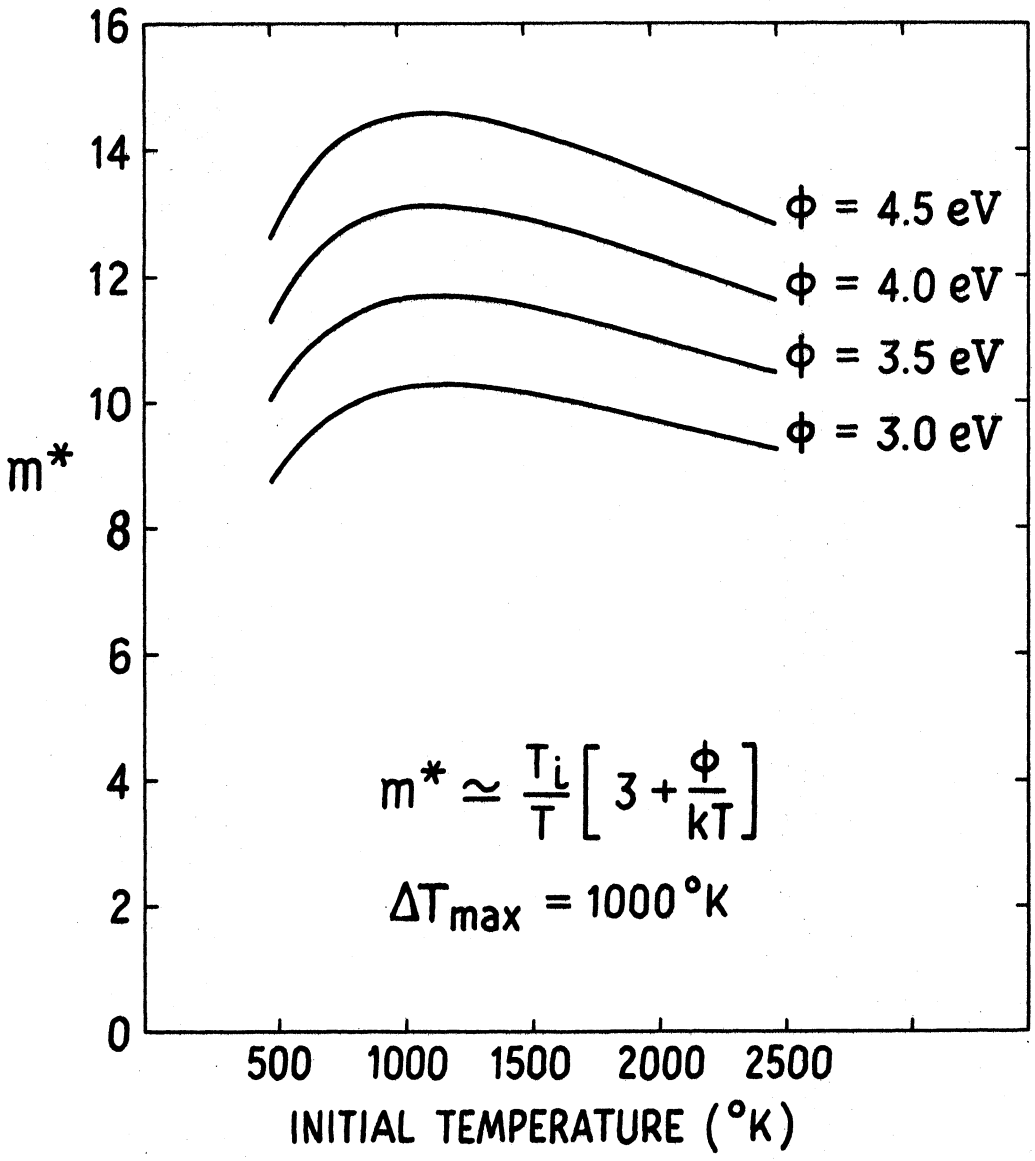

Figure 14. Slope m* Plotted Against Initial Surface Temperature.

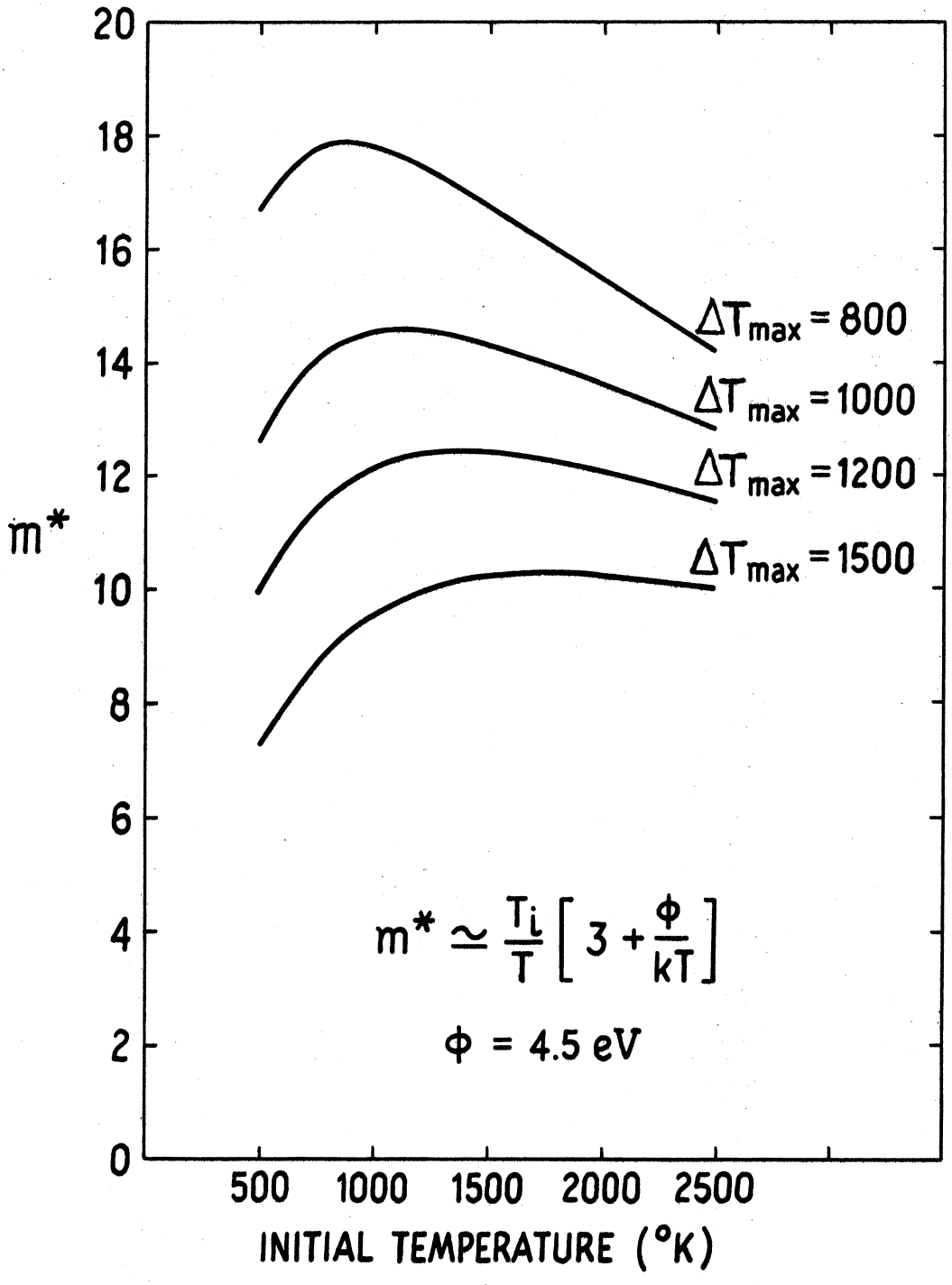

Figure 15. Slope m* Plotted Against Initial Surface Temperature.

In addition to thermionic emission, lasers can produce other types of electron emission from metals. When light strikes a metal surface an electron may be ejected from the surface by the process of photoemission. This effect was discovered in 1887-1888 by Hertz and Hallwachs and was correctly explained by Einstein for which he was awarded the Nobel prize. The Einstein photoelectric equation is

$$h\nu = \varphi + mv^2/2 \tag{3.29}$$

where φ is the work function of the emitter, m is the electron mass, v is the velocity of the electron, ν is the frequency of the incident radiation, and h is Planck's constant. No electron emission can occur unless the frequency of the incident radiation satisfies the condition $h\nu > \varphi$, because the kinetic energy of the emitted electron is always a positive quantity. The emitted electron current will be linearly proportional to the number of incident photons per unit time or, alternately, we can say that the current density is linearly proportional to the incident irradiance. We can express this as

$$J_1 = \eta_1 I \tag{3.30}$$

where η_1 is the frequency dependent photoelectric sensitivity of the surface in units of, for example, amperes/watt. This same relation is often expressed differently by stating a quantum yield, the number of ejected electrons per

incident photon. The relation between sensitivity and the quantum yield Y_1^* is

$$Y_1^* = \eta_1 \frac{h\nu}{e} \tag{3.31}$$

where Y_1^* is the number of electrons per incident photon at a given frequency, and e is the electron charge. Frequently another quantum yield Y_1 is also defined as the number of electrons emitted per absorbed photon. For a surface of reflectivity R, Y_1^* is related to Y_1 by the expression

$$Y_1^* = (1-R)Y_1$$

It has been recognized for some time, however, that if the incident irradiance is sufficiently intense then multiple-photon processes can be observed. A two-photon photoemission process, for example, would obey an energy conservation law of the form

$$2h\nu = \varphi + mv^2/2 \tag{3.32}$$

The corresponding two-photon photoemissive current density J_2 can be written as

$$J_2 = \eta_2 I^2 \tag{3.33}$$

where the two-photon sensitivity is often expressed in units of amperes-cm^2/$megawatt^2$.

It is possible to have still higher order effects, and,

in general, for an n-photon photoemission process the analogues of equations 3.29 and 3.30 are

$$nh\nu = \varphi + mv^2/2 \tag{3.34}$$

and

$$J_n = \eta_n I^n \tag{3.35}$$

There have been several attempts to formulate a theory of multiple-photon photoemission from which the expected sensitivities could be calculated in terms of the incident photon energy and the properties of the irradiated material. These theories, however, have had limited success in that the experimental values of η_2 and η_3 have often differed by as much as several orders of magnitude from the calculated values. Experimental studies on sodium[6] ($\varphi \approx 2.3$ eV) using a pulsed gallium arsenide laser ($h\nu \approx 1.48$ eV) give $\eta_2 \approx 8 \times 10^{-4}$ A-cm^2/MW^2. Other experiments on gold[13] ($\varphi \approx 4.8$ eV) using a frequency doubled ruby laser ($h\nu \approx 3.6$ eV) give $\eta_2 \approx 2.4 \times 10^{-3}$ A-cm^2/MW^2. These experiments were performed with laser irradiances such that the laser induced heating was only a few degrees Kelvin, and the initial temperature of the material was 300 K.

We now return to the process of one-photon photoemission and, in particular, look at the implications of the Einstein photoelectric equation. We note that this equation predicts a sharp cutoff in the electron emission at a frequency ν_o such that $h\nu_o = \varphi$. There is substantial experimental

evidence, however, that indicates the emitted electron current as a function of the incident radiation frequency does not have a sharp cutoff. Moreover, plots of current versus frequency are different at different temperatures for the same metal. This temperature dependence of photoelectron emission near threshold to a large extent has been explained by Fowler.[14]

The Fowler hypothesis is as follows: The quantum yield near threshold is, to a first approximation, proportional to the number of electrons per unit volume of the metal whose "normal" kinetic energy when enhanced by the incident photon energy is sufficient to surmount the potential energy barrier. Specifically, by "normal" kinetic energy we mean that portion of the kinetic energy which is attributed to motion perpendicular to the plane of emission. We will make a slightly different hypothesis but will ultimately arrive at the same final answer that Fowler achieved. Our hypothesis is that the one-photon quantum yield (electrons emitted per absorbed photon) is proportional to the number of electrons impinging in unit surface area per unit time whose "normal" kinetic energy augmented by $h\nu$ is sufficient to escape the potential energy barrier. If this coefficient of proportionality is α_1, we find that this one-photon quantum yield is

$$Y_1 = \alpha_1 \frac{2}{h^3} \int_{-\infty}^{\infty} dp_x \int_{-\infty}^{\infty} dp_y \int_{p_1}^{\infty} dp_z \; \frac{p_z/m}{\exp\left[\frac{p_x^2+p_y^2+p_z^2}{2mkT} - \frac{\epsilon_F}{kT}\right] + 1} \qquad (3.36)$$

where p_1 is defined by the relation

$$h\nu + \frac{p_1^2}{2m} = \epsilon_F + \varphi \tag{3.37}$$

Integrating over p_x and p_y gives

$$Y_1 = \alpha_1 \frac{4\pi kT}{h^3} \int_{p_1}^{\infty} p_z \, dp_z \log \left[1 + \exp\left\{ -\left(\frac{p_z^2}{2m} - \epsilon_F \right) / kT \right\} \right] \tag{3.38}$$

Expanding the logarithm in equation 3.38 and integrating term by term gives the following results:

$$Y_1 = \alpha_1 \frac{4\pi mk^2}{h^3} T^2 \left[\exp\left(\frac{h(\nu-\nu_o)}{kT} \right) - \frac{1}{2^2} \exp\left(\frac{2h(\nu-\nu_o)}{kT} \right) + \frac{1}{3^2} \exp\left(\frac{3h(\nu-\nu_o)}{kT} \right) - \ldots \right] \quad \frac{h(\nu-\nu_o)}{kT} \leq 0 \tag{3.39}$$

$$Y_1 = \alpha_1 \frac{4\pi mk^2}{h^3} T^2 \left[\frac{\pi^2}{6} + \frac{1}{2} \left(\frac{h(\nu-\nu_o)}{kT} \right)^2 - \left\{ \exp\left(- \frac{h(\nu-\nu_o)}{kT} \right) - \frac{1}{2^2} \exp\left(- \frac{2h(\nu-\nu_o)}{kT} \right) + \frac{1}{3^2} \exp\left(- \frac{3h(\nu-\nu_o)}{kT} \right) - \ldots \right\} \right] \tag{3.40}$$

$$\frac{h(\nu-\nu_o)}{kT} \geq 0$$

Expression 3.39 predicts a finite current even if $h\nu < h\nu_o$. One can picture this process as photoelectric emission from the tail of the Fermi-Dirac electron distribution. If

$$\varphi - h\nu \gg kT$$

we can approximate the quantum yield in this region as

$$Y_1 \simeq \alpha_1 (A_r/e) T^2 \exp\left[-(\varphi - h\nu)/kT\right] \qquad (3.41)$$

where A_r is the theoretical value of the Richardson constant $\frac{4\pi mek^2}{h^3}$; this is numerically equal to 120 $A/cm^2/K^2$. The corresponding expression for the electron current density is given by

$$J_1 \simeq \alpha_1 (1-R) \frac{e}{h\nu} I (A_r/e) T^2 \exp\left[-(\varphi - h\nu)/kT\right] \qquad (3.42)$$

The constant α_1 has been determined experimentally[15] to be of the order 10^{-32} - 10^{-33} cm^2-sec for many metals.

Consider now the implications of a laser as the source of radiation for a photoemission experiment. In particular, consider the circumstances in which this laser induced electron emission is described by equation 3.42. If the laser produces substantial heating of the surface, then the time dependence of the surface temperature, as we have previously calculated, may be inserted into equation 3.42 to predict the time evolution of the current density. We note, however, that since the temperature maximum lags the

peak in the incident irradiance for a temporally Gaussian laser pulse, the emitted current pulses will be time delayed with respect to the incident laser pulse. We will henceforth designate this laser produced photoemission augmented by laser produced surface heating the following: one-photon assisted thermionic emission. We choose to emphasize the thermal aspect of the effect because experiments on photoemission (with no concomitant temperature change) indicate that there is no time delay in the electron emission process. To the extent that equation 3.41 is a good approximation of equation 3.39, we expect the one-photon assisted thermionic emission current density to be given by equation 3.42.

In addition to one-photon assisted thermionic emission we can naturally generalize our arguments to include n-photon assisted thermionic emission. As a specific example we shall consider a two-photon assisted thermionic emission effect. We shall postulate that the number of electrons emitted per unit area per unit time is proportional to the square of the number of absorbed photons per unit area per unit time and linearly proportional to the number of electrons impinging from within on unit surface area per unit time whose "normal" kinetic energy augmented by $2h\nu$ is sufficient to escape the energy barrier. The two-photon quantum yield Y_2, the number of emitted electrons per absorbed photon, is now proportional to the number of absorbed photons per unit area per unit time. The expressions analogous to equations 3.39 and 3.40 become

$$Y_2 = \alpha_2 \frac{e}{h\nu} (1-R) I \frac{A_r}{e} T^2 \left[\exp\left[h(2\nu-\nu_o)/kT\right] \right.$$

$$\left. - \frac{1}{2^2} \exp\left[2h(2\nu-\nu_o)/kT\right] + \frac{1}{3^2} \exp\left[3h(2\nu-\nu_o)/kT\right] - \ldots \right]$$

$$\frac{h(2\nu-\nu_o)}{kT} \leq 0$$

$$Y_2 = \alpha_2 \frac{e}{h\nu} (1-R)\ I \frac{A_r}{e} T^2 \left[\frac{\pi^2}{6} + \frac{1}{2} \left(\frac{h(2\nu-\nu_o)}{kT} \right)^2 \right.$$

$$- \left\{ \exp\left[- h(2\nu-\nu_o)/kT \right] - \frac{1}{2^2} \exp\left[- 2h(2\nu-\nu_o)/kT \right] \right.$$

$$\left. \left. + \frac{1}{3^2} \exp\left[- 3h(2\nu-\nu_o)/kT \right] - \ldots \right\} \right]$$

$$\frac{h(2\nu-\nu_o)}{kT} \geq 0$$

Again if

$$\varphi - 2h\nu \gg kT$$

we can approximate Y_2 by the expression

$$Y_2 \simeq \alpha_2 \frac{e}{h\nu} (1-R)\ I \frac{A_r}{e} T^2 \exp\left[-(\varphi-2h\nu)/kT \right] \qquad (3.45)$$

The corresponding expression for the two-photon assisted thermionic emission current density is

$$J_2 \simeq \alpha_2 \left(\frac{e}{h\nu}\right)^2 (1-R)^2 \, I^2 \, \frac{A_r}{e} \, T^2 \exp\left[-(\varphi-2h\nu)/kT\right] \qquad (3.46)$$

If we return to one-photon assisted thermionic emission we may now compute the total current produced by a spatially Gaussian incident irradiance. Assuming a temperature distribution of the form

$$T = T_i + \Delta T \, e^{-(r/d)^2} \qquad (3.47)$$

we find that the total current is given by

$$i = 2\pi \int_0^d J_1 \, r dr \qquad (3.48)$$

where J_1 is given by equation 3.42. The result of the integration gives

$$i = \pi d^2 \alpha_1 (1-R) \frac{A_r}{h\nu} \, \frac{I}{\Delta T} \left(\frac{\varphi-h\nu}{k}\right)^3 \left[\Gamma\left(-3, \frac{\varphi-h\nu}{k(T_i+\Delta T)}\right) - \Gamma\left(-3, \frac{\varphi-h\nu}{k(T_i+\frac{\Delta T}{e})}\right)\right] \qquad (3.49)$$

If $T_i \ll \Delta T$, we can take the leading term in the expansion of the incomplete gamma function to find

$$i \simeq \pi d^2 \alpha_1 (1-R) \frac{A_r}{h\nu} I \frac{k}{\varphi - h\nu} (T_i+\Delta T)^3 \exp\left[-(\varphi-h\nu)/k(T_i+\Delta T)\right] \tag{3.50}$$

As with laser induced thermionic emission we can calculate the expected slope of a log-log plot of maximum electron current, i_{max}, versus maximum laser irradiance I_o. Defining this variable as m_1 for a one-photon assisted thermionic emission process, we find by using equation 3.50

$$m_1 \equiv \frac{d\ (\ln i_{max})}{d\ (\ln I_o)} \simeq \frac{T - T_i}{T} \left[4 + \frac{\varphi - h\nu}{kT} \right] \tag{3.51}$$

Again as with thermionic emission, the variable m_1 is written implicitly in terms of the maximum surface temperature, T, and the initial temperature T_i, instead of explicitly in terms of the maximum irradiance I_o. The variable m_1 is plotted in Figure 16 as a function of the maximum surface temperature for an incident photon energy of 1.8 eV and for several values of work function. The initial surface temperature is assumed to be 300 K. If we compare the results of Figure 13 with those of Figure 16, we conclude that for a given maximum surface temperature and a given work function the slope of a log-log plot of maximum current versus maximum irradiance is less for one-photon assisted thermionic emission than for thermionic emission.

The slope m_1^* associated with the change in current

produced by a change in initial temperature, T_i, can be calculated for a one-photon assisted thermionic emission. For this case

$$m_1^* \equiv \frac{d\ (\ln i_{max})}{d\ (\ln T_i)} \simeq \frac{T_i}{T}\left[3 + \frac{\varphi - h\nu}{kT}\right] \qquad (3.52)$$

In Figure 17 m_1^* is plotted against initial temperature for a work function of 4.5 eV and several values of ΔT_{max}, the maximum change in surface temperature produced by the laser.

We should note that the rather simple expressions for m_1 and m_1^* given in equations 3.51 and 3.52 respectively are only approximations for these derivatives. If we compare the results of these simple expressions, which are used for Figures 16 and 17, with more sophisticated computer calculations based on equation 3.49, we find that the two methods give consistent results to within ten percent. A comparison of the computer calculations performed on the University of Michigan High Energy Physics PDP-10 computer with the results given in Figures 16 and 17 is given in Table 1.

For two-photon assisted thermionic emission produced by a spatially Gaussian incident irradiance the surface temperature once again is given by

$$T = T_i + \Delta T\ e^{-(r/d)^2} \qquad (3.53)$$

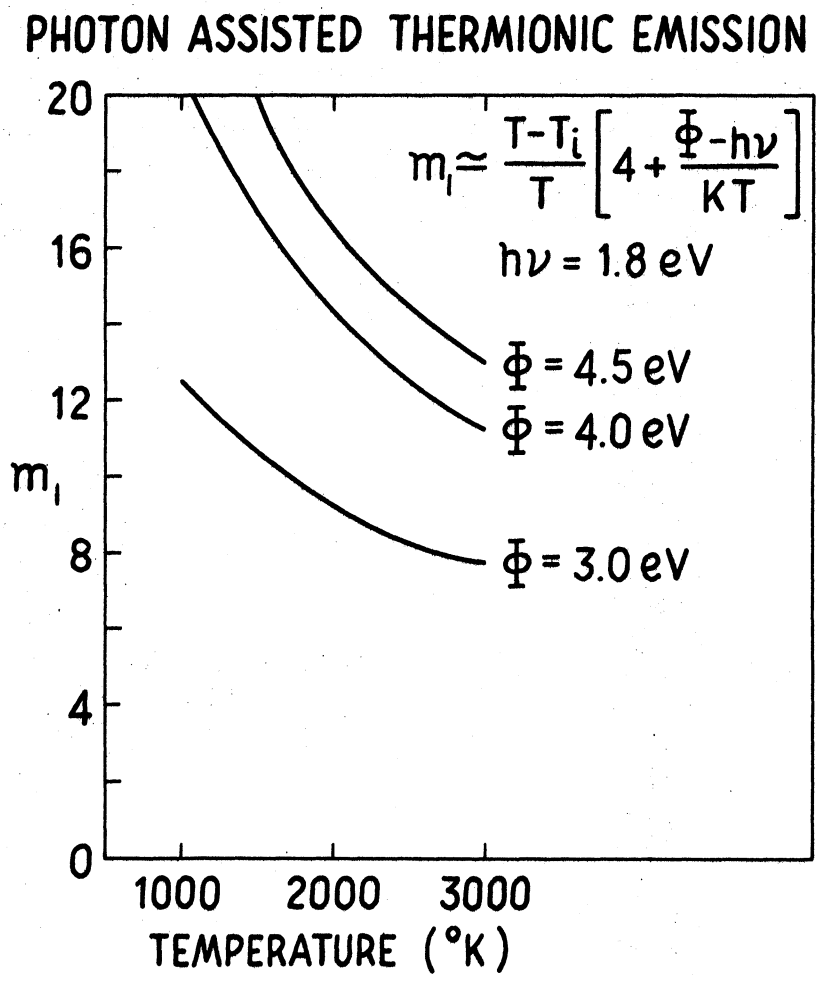

Figure 16. Slope m_l Plotted Against Maximum Surface Temperature. T_i=300 K.

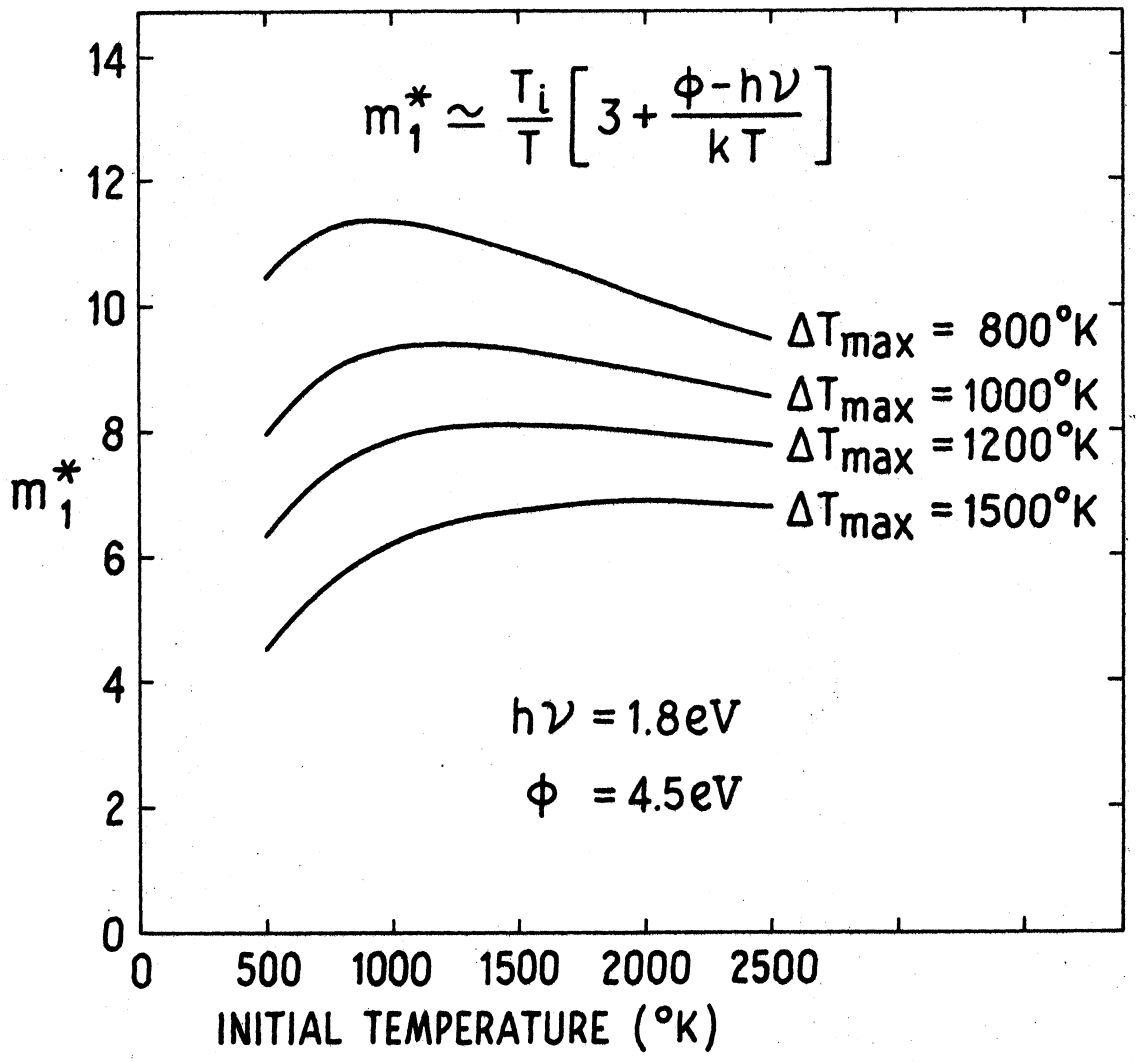

Figure 17. Slope m_1^* Plotted Against Initial Surface Temperature.

$h\nu$ = 1.8 eV	m_1 COMPUTER	m_1 (eq. 3.51)
φ=4.5 eV; T_i=300 K; ΔT=1000 K	21.5	21.6
φ=4.5 eV; T_i=300 K; ΔT=1500 K	17.7	17.8
φ=3.5 eV; T_i=300 K; ΔT=1000 K	14.6	14.8
φ=3.5 eV; T_i=300 K; ΔT=1500 K	12.3	12.5
	m_1^* COMPUTER	m_1^* (eq. 3.52)
φ=4.5 eV; ΔT=1000 K; T_i=1000 K	9.7	9.3
φ=4.5 eV; ΔT=1000 K; T_i=1500 K	9.7	9.3
φ=3.5 eV; ΔT=1000 K; T_i=1000 K	6.8	6.4
φ=3.5 eV; ΔT=1000 K; T_i=1500 K	6.8	6.5

Table 1. A Comparison of Calculated Slopes: One-Photon Assisted Thermionic Emission.

The total current is thus

$$i = 2\pi \int_0^d J_2 \, r \, dr \tag{3.54}$$

where J_2 is given by equation 3.46. The result of the integration gives

$$i = \pi d^2 \alpha_2 (1-R)^2 \left(\frac{e}{h\nu}\right)^2 \frac{A_r}{e} \frac{I^2}{\Delta T^2} \left[\left(\frac{\varphi - 2h\nu}{k}\right)^4 \left\{ \Gamma\left(-4, \frac{\varphi-2h\nu}{k(T_i+\Delta T)}\right) - \Gamma\left(-4, \frac{\varphi-2h\nu}{k(T_i+\frac{\Delta T}{e})}\right)\right\} - T_i \left(\frac{\varphi-2h\nu}{k}\right)^3 \left\{ \Gamma\left(-3, \frac{\varphi-2h\nu}{k(T_i+\Delta T)}\right) - \Gamma\left(-3, \frac{\varphi-2h\nu}{k(T_i+\frac{\Delta T}{e})}\right)\right\}\right] \tag{3.55}$$

If $T_i \ll \Delta T$, then the current may be approximated by

$$i = \pi d^2 \alpha_2 (1-R)^2 \left(\frac{e}{h\nu}\right)^2 \frac{A_r}{e} I^2 \frac{(T_i+\Delta T)^3 k}{\varphi - 2h\nu} e^{-\frac{\varphi-2h\nu}{k(T_i+\Delta T)}} \tag{3.56}$$

Again we can calculate the expected slope of a log-log plot of maximum electron current, i_{max}, versus maximum laser irradiance I_o. Defining this variable as m_2 for a two-photon assisted thermionic emission process, we find by using equation 3.56

$$m_2 \equiv \frac{d\,(\ln i_{max})}{d\,(\ln I_o)} \simeq \frac{T-T_i}{T}\left[5 + \frac{\varphi-2h\nu}{kT}\right] \tag{3.57}$$

The variable m_2 is plotted in Figure 18 as a function of the maximum surface temperature for an incident photon energy of 1.8 eV and for several values of the work function. The initial surface temperature is assumed as 300 K.
If we compare the results as shown in Figure 18 with the results depicted in Figures 13 and 16, we conclude that for a given surface temperature and a given work function the slope of a log-log plot of maximum current versus maximum irradiance is still smaller for the two-photon assisted thermionic emission than for either the one-photon assisted thermionic emission or the thermionic emission process.

The slope m_2^* associated with the change in current produced by a change in initial temperature, T_i, when calculated for the two-photon assisted thermionic emission is found to be

$$m_2^* \equiv \frac{d\ (\ln i_{max})}{d\ (\ln T_i)} \simeq \frac{T_i}{T}\left[3 + \frac{\varphi - 2h\nu}{kT}\right] \qquad (3.58)$$

In Figure 19 m_2^* is plotted versus initial temperature for a work function of 4.5 eV and for several values of ΔT_{max} the maximum change in the surface temperature produced by the laser.

A comparison of computer calculations of m_2 and m_2^* with the predictions of the simple expressions in equations 3.57 and 3.58 is given in Table 2.

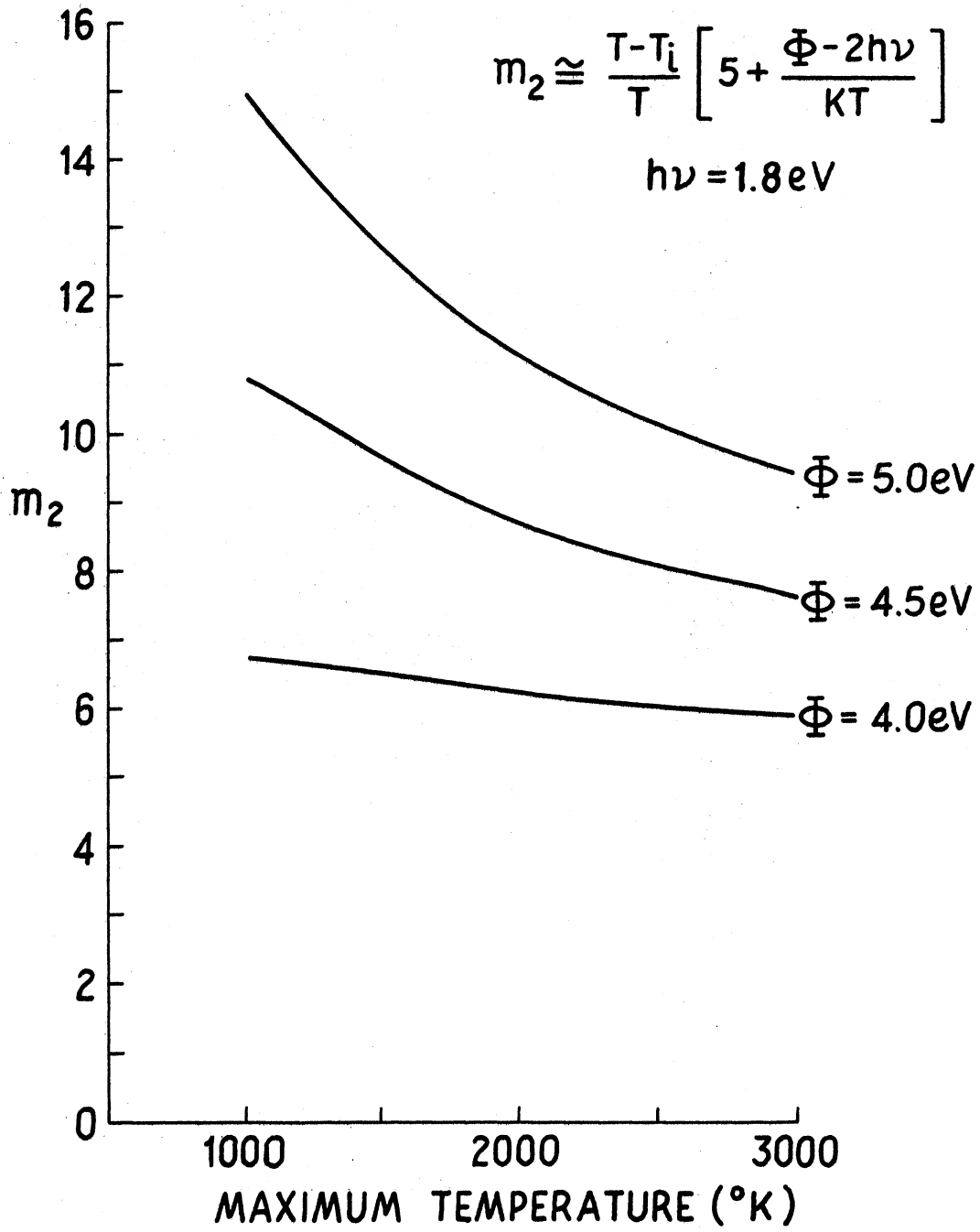

Figure 18. Slope m_2 Plotted Against Maximum Surface Temperature. T_i = 300 K.

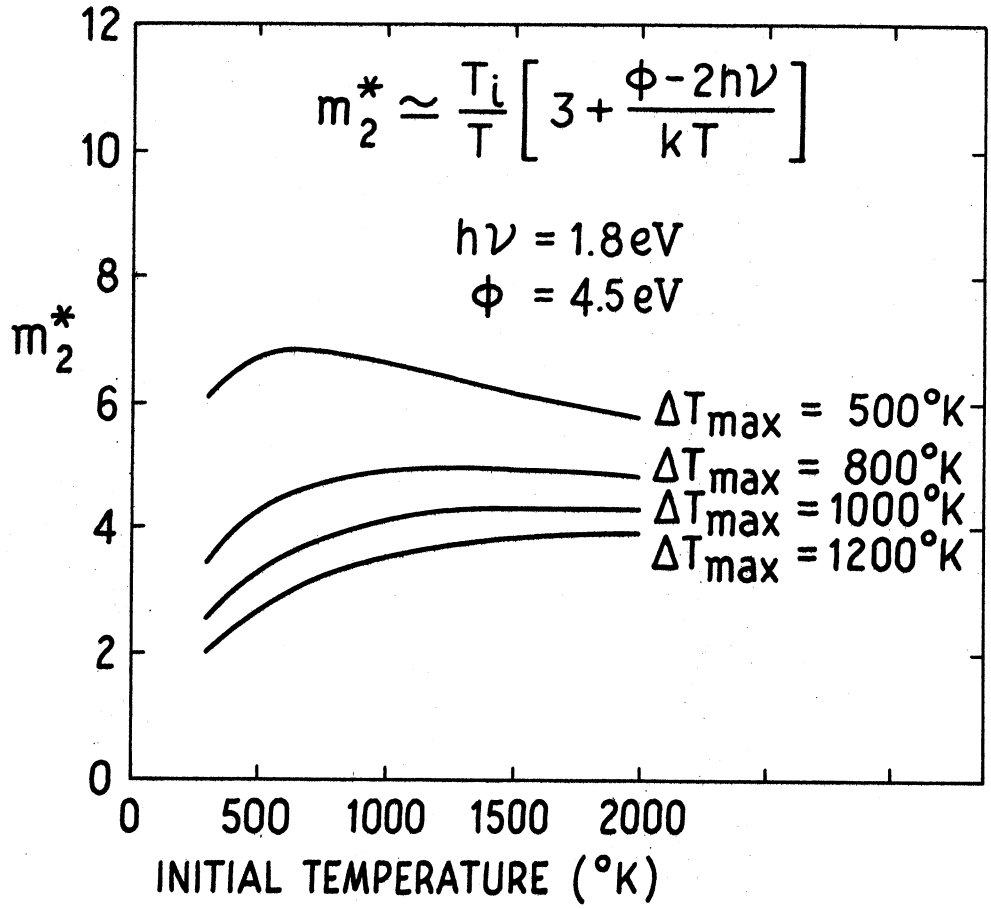

Figure 19. Slope m_2^* Plotted Against Initial Surface Temperature.

Table 2. Comparison of Calculated Slopes: Two-Photon Assisted Thermionic Emission.

$2h\nu$ = 3.6 eV	m_2 COMPUTER	m_2 (eq. 3.57)
φ=4.5 eV; T_i=300 K; ΔT=1000 K	10.0	10.1
φ=4.5 eV; T_i=300 K; ΔT=1500 K	8.8	9.0
φ=4.5 eV; T_i=300 K; ΔT=1800 K	8.3	8.5
φ=4.0 eV; T_i=300 K; ΔT=1000 K	6.4	6.6
φ=4.0 eV; T_i=300 K; ΔT=1500 K	6.0	6.3
φ=4.0 eV; T_i=300 K; ΔT=1800 K	5.8	6.2
	m_2^* COMPUTER	m_2^* (eq. 3.58)
φ=4.5 eV; ΔT=1000 K; T_i= 500 K	3.5	3.3
φ=4.5 eV; ΔT=1000 K; T_i=1000 K	4.2	4.1
φ=4.5 eV; ΔT=1000 K; T_i=1200 K	4.3	4.2
φ=4.0 eV; ΔT=1000 K; T_i= 500 K	2.1	2.0
φ=4.0 eV; ΔT=1000 K; T_i=1000 K	2.6	2.6
φ=4.0 eV; ΔT=1000 K; T_i=1200 K	2.6	2.8

CHAPTER IV

EXPERIMENTAL RESULTS

In our experiments on laser induced electron emission we have studied several types of cathode geometries and have used two different ruby lasers. We shall consider first those experiments in which we used metal rods as cathode material. Finally, we shall consider those experiments in which we used tungsten ribbons as cathodes.

The tungsten field emission cathode was fabricated from a KOH etched 0.04 inch diameter rod. The details of the tube preparation have been given in Chapter II. Before irradiating the cathode with the laser, we measured the d.c. current-voltage relation for this cathode. We have plotted the data in the form of the usual Fowler-Nordheim plot in Figure 20. The magnitude of the slope of this plot is approximately 4×10^4 volts, and the theory of field emission has been reviewed in Appendix II.

The relation between maximum emitted current and the maximum incident irradiance is given for the field emission cathode in Figures 21,22, and 23. This data was taken at the Hughes Research Laboratories and clearly demonstrates the nonlinear relation between the maximum current and the maximum laser irradiance. The pressure in the electron tube was 1×10^{-9} torr, and the temperature of the cathode prior

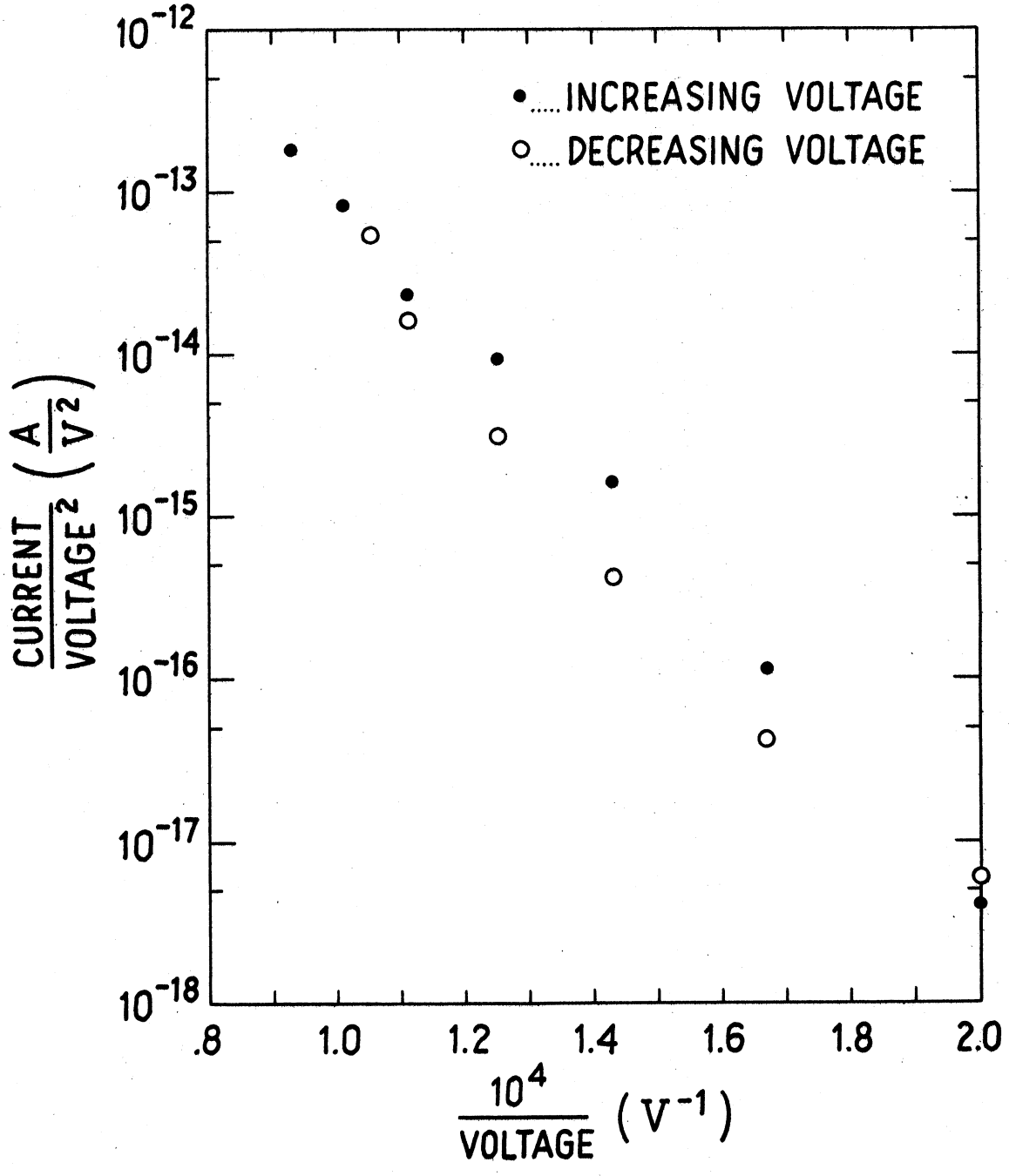

Figure 20. Fowler-Nordheim Plot of Current-Voltage Relation.

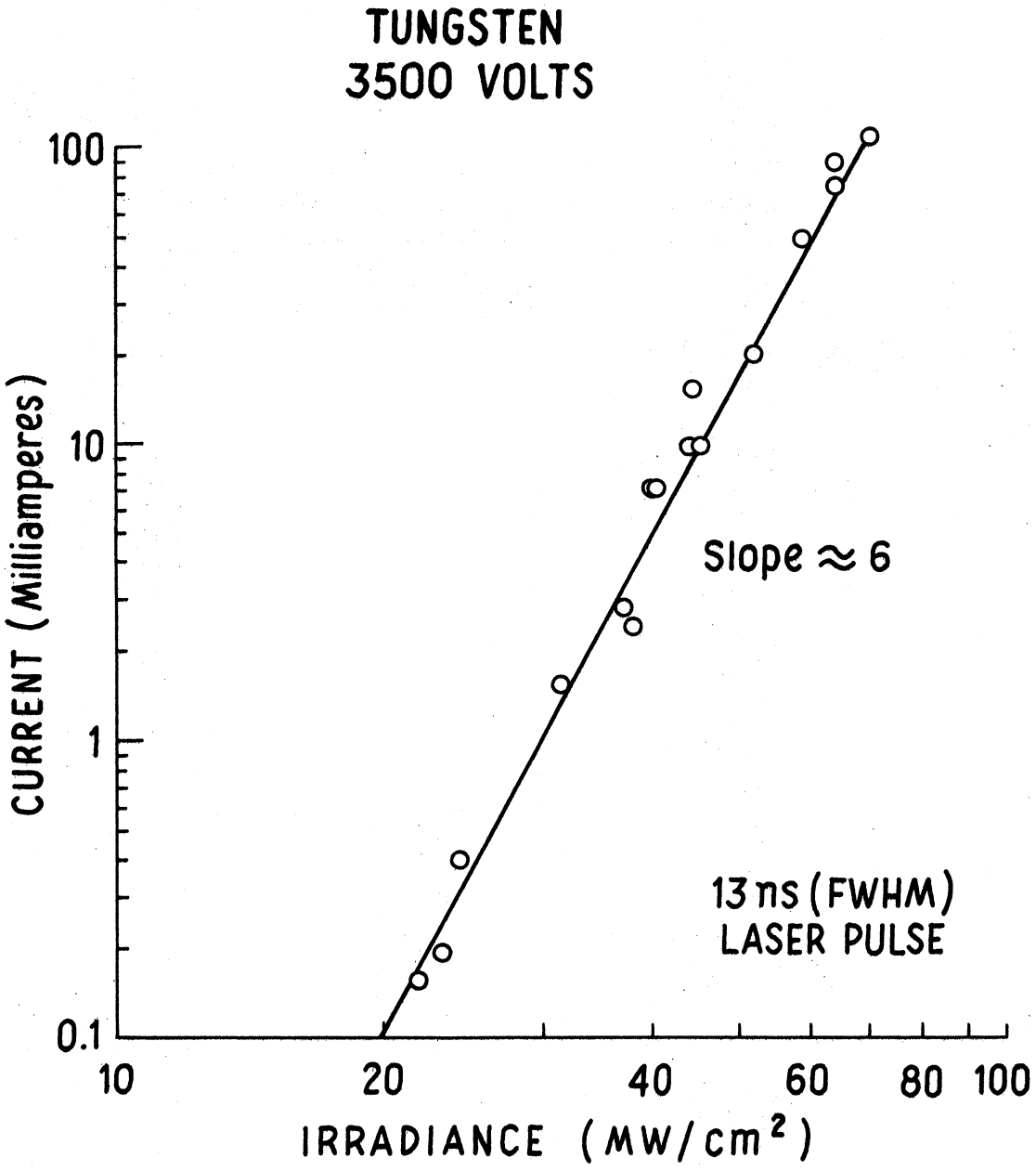

Figure 21. Maximum Laser Induced Current Versus Maximum Incident Irradiance.

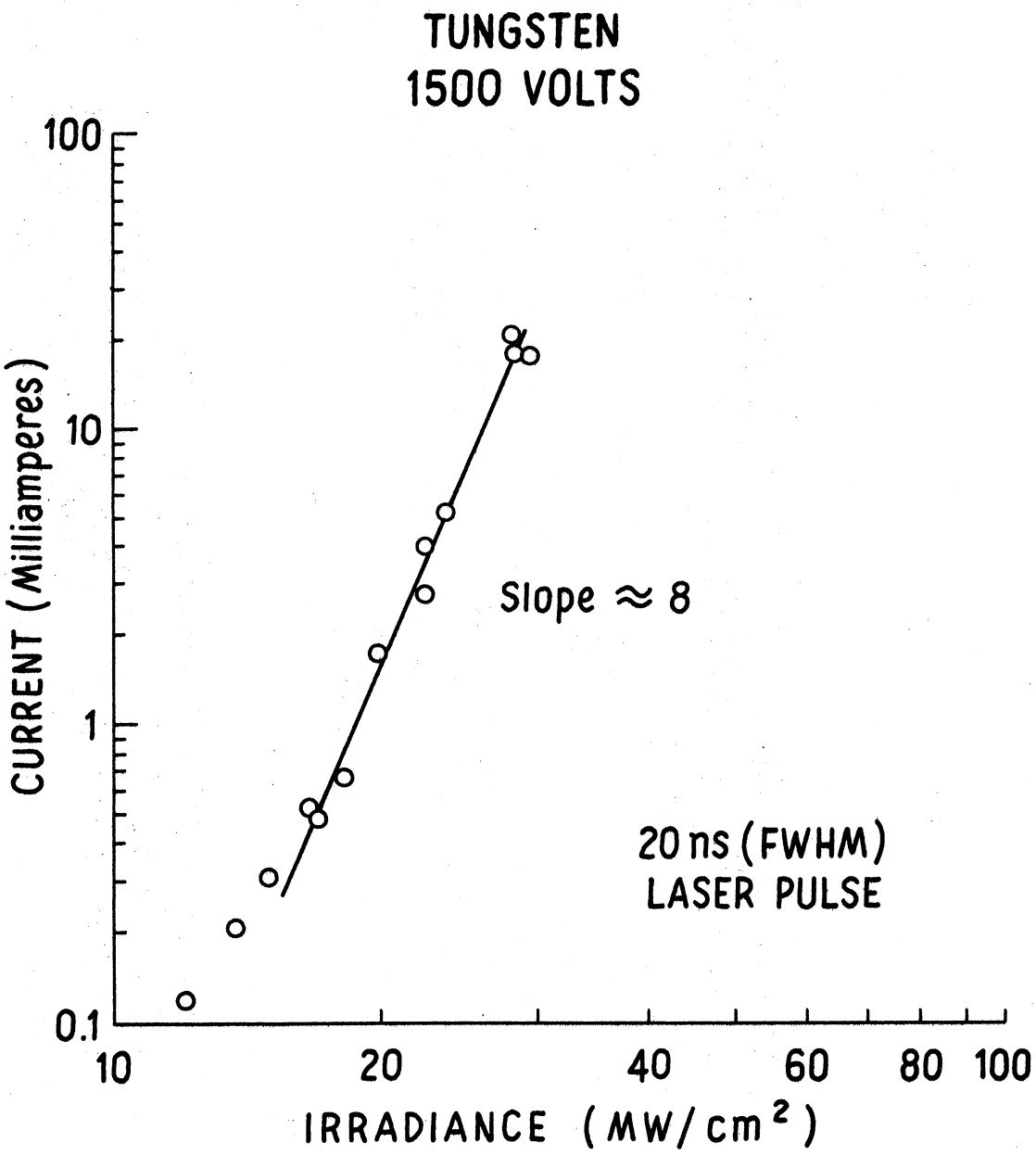

Figure 22. Maximum Laser Induced Current Versus Maximum Incident Irradiance.

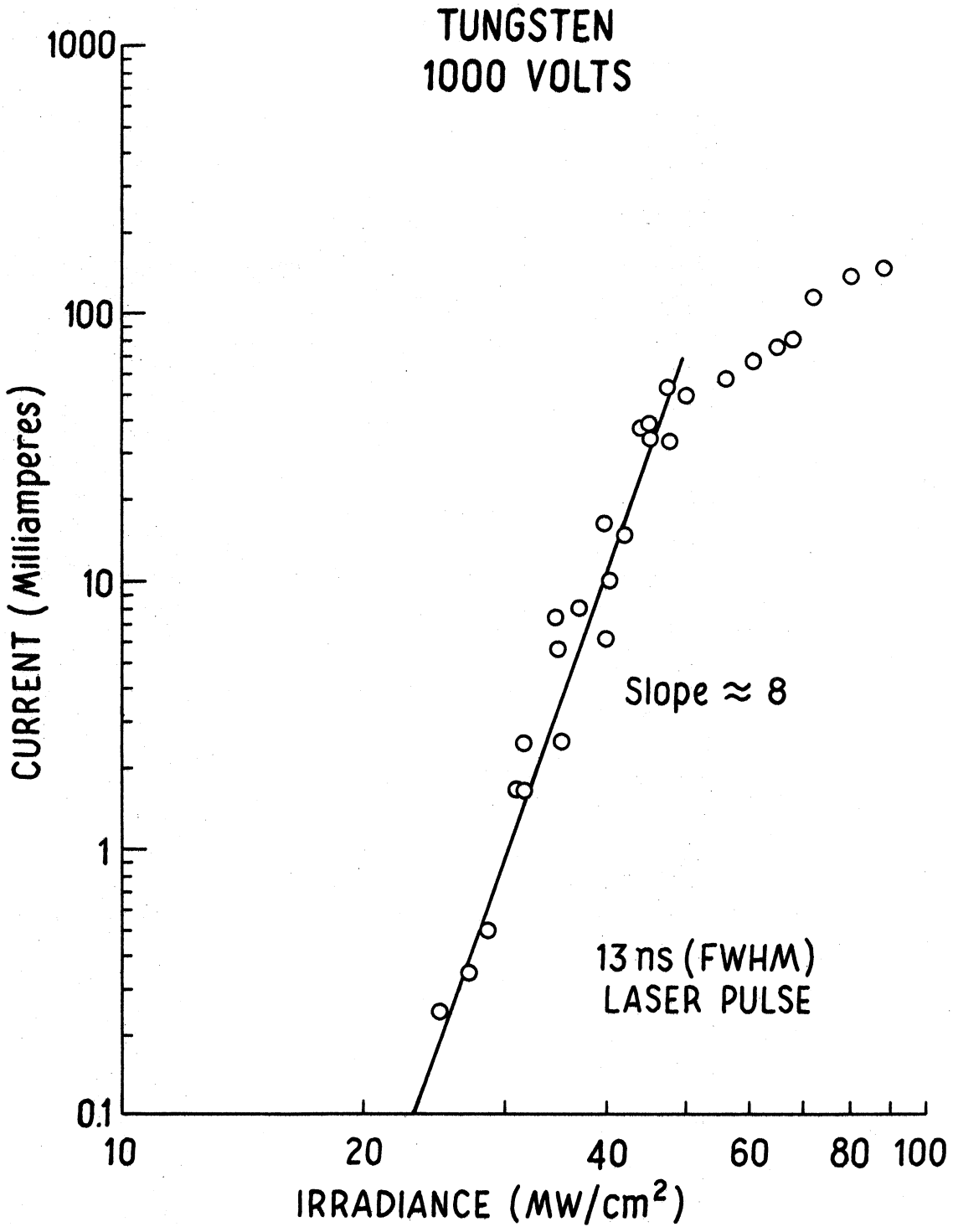

Figure 23. Maximum Laser Induced Current Versus Maximum Incident Irradiance.

to being irradiated by the laser was 300 K. The cathode to anode spacing in the field emission tube was 3 mm, and the applied voltage is listed at the top of each graph. The laser output was nearly a single longitudinal and single transverse mode, and the difference in the duration of the output was due to a difference in the dye of the Q-switch used in the different runs. The effective area of the laser, πd^2, (compare equation 3.18) was found to be 4.5×10^{-2} cm^2 for the laser at the Hughes Research Laboratories. The pulse energy and power were monitored by using calibrated photodiodes, and we estimate the accuracy of both the power measurements and the area measurements to be 10 percent. The polarization of the electric field of the laser was perpendicular to the line connecting cathode and anode.

From Figures 21, 22, and 23 we find that the log-log plot of maximum current versus maximum laser irradiance is approximately linear in the region of a few tens of megawatts per square centimeter. The slopes of these lines vary from approximately 6 to 8.

In order to see if the electron emission was characteristic of tungsten, we performed similar experiments on molybdenum and platinum. The results of these experiments are given in Figures 24 and 25. Both of these materials were sealed in the same vacuum tube, and each served as one of the two electrodes. Each electrode was a blunt rod of diameter 0.045 inches (platinum) and 0.04 inches (molybdenum). The two electrodes were separated by a spacing of approxi-

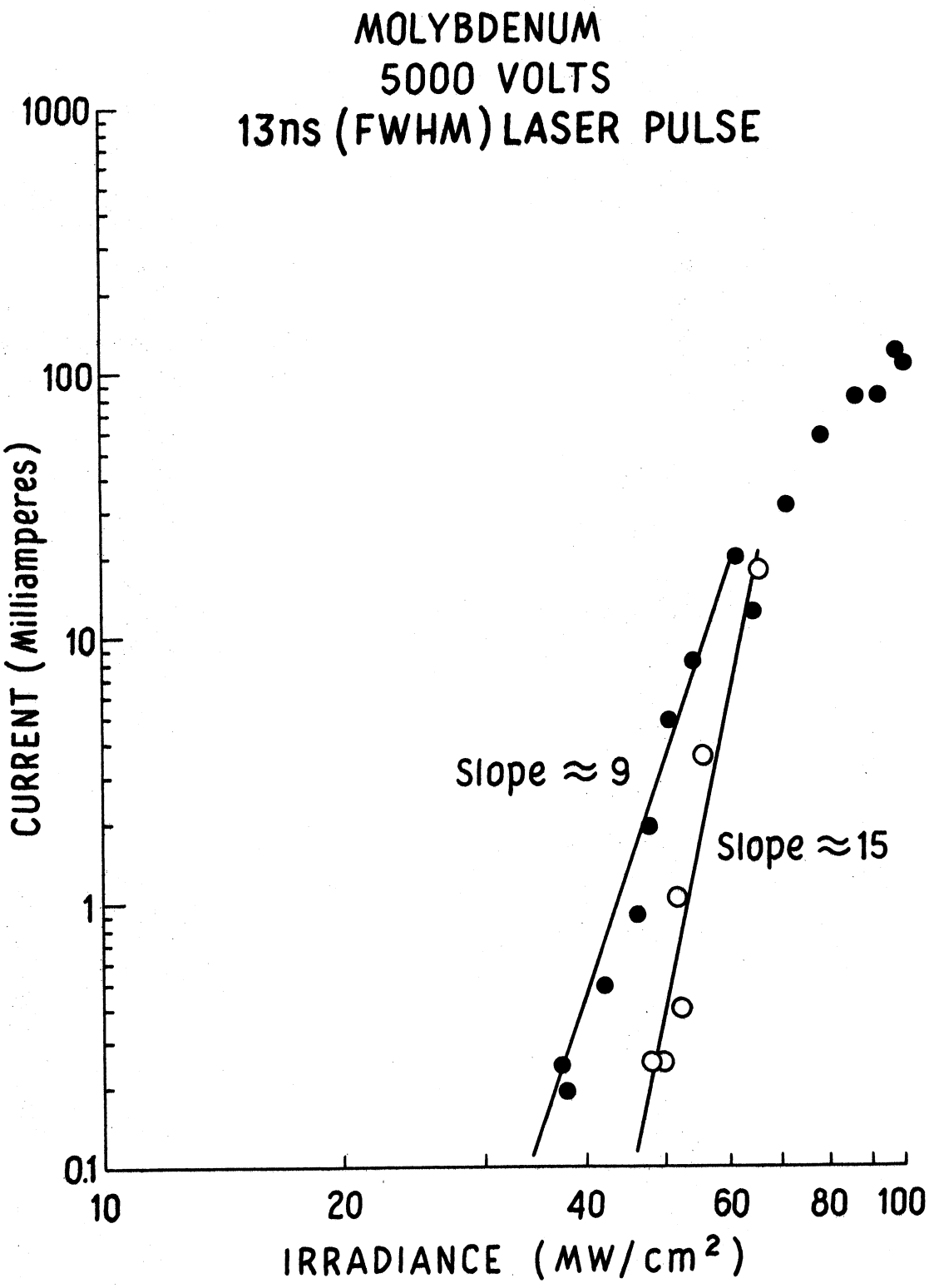

Figure 24. Maximum Laser Induced Current Versus Maximum Incident Irradiance.

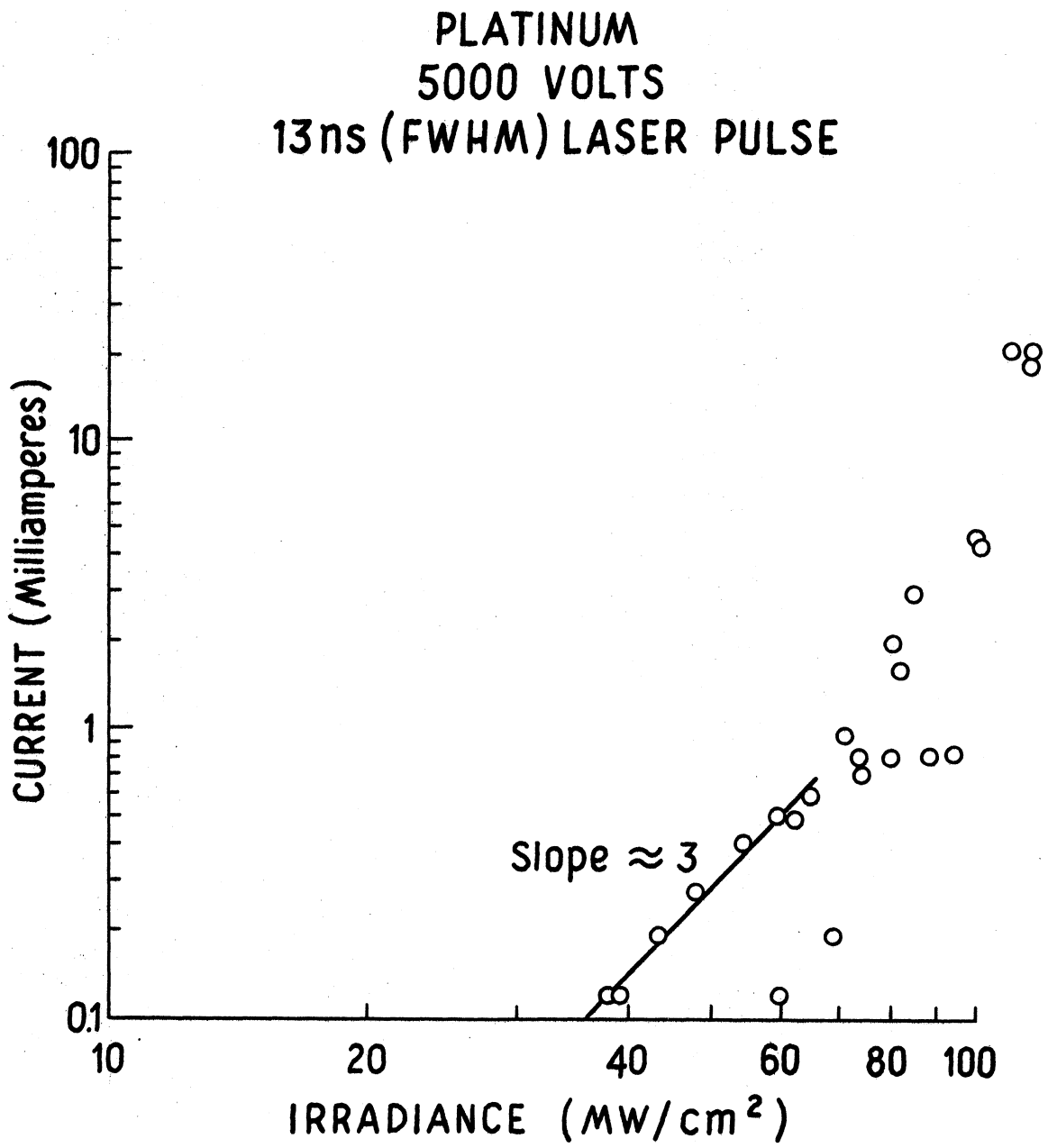

Figure 25. Maximum Laser Induced Current Versus Maximum Incident Irradiance.

mately 0.5 cm, and the pressure in the vacuum diode was 1×10^{-7} torr. Although this pressure was somewhat higher than in the other electron tubes, we employed the same bake-out proceedure used for the other tubes. We do not feel that this pressure, which represents about 10^{10} molecules per cubic centimeter, significantly altered our results. Again the data was taken using the Hughes laser, and the cathode-anode voltage difference was maintained at 5000 volts.

The results of the experiments on platinum and molybdenum exhibit a very nonlinear current-irradiance dependence. The data for platinum indicates a substantially higher threshold irradiance necessary for observable electron emission and a somewhat less steep slope compared to tungsten. Figure 25 presents data for molybdenum and shows two distinct slopes. That portion of the data labeled "slope approximately equal to 9" was for increasing laser power, whereas that portion labeled "slope approximately equal to 15" was for decreasing laser power. This hystresis like effect was not observed in the tungsten data.

In addition to measuring the current versus irradiance, we have looked for a voltage dependence of the electron emission from tungsten at nearly constant laser power per unit area. Data is given in Figures 26 and 27 for the maximum current versus the cathode-anode voltage difference. This data was taken using the University of Michigan laser, the pulse duration of which is about 20 nanoseconds. This

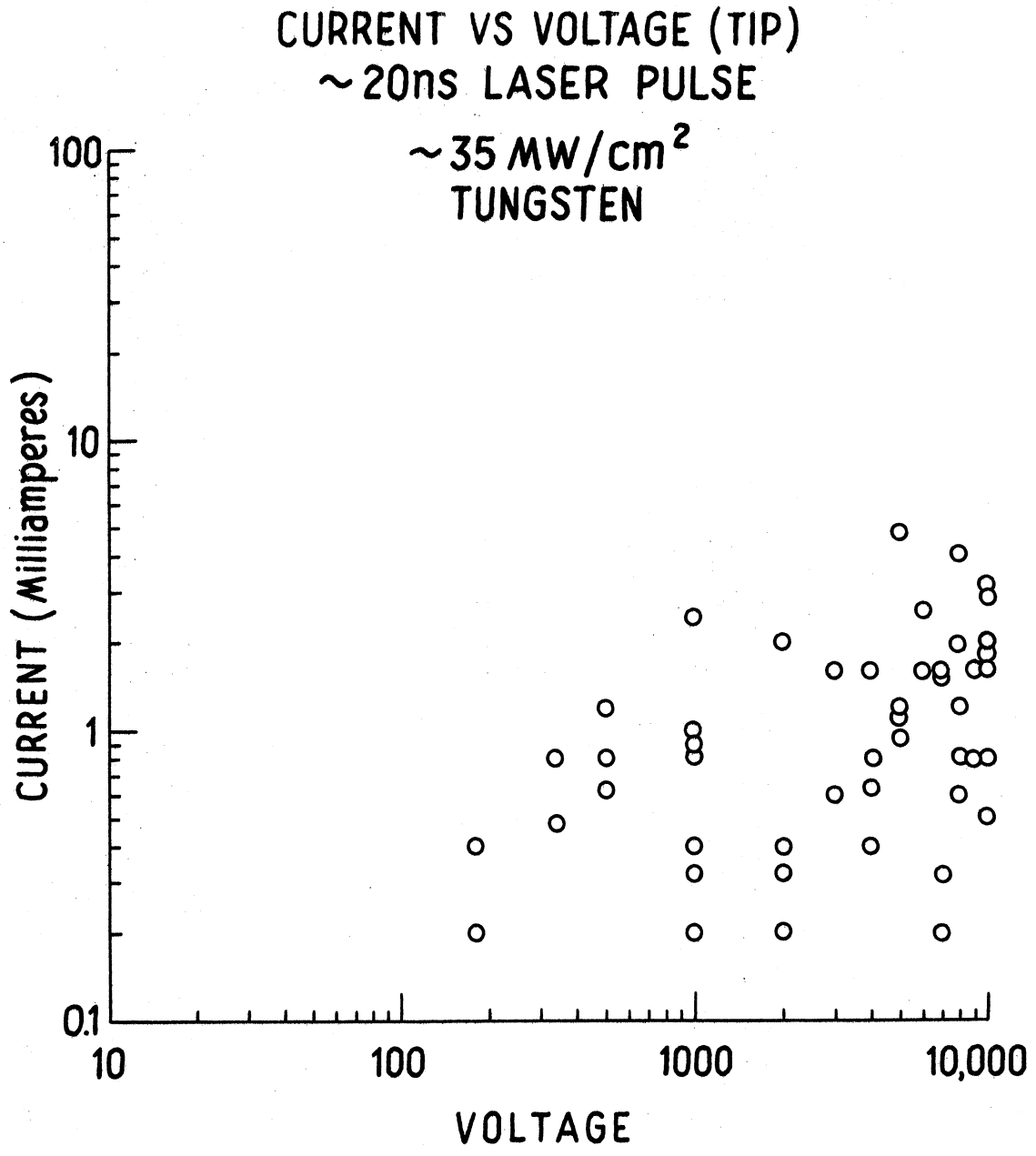

Figure 26. Maximum Laser Induced Current Plotted Against Cathode-Anode Voltage Difference.

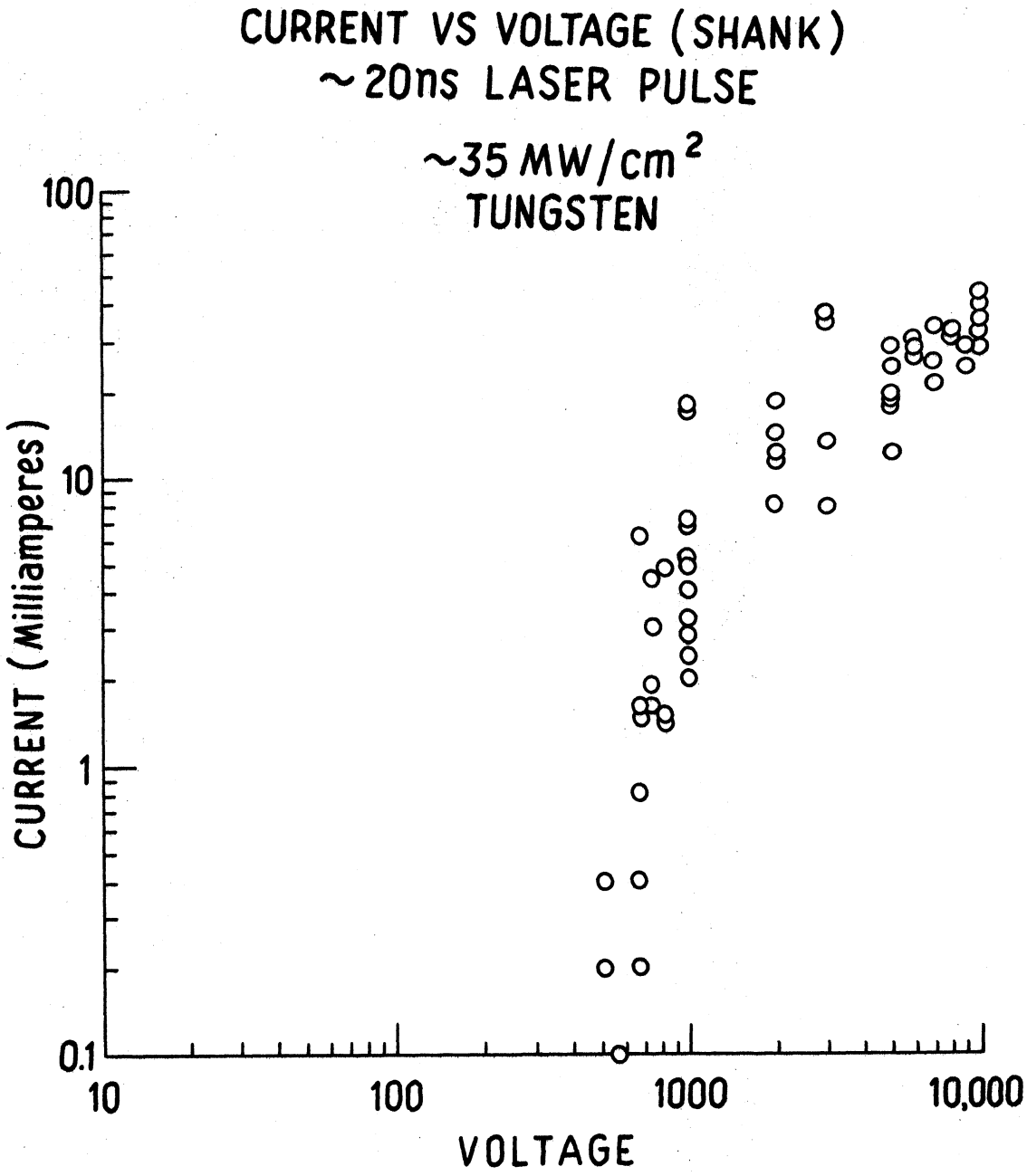

Figure 27. Maximum Laser Induced Current Plotted Against Cathode-Anode Voltage Difference.

laser operates in nearly a single transverse mode, but it oscillates in several longitudinal modes. The average peak irradiance for the data given in Figures 26 and 27 is approximately 35 MW/cm^2. The effective area, πd^2, of this laser was measured to be 1.25×10^{-2} cm^2. Figure 26 presents data for the laser beam centered on the field emission point, and Figure 27 shows the corresponding data for the laser beam centered on the shank of the tungsten rod several millimeters above the point. A comparison of these two figures reveals that the threshold voltage for detectable electron current is less for the laser irradiating the field emission point cathode compared to the shank of the cathode. At voltages greater than 1000 volts, however, the total emitted current is larger for the irradiated shank than for the tip because the shank intercepts a larger portion of the laser beam. In addition, Figures 26 and 27 demonstrate that the field emission point is not per se requisite for the emission process.

Figure 28 is a picture of the current pulse obtained by using the University of Michigan laser. The combination of two longitudinal modes produces the 200 megahertz modulation in the current, and the degree of this modulation varied from shot to shot. In fact the primary motivation for doing some of the experiments at the Hughes Research Laboratories was to eliminate this complexity.

In Chapter III we have observed that the peak temperature produced by a temporally Gaussian laser pulse is time

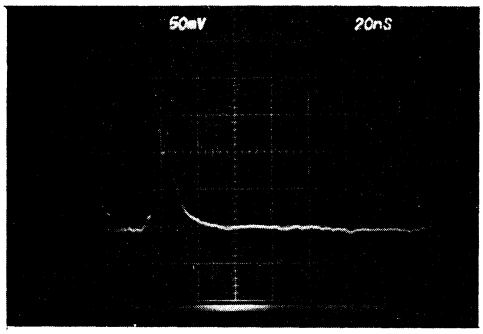

Figure 28. Modulated Current Pulse Produced by Longitudinal Mode Beating.

delayed with respect to the maximum incident irradiance; consequently, any electron emission associated with the laser produced temperature change should be delayed with respect to the incident irradiance. In contrast, a pure multiple-photon photoelectric effect should exhibit no time delay. Using the field emission cathode we have looked for a shift in time of the maximum current with respect to the maximum incident irradiance. We have observed that the peak electron current is delayed with respect to the peak irradiance by approximately 5 nanoseconds.

The experiments described hitherto were performed in the sequence that they have been presented. We hasten to observe that the time delay experiment strongly suggests that the electron emission is a thermal effect; however, the experiments reported in Figures 21, 22, and 23 strongly suggest that the emission process is not thermionic emission. The slope of the log-log plot of current versus laser irradiance is simply not steep enough by approximately a factor of three.

Since the previously described data portends a new type of electron emission, we have performed other experiments of a somewhat different character to form an independent test of the emission process. These experiments consisted in observing the emitted current for a changing initial surface temperature at constant laser power.

In order to change the initial surface temperature of

the cathode we electrically heated a tungsten ribbon by passing an a.c. current through it. The filament power supply was a small Variac that was connected to a filament transformer which provided 10,000 volts isolation. The temperature of the ribbon was monitored by a Leeds and Northrup Model 8632-C optical pyrometer. The maximum laser induced current is plotted against the initial surface temperature of the ribbons in Figures 29 and 30.

Because of the unusual results on the tungsten rod material, we studied laser induced electron emission from both a KOH etched tungsten ribbon and an unetched ribbon. We have found no salient difference between the emission characteristics of either ribbon, and the results are plotted in Figures 29 and 30. The data in Figure 29 is for a 0.003 inch thick unetched ribbon. The data in Figure 30 is for a geometrically similar but etched ribbon. Both ribbons were 0.04 inches wide and 0.003 inches thick. The cathode-anode voltage difference was maintained at 5000 volts in both ribbon experiments. The average peak irradiance of the incident light was approximately 35 MW/cm^2. The initial pressure in each vacuum tube was $1x10^{-9}$ torr, but this pressure increased to $5x10^{-8}$ torr for a ribbon temperature of 2000 K. All data on the ribbon cathodes was acquired using the University of Michigan laser, and the laser beam was directed at normal incidence onto the ribbon.

Figure 31 shows data obtained from the etched tungsten

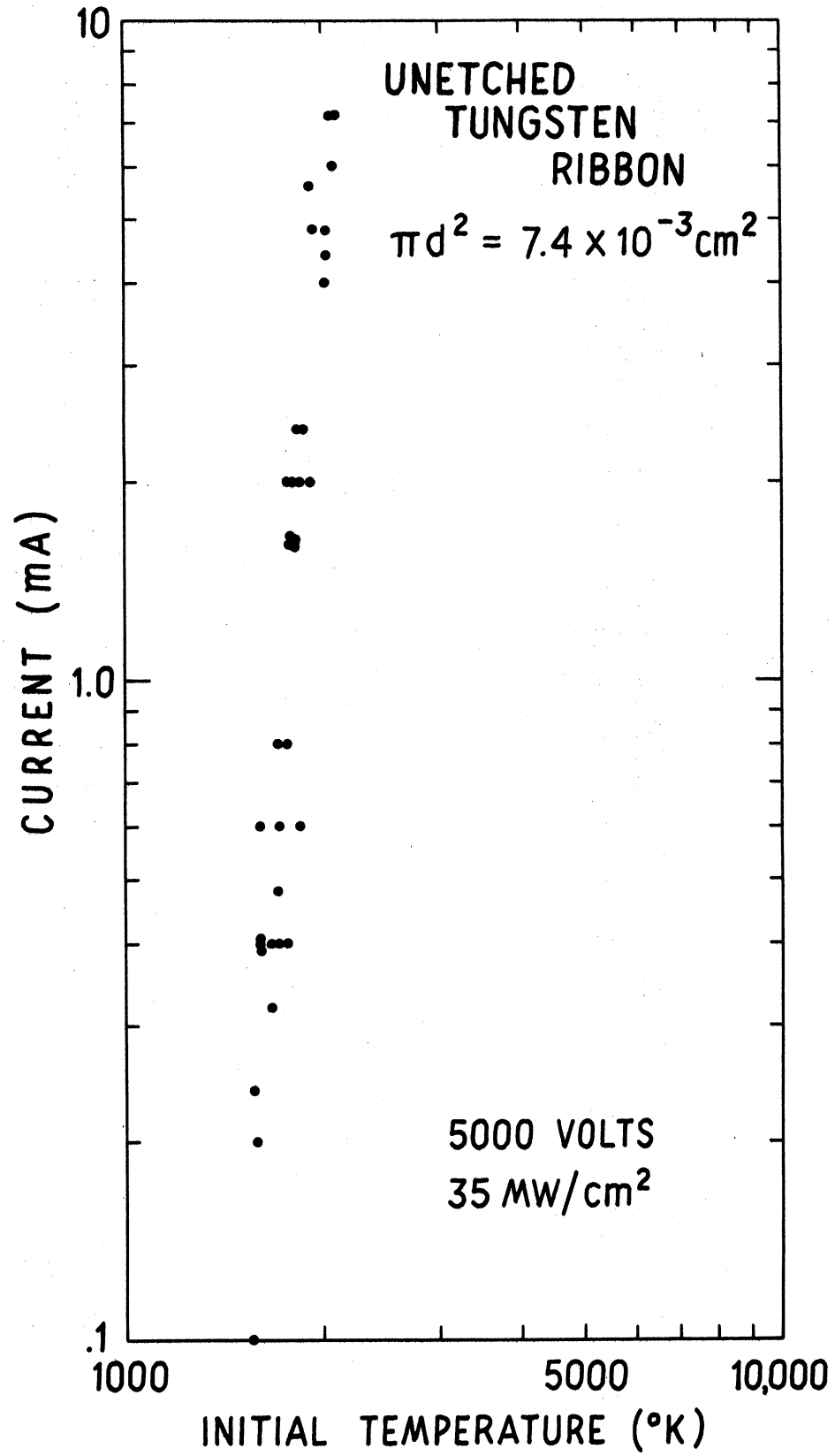

Figure 29. Maximum Laser Induced Current Plotted Against Initial Temperature of Cathode.

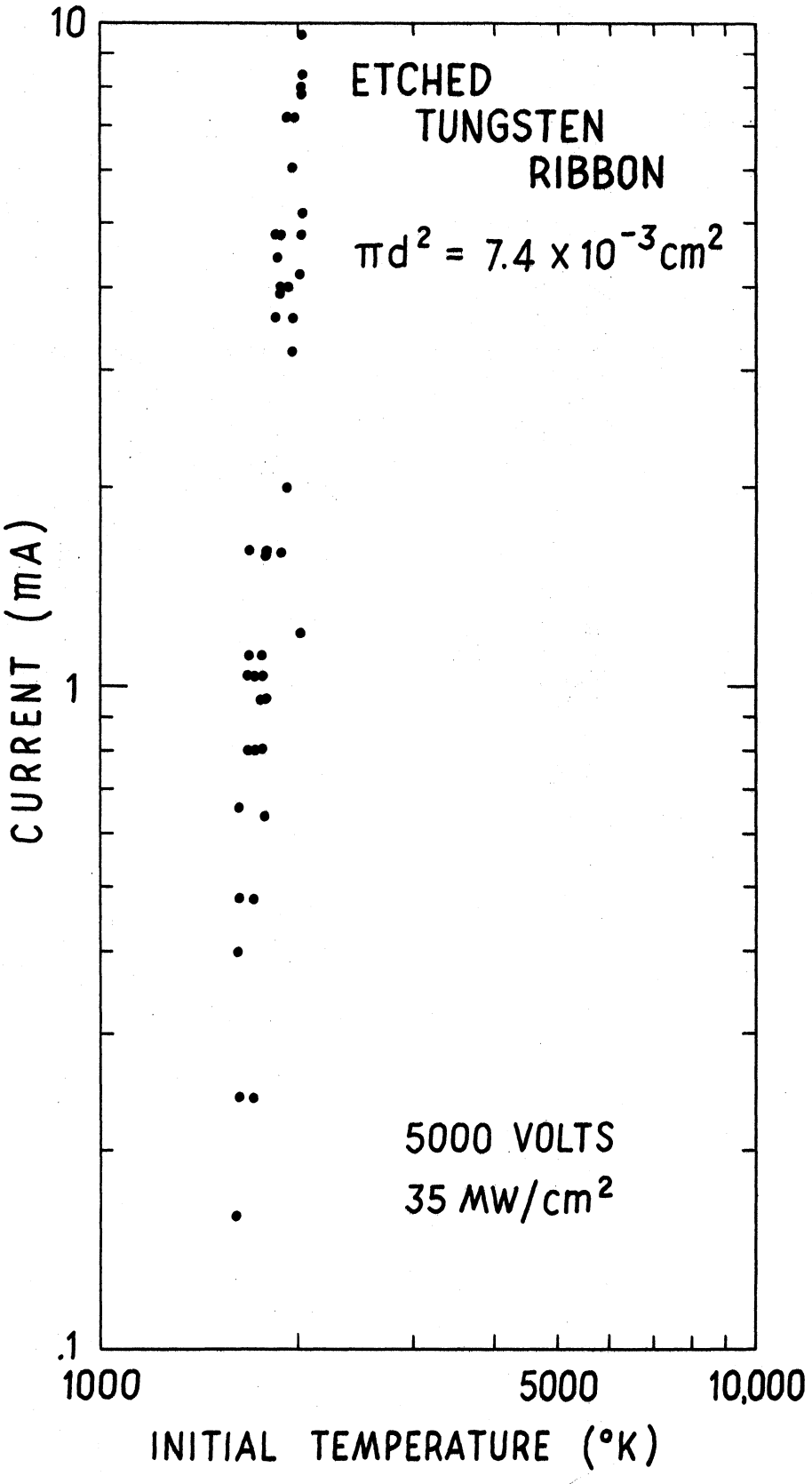

Figure 30. Maximum Laser Induced Current Plotted Against Initial Temperature of Cathode.

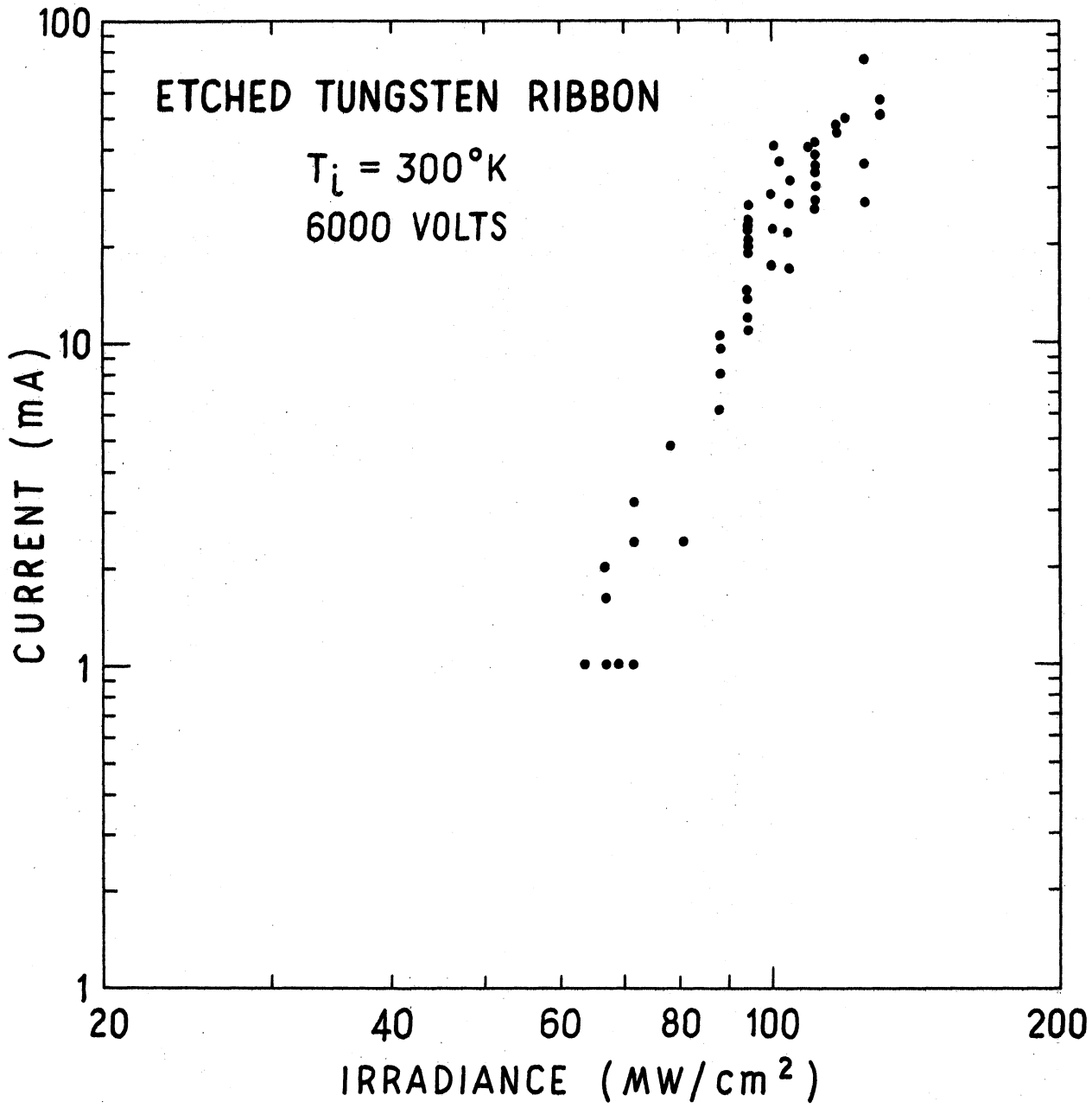

Figure 31. Maximum Laser Induced Current Versus Maximum Incident Irradiance.

ribbon with an initial temperature of 300 K. In order to obtain a detectable electron emission it was necessary to partially focus the laser beam such that at the surface of the ribbon the effective area of the laser, πd^2, was 1.7×10^{-3} cm^2. The threshold current of 1 mA corresponds to a current per effective laser area of about 0.6 A/cm^2. Both the current pulse and the monitor photodiode output were displayed on the same CRO trace, and an example of this trace is given in Figure 32. The initial pulse is the current pulse from the tungsten ribbon, and the second pulse is the output of the FW-114A photodiode. The second pulse was delayed by passing the signal through a low loss coaxial cable, and the difference in the polarity of the two pulses was due to a convenience in the biasing of the diodes with respect to ground. The irradiance impinging on the tungsten ribbon was changed by changing the concentration of a solution of $CuSO_4$ dissolved in distilled water.

We note that the graph in Figure 31 is the same type of plot as that given in Figures 21, 22, and 23; moreover, the slope of the graph in Figure 31 is nearly the same as the slopes in Figures 21, 22, and 23. However, it is by no means obvious that the emission process is the same for these different graphs. The effective laser area, πd^2, for the data in Figure 31 is more than a factor of 25 less than the effective laser area for the data in Figures 21, 22, and 23. Thus, any space charge effects will be more severe for the data in Figure 31 than for the data in the

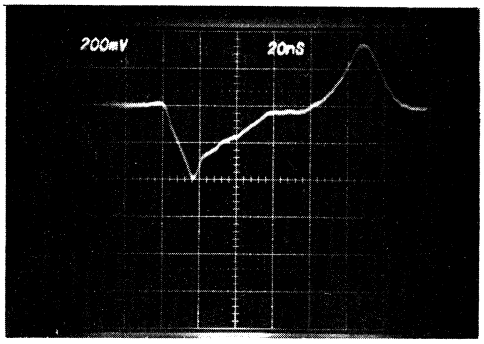

Figure 32. Photograph of Current Pulse and Photodiode Monitor Pulse. The first signal is from the tungsten ribbon, and the second signal is from the FW-114A photodiode. The initial temperature of the ribbon is 300 K, and the peak irradiance of the incident 20 nanosecond laser pulse is approximately 105 MW/cm^2.

other aforementioned graphs. In addition, we observe that the current pulse in Figure 32 has different rise and fall times and that the full-width-at-half-maximum is approximately the same as the laser pulse. This strongly suggests that the emission process for this particular set of data points is accompanied by some type of plasma effect that lengthens the current pulse and neutralizes space charge fields near the cathode.

In Figure 33 data is presented for the etched tungsten ribbon at initial temperatures of 1515 K and 1850 K. The current per effective laser area is plotted against incident irradiance, and the cathode-anode voltage difference is 6000 volts. From this graph we observe that the incident irradiance necessary for a current density of a few tens of amperes per square centimeter is approximately 10-20 MW/cm^2 higher for the initial temperature of 1515 K compared to an initial temperature of 1850 K.

A comparison of the data from the tungsten rod cathodes and from the tungsten ribbon cathodes reveals that the threshold irradiance for minimum detectable current from both ribbon cathodes was nearly a factor of 3 higher than the threshold irradiance for the tungsten rod cathode material. In order to determine if there was an appreciable difference in the chemical compositions of the ribbon and rod materials, both were analyzed with an electron microprobe. Both materials were found to be tungsten with the ribbon material having a small amount of selenium present

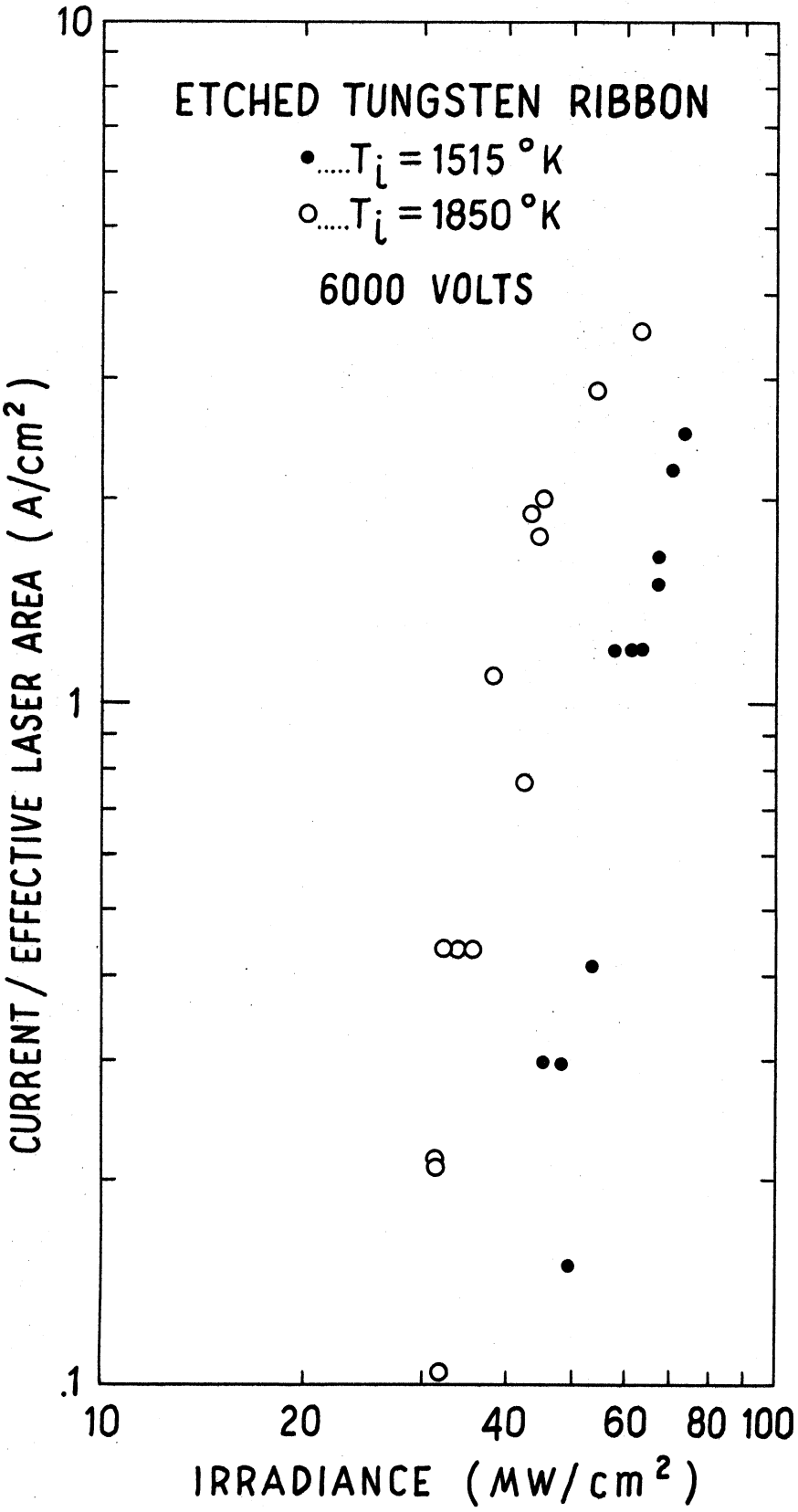

Figure 33. Maximum Current per Effective Laser Area Plotted Against Maximum Incident Irradiance.

(about 1%). The electron microprobe used was a part of the facilities of the University of Michigan, Department of Materials and Metallurgical Engineering. We note, however, that the electron microprobe used in the above analysis was not sensitive to elements with atomic number less than eleven. Therefore, oxides or carbides of tungsten would not have been observed. Finally, we do not feel that the small amount of selenium detected influenced the experiment.

CHAPTER V

DISCUSSION AND SUMMARY

Several years ago we began an experiment to look for laser modulated electron currents from a tungsten field emission cathode. We used a Q-switched ruby laser to irradiate a field emission tip in order to provide a modulation to the emitted current. We have not yet observed effects associated with this modulation (a detailed summary of this experiment is given in Appendix I); however, we did observe copious electron emission from the laser irradiated metal. Because of the difficulties encountered in the original experiment, we decided to investigate the electron emission phenomena rather than pursue our original objective.

Our initial observations were that the electron emission from the tungsten cathode was a very nonlinear function of the incident irradiance and that there was a time delay of nearly 5 nanoseconds between the maximum incident irradiance and the maximum emitted current. This time delay is consistent with the calculated temperature change and thus suggests that the electron emission is a thermal effect.

Our initial experiments were performed with a single transverse mode laser at the University of Michigan; however, this laser oscillated in several longitudinal modes, and we

quickly observed that the mode beating in the output of this laser made a detailed study of the emission process nearly impossible. Fortunately, we were able to use a single longitudinal and single transverse mode ruby laser at the Hughes Research Laboratories. We found that if we plotted the maximum current versus the maximum laser irradiance on a log-log scale then the slope of the resulting data points was nearly a straight line with a slope of approximately 6-8. If the emission were thermionic, then we would expect the slope of this log-log plot to be nearly 20. Moreover, for the 13 nanosecond laser pulse with a maximum irradiance of 40 MW/cm^2 the calculated maximum surface temperature was only 1400 K. We observed a current of more than 1 mA at this irradiance, and the temporal shape of the emitted current pulse was more narrow than the incident laser pulse. Again we measured a 5 nanosecond time delay.

Although the time delay is consistent with thermionic emission, the calculated temperature of the surface is less than the temperature needed to achieve the observed current. In addition, as we have previously noted, the slope of the log-log plot of maximum current versus maximum incident irradiance is substantially less than the slope one would expect for a purely thermionic process with laser heating of the surface as we have described in Chapter III. We could obtain the slope of 6-8 for the log-log plot of maximum current versus maximum irradiance for a thermionic emission effect but only at the expense of assuming a sublinear relation

between incident irradiance and the laser induced temperature change. This assumption, however, would make the surface temperature even less than the value cited in the previous paragraph.

To explain the results of our data we have considered the possibility that these phenomena are due to a two-photon assisted thermionic emission effect. For this effect the laser acts not only as a photon source but also as a heat source. The electron emission originates by a two-photon photoemission from the electrons in the Fermi tail of the electron distribution within the metal. Since the number of electrons in the tail is a sensitive function of the temperature, we expect a time delay for this emission process. Moreover, we find that the slope predicted by this model is consistent with our data.

To provide an additional test of this hypothesis we have performed other experiments on tungsten ribbons, the initial temperature of which could be varied by changing the a.c. current flowing through them. Since the field emission cathode had been prepared by a chemical etching, both etched and unetched ribbons were studied. For both types of ribbons with initial temperatures from 1500-2000 K and an incident maximum irradiance of 35 MW/cm^2 for a 20 nanosecond laser pulse we find that the slope of a log-log plot of maximum current versus initial temperature is between 10 and 14. The results of this experiment are, therefore, consistent with thermionic emission, the theoretically predicted value

of the slope being 12. The theoretically predicted value of this slope for a two-photon assisted thermionic emission process is 3-4, substantially less than the experimental results.

The central result of this experiment is that the tungsten ribbons give laser induced electron emission that is best explained as thermionic emission whereas the tungsten rod material used in the field emission cathode gives results that are best explained as two-photon assisted thermionic emission. We can estimate the two-photon parameter α_2, as given in equation 3.50, by using the data in Figure 21 to obtain $\alpha_2=4\text{x}10^{-47}$ m^4-sec^2/coul. Moreover, we can use the data in Figure 33 to obtain an upper bound on α_2, assuming that the data in Figure 33 corresponds to thermionic emission. Using $T_i=1500$ K, $I=50$ MW/cm^2, and $i/\pi d^2=0.3$ A/cm^2, we find that α_2 is less than $2\text{x}10^{-49}$ m^4-sec^2/coul. This is a factor of 200 less than the corresponding result for the rod material. Our conclusion is, therefore, that for as yet unexplained reasons the value of the two-photon parameter α_2 is some 200 times greater for the rod material than it is for the ribbon material.

Finally, our results for platinum indicate that near our threshold detectable current the slope of the log-log plot of maximum current versus maximum incident irradiance is approximately 3. This slope is consistent with a three-photon photoemission process. Since the energy of three ruby laser photons exceeds the work function of platinum,

we expect the thermal assist mechanism to play a less dramatic role in the emission process. Moreover, the observed time delay from the platinum rod was several nanoseconds less than from either the tungsten or the molybdenum samples.

APPENDIX I

THE ORIGINAL EXPERIMENT

In the autumn of 1970 I became interested in the possibility of modulating electron beams at frequencies in or near the optical region of the spectrum. My initial interest was stimulated by the announcement by Schwarz and Hora[16] that they had observed an effect associated with an electron beam modulated at the frequency of an argon ion laser. My intent was to look for optical modulation of thermionic emission; i.e. the laser electric field normal to a thermionic cathode should produce a change in the apparent work function of the cathode (Schottky effect). It was not clear to me that the frequency response of thermionic emission would be sufficiently great to observe this effect; however, it was suggested to me by Peter Franken that looking for optical modulation of high field emission might prove to be a more interesting and feasible experiment. Let us examine in detail, now, the effects that might be expected.

The method that we hoped to use to generate an optically modulated electron beam was to let the laser electric field modulate the potential energy barrier thickness of a field emission diode. If the static electric field near the cathode is of the order of 10^7-10^8 volts/cm, a field emission current should be observed. For laser

irradiances of 10 MW/cm^2 the laser electric field is approximately 10^5 volts/cm, nearly a thousand times less than the static electric field. The field emission current is, however, a nonlinear function of the applied electric field; therefore, a fractional modulation of the current can be significantly larger than the ratio of the laser field to the static field. Moreover, the nonlinearity of the Fowler-Nordheim equation with respect to the electric field means that the current will contain not only frequency components at the laser frequency but also frequency components at integral multiples of the laser frequency. When these high frequency components of electron current strike the anode one expects to observe radiation at these frequencies. It would be well-nigh impossible to observe this reradiation at the fundamental frequency because of the laser background. Nevertheless, it should be possible to detect the harmonic components by using suitable filters and sensitive detectors. Finally, we observe that the tunnelling time for the field emission process is extremely rapid; it is typically 10^{-16} seconds[17] for sufficiently large static electric fields. Thus we can expect to modulate the electron beam up to frequencies approaching 10^{16} hertz.

Having discussed qualitatively what we would expect from this type of experiment, we can now derive some quantitative results.

The current density of a field emission cathode is given by the usual Fowler-Nordheim equation

$$J \approx \frac{AF^2}{\varphi} \exp\left[\frac{-B\,\varphi^{3/2}}{F}\right] \qquad \text{AI.1}$$

where J is the current density, φ is the work function, A and B are constants, and F is the total electric field at the surface of the cathode. We let F be given by

$$\begin{aligned} F &= F_o + F_1 \cos \omega t \;\; = F_o \,(\, 1 + \alpha x \,) \\ x &= \cos \omega t \\ \alpha &= F_1/F_o \ll 1 \end{aligned} \qquad \text{AI.2}$$

F_o is the static electric field and F_1 is the electric field produced by the laser. In the above approximation we are neglecting the Nordheim elliptic functions in equation AI.1; this is equivalent to neglecting the image charge effect.

If we now expand the current density J in a Taylor series about $\alpha=0$, we find

$$J = J(\alpha=0) + \left.\frac{dJ}{d\alpha}\right|_{\alpha=0} \alpha \;+\; \frac{1}{2!} \left.\frac{d^2J}{d\alpha^2}\right|_{\alpha=0} \alpha^2 \;+\; \cdots \qquad \text{AI.3}$$

where we have kept terms only up to α^2. From this expression and straightforward differentiation we find

$$J \approx \frac{A F_o^2}{\varphi} \exp\left[\frac{-B \varphi^{3/2}}{F_o}\right]\left[1 + \left(2 + \frac{2 B \varphi^{3/2}}{F_o} + \frac{B^2 \varphi^3}{F_o^2}\right)\frac{F_1^2}{4F_o^2} + \left(\frac{F_1}{F_o}\left(2 + \frac{B \varphi^{3/2}}{F_o}\right)\right) \cos \omega t + \left(\left(2 + \frac{2 B \varphi^{3/2}}{F_o} + \frac{B^2 \varphi^3}{F_o^2}\right)\frac{F_1^2}{4F_o^2}\right) \cos 2\omega t + \ldots\right]$$

AI.4

To ascertain the magnitude of the quantities involved in this expression let us assume the following values:

$F_1 = 10^5$ volts/cm $F_1/F_o = 2.5 \times 10^{-3}$

$F_o = 4 \times 10^7$ volts/cm $B \varphi^{3/2}/F_o = 16$

$\varphi = 4.5$ eV

From this we find

$$J \approx J_o \left(1.0005 + .05 \cos \omega t + .0005 \cos 2\omega t + \ldots\right)$$

AI.5

This expression shows that the expected modulation of the beam is a few percent at the laser frequency and a few hundreths of a percent at the second harmonic (twice the laser frequency).

If we now consider a modulated electron beam of the form $i_o (1 + \alpha \cos \omega t)$, where i_o is the d.c. current,

we expect the power radiated at the angular frequency ω to be given by

$$\frac{dP}{d\Omega} \approx \frac{i_o^2 \alpha^2 \beta^2}{2\pi c} \quad \frac{\sin^2 \theta}{(1 - \beta^2 \cos^2 \theta)^2} \qquad \text{AI.6}$$

and

$$P = \int \frac{dP}{d\Omega} d\Omega \approx \frac{i_o^2 \alpha^2 \beta^2}{c} \left[\frac{\beta^2+1}{4\beta^3} \ln \frac{1+\beta}{1-\beta} - \frac{1}{2\beta^2} \right] \qquad \text{AI.7}$$

If $\beta << 1$, we can use $\ln \frac{1+x}{1-x} \approx 2x + \frac{2}{3}x^3$ to find

$$P \approx \frac{2 i_o^2 \alpha^2 \beta^2}{3 c} \qquad \text{AI.8}$$

The efficiency in the nonrelativistic limit is thus

$$\eta \approx \frac{4}{3} \frac{e}{mc^3} \alpha^2 i_o \qquad \text{AI.9}$$

The corresponding nonrelativistic expressions for radiative power and efficiency in MKS units are

$$P \approx \frac{i_o^2 \alpha^2 \beta^2}{6\pi} \sqrt{\frac{\mu_o}{\epsilon_o}} \approx 20\, i_o^2 \alpha^2 \beta^2 \qquad \text{AI.10}$$

$$\eta \approx \frac{1}{3\pi} \frac{e}{mc^2} \alpha^2 i_o \sqrt{\frac{\mu_o}{\epsilon_o}} \approx 8 \times 10^{-5} \alpha^2 i_o \qquad \text{AI.11}$$

If we now assume that $\beta = .1$, which corresponds to an electron with an energy of about 2500 electron volts, and assume that $i_o \approx 10^{-5}$ ampere, we find from equation AI.10 that the expected radiative power is about 5×10^{-18} watts with the assumption that $\alpha = 5 \times 10^{-4}$. If this emission occurs for a time of 10^{-8} seconds (the duration of the Q-switched laser pulse) and the frequency is twice the ruby laser frequency, then this corresponds to much less than one photon per pulse. We note that if substantially larger currents can be achieved, say one ampere, then the total power radiated would be nearly 10 orders of magnitude larger than that given above.

In the spring of 1971 experiments were performed by Peter Franken, William Hall, and Gary Cochran in an attempt to observe a reradiation of the electron beam at twice the ruby laser frequency. Their experiments were not conclusive; however, they did observe substantial electron emission from the field emission cathode when the laser radiation impinged on it. This electron pulse was much more narrow than the laser pulse, and the emitted current was a very nonlinear function of the laser power per unit area. These features are both consistent with an optical field emission process. At that time we could only speculate that somehow the laser field was being spectacularly enhanced at the surface. I should paren-

thetically note that the small signal analysis of optical field emission as given above would not be valid. In this case the parameter α would not be small. Unfortunately, we were not able to find any plausible mechanism for a large enhancement of the laser field. In June of 1971 I arrived in Ann Arbor and started to work on the experiments that were then in progress. We finally decided to study the origin of the electron current pulses in an attempt to understand the observed phenomena. I was able to show that the current pulses were not optical field emission because there was a time delay of a few nanoseconds between the peak of the laser pulse and the maximum in the current. Moreover, the current was not originating at the tip but rather was coming from any portion of the metal that was irradiated by the laser. In addition, I repeated the second harmonic experiment and could find no change in the number of collected second harmonic photons as I changed the d.c. current in the field emission diode. The largest d.c. currents that we were able to achieve were a few tens of microamperes. For this current and with no laser field enhancement, then as we have previously calculated, the total power at angular frequency 2ω is approximately 10^{-18} watts. This power is certainly consistent with our observation that no change in second harmonic signal was detected as a result of changing the d.c. field emission current.

APPENDIX II

REVIEW OF FIELD EMISSION

In this appendix we review the basic theory of field emission of electrons from a metal surface. This process was discovered by R.W. Wood[18] in 1897, but it wasn't until after the advent of quantum mechanics by Schrodinger and Heisenberg that a generally accepted theory was formulated. The theoretical explanation is attributed to two papers, one a collaboration by Fowler and Nordheim[19] and the other by Nordheim[20] alone. The Fowler-Nordheim model treats field emission as the penetration of the electrons through the one-dimensional energy barrier at the surface of the metal. The height and the width of this barrier are determined by the work function and the applied electric field. This model was modified by Nordheim by including the effects of the image charge on the emitted electron. The outline presented here follows the more comprehensive review by Good and Muller[21], although more recent results are also included.

The important assumptions of the Fowler-Nordheim treatment of field emission may be characterized as follows:

1) The electrons within the metal are considered as a free electron gas that obeys Fermi-Dirac statistics. Within the metal each electron is assumed to

have a constant average potential energy $-W_a$. The magnitude of W_a is given by

$$W_a = \varphi + \epsilon_f$$

where φ is the work function and ϵ_f is the Fermi energy.

2) The transmission coefficient of the energy barrier as a function of the electron energy is determined either by a direct solution of the Schrodinger equation or by a WKB approximation.

3) The current density is calculated by integrating over all possible energies the product of the transmission coefficient and the electron flux on the surface energy barrier. The total emission current density is thus given by

$$J = e \int N(W,T)\, D(W,F)\, dW \qquad \text{AII.1}$$

with $N(W,T)$ the number of electrons per unit area per unit time striking the surface, and $D(W,F)$ the transmission coefficient of the energy barrier. The electric field at the surface is denoted by the variable F, the temperature of the metal is denoted by T, and W is defined such that

$$W = E - \frac{p_x^2}{2m} - \frac{p_y^2}{2m}$$

where E is the total energy of the electron and the momentum p_x and p_y are in the plane of the emitting surface.

4) The explicit solution for the current density is predicated on several other assumptions. These assumptions are that the surface is mathematically flat, that the classical expression for the image charge potential energy is valid for any distance from the surface, and that the temperature is 0 K.

The final result for the current density is found to be

$$J = \frac{e^3 F^2}{8\pi h\varphi t^2(\frac{(e^3F)^{1/2}}{\varphi})} \exp(-\frac{4(2m)^{1/2}\varphi^{3/2}}{3ehF} v(\frac{(e^3F)^{1/2}}{\varphi})) \qquad \text{AII.2}$$

$$= \frac{1.5\text{x}10^{-6} F^2}{\varphi t^2(3.79\text{x}10^{-4}\frac{F^{1/2}}{\varphi})} \exp(-6.83\text{x}10^7 \frac{\varphi^{3/2}}{F} v(3.79\text{x}10^{-4}\frac{F^{1/2}}{\varphi}))$$

where F is in volts/cm and φ is in electron volts. This equation is called the Fowler-Nordheim equation, and the elliptic functions t(y), v(y), and s(y) are plotted in Figure 34.

The variables that appear in the Fowler-Nordheim equation are the current density J and the electric field at the cathode F; however, the experimentally determined quantities are the total current i and the cathode-anode voltage difference V. To convert the Fowler-Nordheim

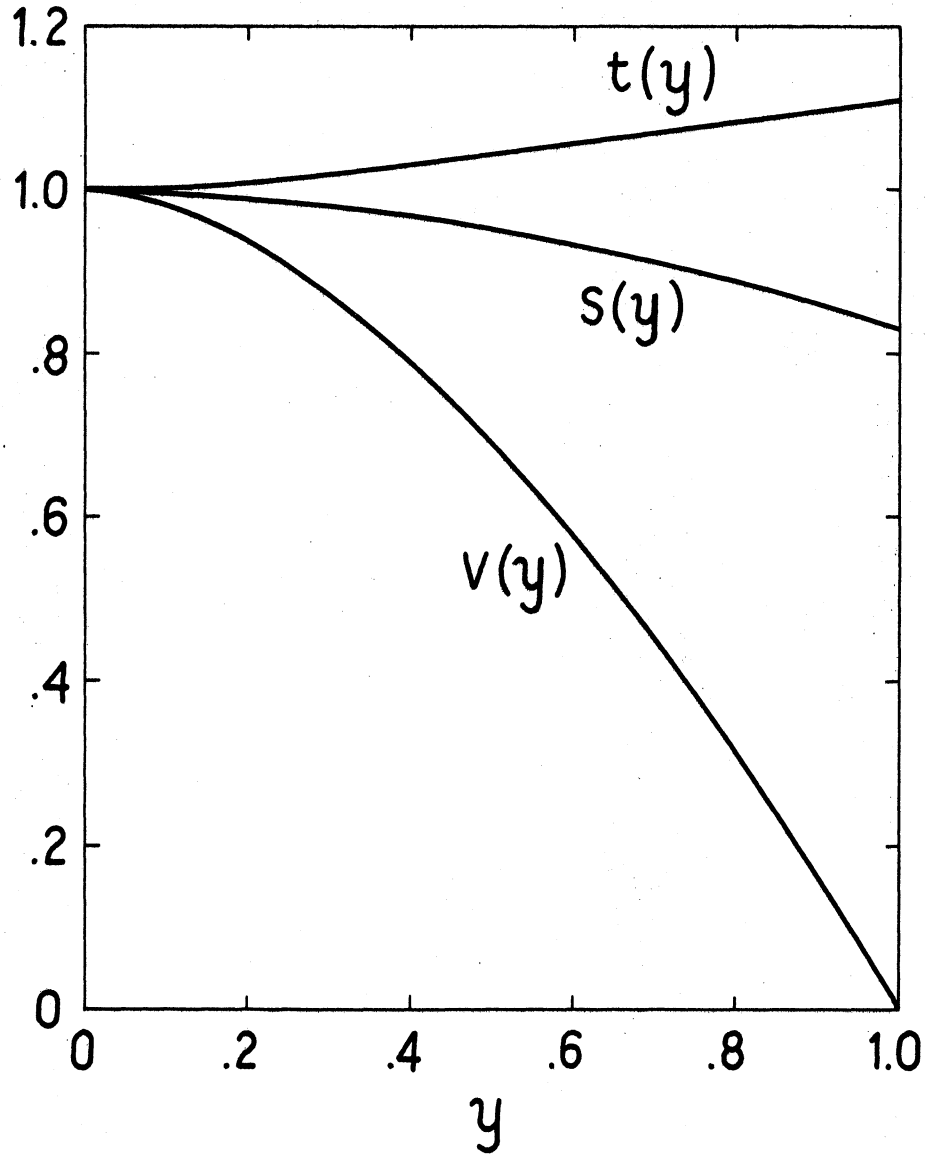

Figure 34. Elliptic Functions for Fowler-Nordheim Theory (compare Reference 21).

equation into an equation expressed in terms of the experimental variables we introduce the effective emitting area S and the inverse length β that relates the field to the voltage.

$$F = \beta V \qquad \text{AII.3}$$

Inserting this into the Fowler-Nordheim equation we find

$$\ln \frac{i}{V^2} = \ln \frac{SA\beta^2}{\varphi} - \frac{B\varphi^{3/2}}{\beta V} v(y) \qquad \text{AII.4}$$

where A, B, and y are given by

$$A = \frac{e^3}{8\pi h t^2(y)} = \frac{1.54 \times 10^{-6}}{t^2(3.79 \times 10^{-4} \frac{\sqrt{F}}{\varphi})} \qquad \text{AII.5}$$

$$B = \frac{4\sqrt{2m}}{3\hbar e} = 6.83 \times 10^7 \qquad \text{AII.6}$$

$$y = \frac{(e^3 F)^{1/2}}{\varphi} = 3.79 \times 10^{-4} \frac{\sqrt{F}}{\varphi} \qquad \text{AII.7}$$

The numerical values are appropriate for F(volts/cm), $S(cm^2)$, φ(eV), β (cm^{-1}), and i(amperes).

If we now plot $\log_{10} i/V^2$ versus 1/V (a Fowler-Nordheim plot) then the magnitude of the slope of this line is given by

$$m_{FN} = \frac{B\varphi^{3/2}}{2.3\beta}\, s(y) = 2.97\times10^{7}\,\frac{\varphi^{3/2}}{\beta}\, s(y) \qquad \text{AII.8}$$

with

$$s(y) = v(y) - \frac{y}{2}\frac{dv(y)}{dy}$$

and as we see in Figure 34 , s(y) is nearly unity. The slow decrease in the slope with increase in the field is a consequence of the image charge interaction. If we neglect the image force, then s(y) would be unity. This predicted change in the slope of the Fowler-Nordheim plot is, however, small and it is doubtful that it can be observed under realistic experimental conditions. In addition, space-charge effects, which are neglected in the Fowler-Nordheim theory, tend to decrease the slope of the Fowler-Nordheim plot at high current densities.

An interesting aspect of field emission is that we may determine the current density without knowing the factor β and by making only limited assumptions about the work function φ. This method of obtaining the current density was first proposed by Charbonnier and Martin[22], and their method is described here in some detail since it leads to useful results.

Charbonnier and Martin's argument is derived from the following observation: If we use the above expression for the magnitude of the slope of the Fowler-Nordheim plot, we may express the electric field strength in terms of the

slope and the voltage as

$$F = \beta V = \frac{B\,\varphi^{3/2}}{2.3\ \frac{m_{FN}}{V}}\, s(y) \qquad \text{AII.9}$$

Inserting this expression into the Fowler-Nordheim equation gives

$$J = \frac{AB^2\varphi^2 s(y)^2}{(2.3)^2 \left(\frac{m_{FN}}{V}\right)^2} \exp\left(- 2.3 \frac{m_{FN}}{V} \frac{v(y)}{s(y)} \right) \qquad \text{AII.10}$$

If now we expand s(y) and v(y) about y=.5, we find

$$\begin{aligned} s(y) &= .956 \\ v(y) &= .956 - 1.062\ y^2 \end{aligned} \qquad \text{AII.11}$$

These expression, if inserted into equation AII.10, give

$$J(A/cm^2) = 1.14 \times 10^9 \left(\varphi^2 e^{10.4/\sqrt{\varphi}} \right) \frac{\exp(-2.3 m_{FN}/V)}{(m_{FN}/V)^2} \qquad \text{AII.12}$$

for φ expressed in eV and V expressed in volts.

The function $g(\varphi) = \varphi^2 \exp(10.4/\sqrt{\varphi})$, however, has a broad minimum near $\varphi = 6.75$ eV; therefore, if we assume that the work function of the metal is in the range of 4 - 10 eV, we can find the current density appropriate to a known value of m_{FN}/V (compare Figure 35.).

A graph of the current density versus m_{FN}/V is given

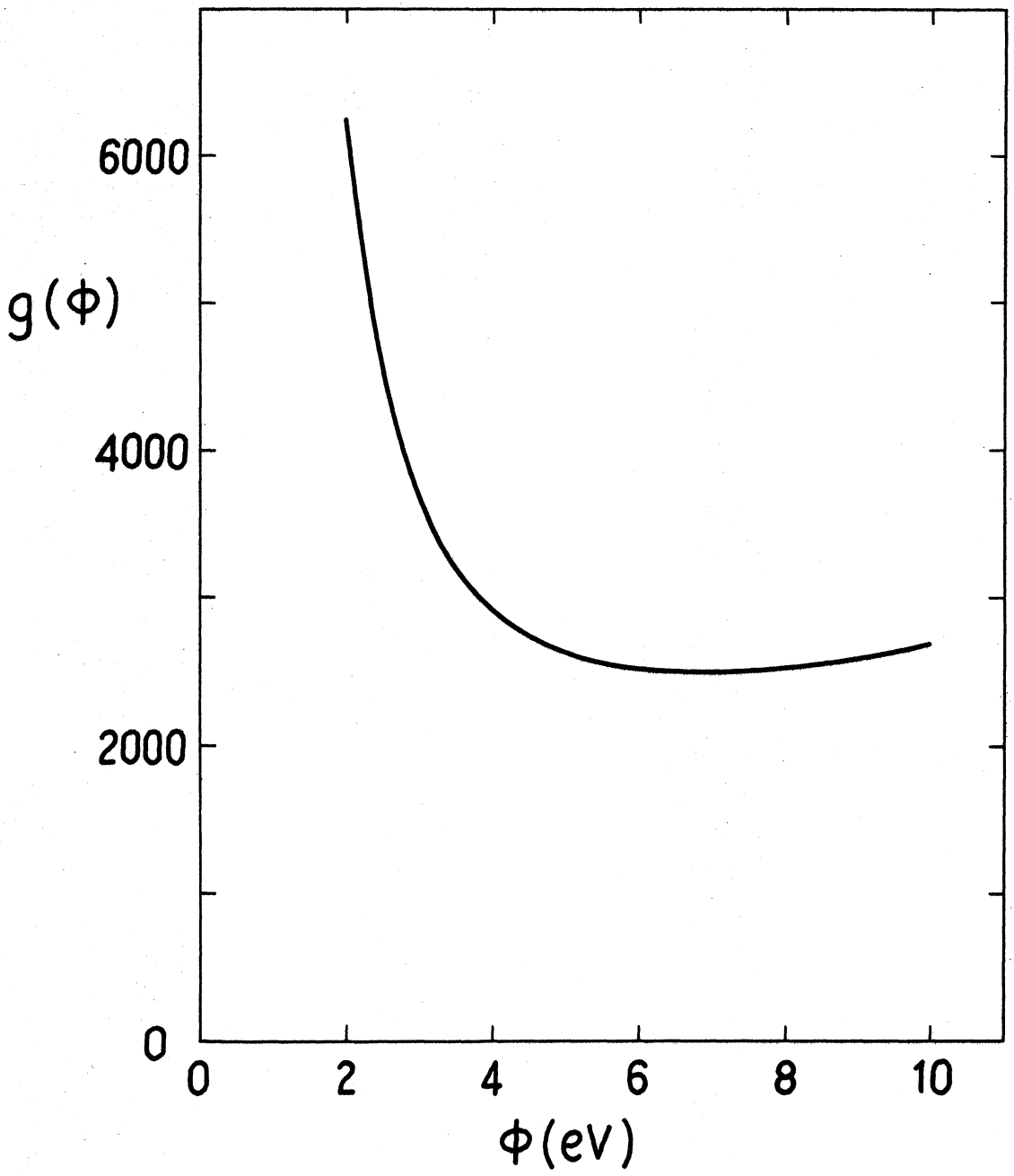

Figure 35. Function g(φ) for Charbonnier and Martin's Analysis of Fowler-Nordheim Equation.

in Figure 36. This graph is identical to the one given by Charbonnier and Martin except that only curves corresponding to $\varphi = 4.5$ eV and $\varphi = 2$ eV are given here. Charbonnier and Martin state that the appproximations used to obtain equation AII.12 are valid for $10\ A/cm^2 \leq J \leq 10^4\ A/cm^2$, which corresponds approximately to $7 \leq m_{FN}/V \leq 10$. However, in the experiments reported here values of m_{FN}/V less than 7 were often observed.

There is no reason to expect the validity of Charbonnier and Martin's result extrapolated to current densities $> 10^4\ A/cm^2$. We may obtain results for high current densities, however, by returning to equation AII.8. If we choose a work function φ, then m_{FN}/V may be calculated for different values of F from

$$\frac{m_{FN}}{V} = \frac{B\,\varphi^{3/2}\,s(y)}{2.3\,F} \qquad \text{AII.13}$$

But for a given value of φ and F the current density is uniquely specified by the Fowler-Nordheim equation; therefore, we can construct plots of J versus m_{FN}/V for a given value of φ without making the approximation (equation AII.11) used by Charbonnier and Martin. Essentially all that we are doing is transforming $J(\varphi,F)$ into $J(\varphi,m_{FN}/V)$, and equation AII.13 allows us to make this transformation. The truly interesting feature of this transformation is displayed in Figures 37 and 38. We observe that the current density for a given value of m_{FN}/V is almost

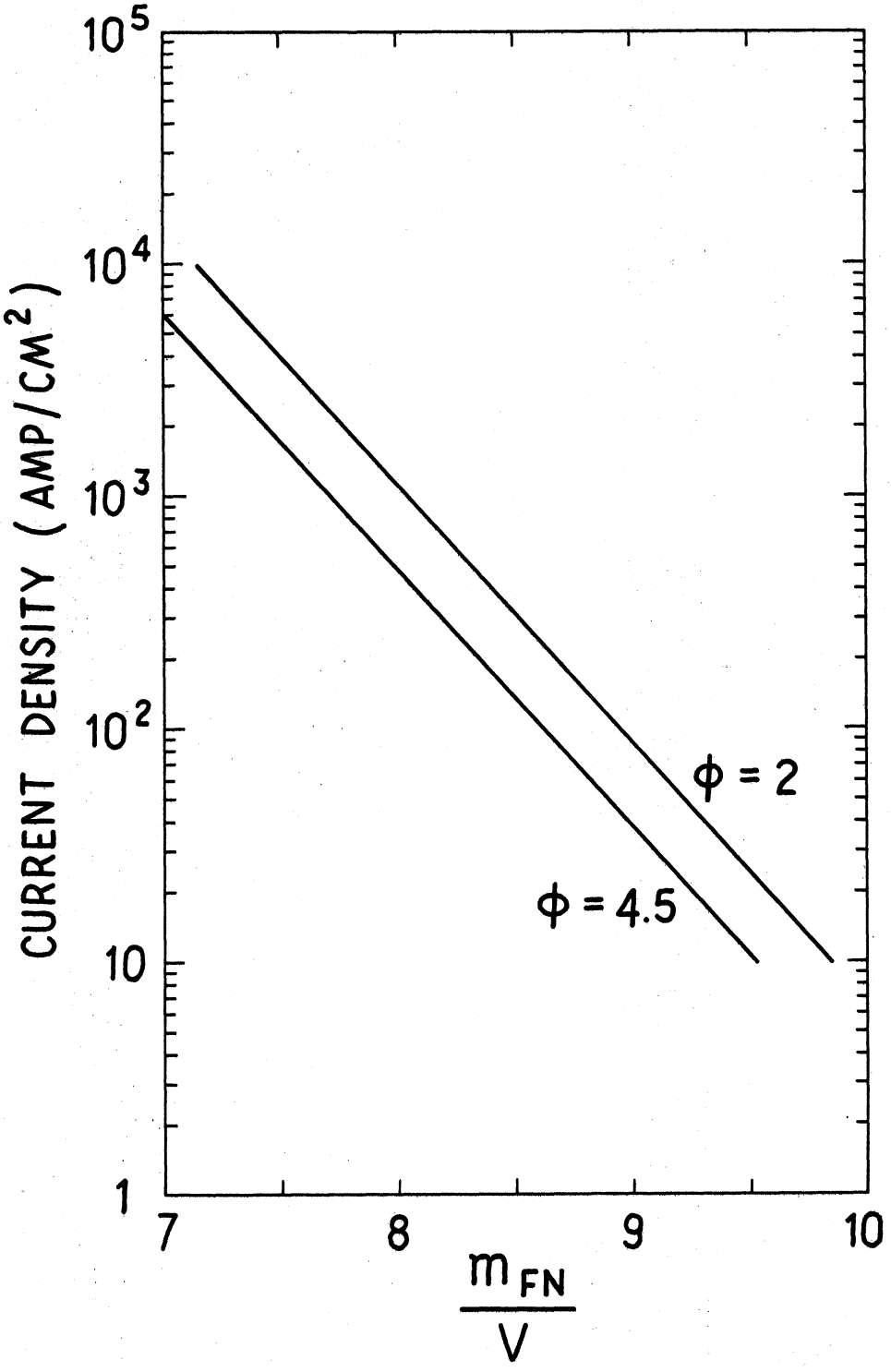

Figure 36. Charbonnier and Martin's Plot of Current Density Versus Parameter m_{FN}/V.

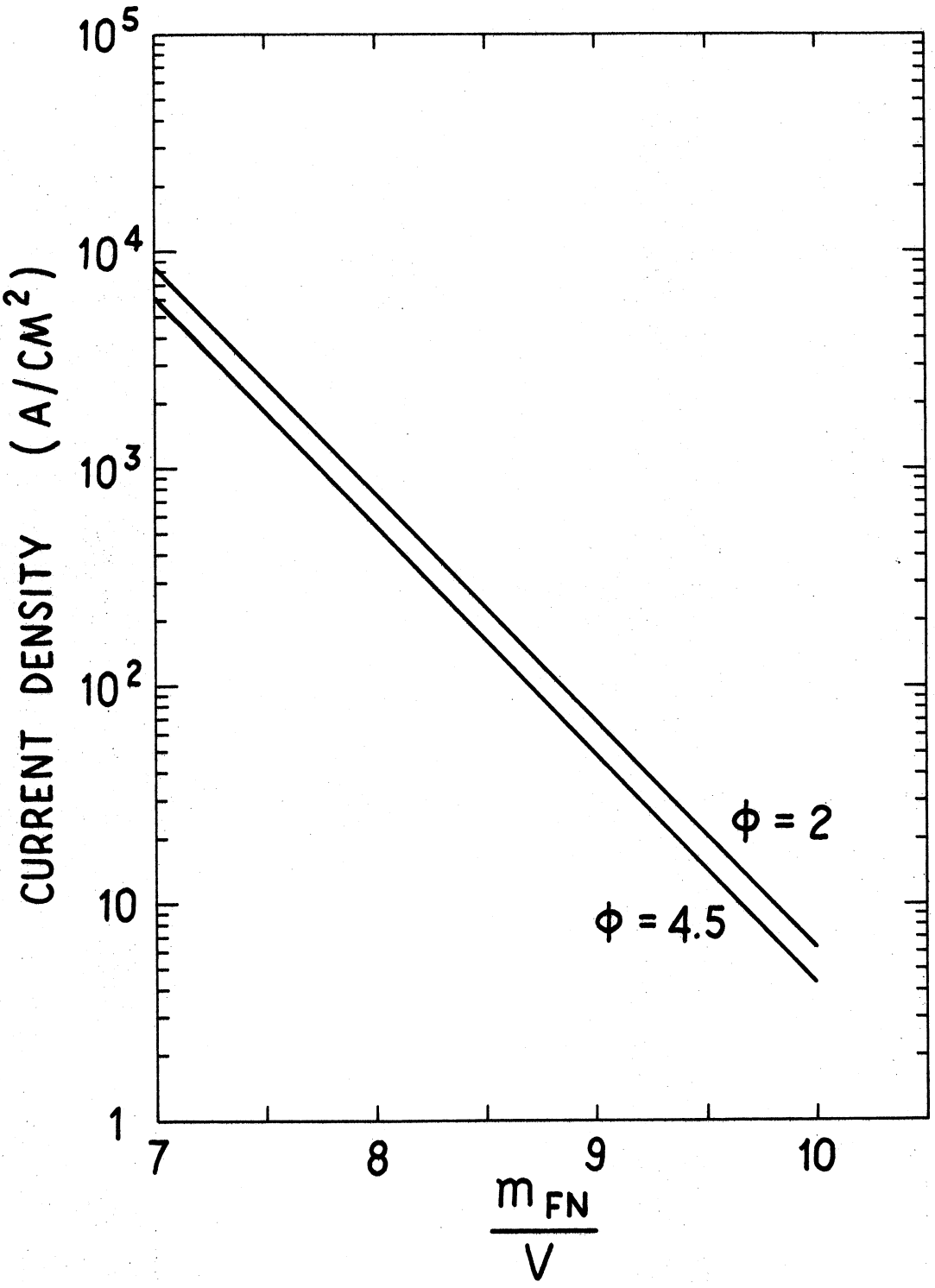

Figure 37. Extended Analysis of Fowler-Nordheim Equation. Plot of current density versus parameter m_{FN}/V.

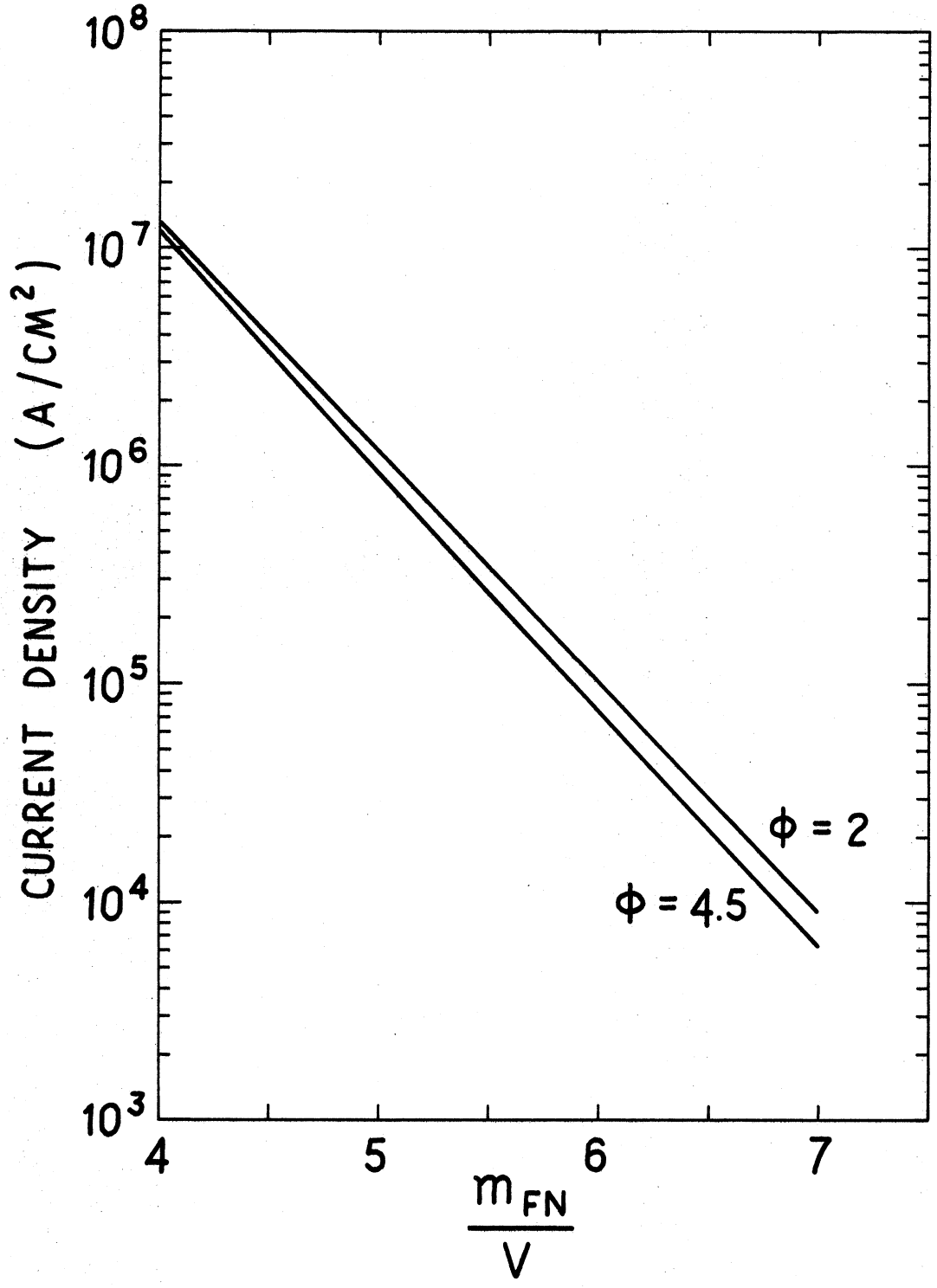

Figure 38. Extended Analysis of Fowler-Nordheim Equation. Plot of current density versus parameter m_{FN}/V.

independent of the work function if $m_{FN}/V > 5$. Thus for a given voltage, the current density can be inferred from these graphs, and because at a given voltage both the current density and the current are known, the effective area of emission can be determined.

REFERENCES

1. D. Lichtman and J.F. Ready, Phys. Rev. Letters 10, 342 (1963)

2. R.E. Honig and J.R. Woolston, Appl. Phys. Letters 2, 138 (1963)

3. C.M. Verber and A.H. Adelman, Appl. Phys. Letters 2, 220 (1963)

4. F. Giori, L.A. MacKenzie, and E.J. McKinney, Appl. Phys. Letters 3, 25 (1963)

5. J.F. Ready, Phys. Rev. 137, A620 (1965)

6. M.C. Teich and G.J. Wolga, Phys. Rev. 171, 809 (1968)

7. E.M. Logothetis and P.L. Hartman, Phys. Rev. 187, 460 (1969)

8. C.R. Giuliano, D.F. Dubois, R.W. Hellwarth, and G.R. Rickel, Damage Threshold Studies in Laser Crystals: Intensity Profile and Self-Focusing., Semi-Annual Rep. No. 3, Contract No. F19628-69-C-0277, Proj. No. 8693 (January 1971)

9. H.S. Carslaw and J.C. Jaeger, Conduction of Heat in Solids, 2ed ed. (Oxford U.P., London, 1959), p. 80.

10. H.B.G. Casimir and J. Ubbink, Philips tech. Rev. 28, 300 (1967)

11. Reference 9, Sec. 2.9

12. American Institute of Physics Handbook, 3ed ed. (McGraw-Hill, New York, 1972)

13. E.M. Logothetis and P.L. Hartman, Phys. Rev. Letters 18, 581 (1967)

14. R.H. Fowler, Phys. Rev. 38, 45 (1931)

15. R.J. Maurer in Handbook of Physics, edited by E.U. Condon and H. Odishaw (McGraw-Hill, New York, 1958), p. 8-67.

16. H. Schwarz and H. Hora, Appl. Phys. Letters 15, 349 (1969)

17. T.E. Hartman, J. Appl. Phys. 33, 3427 (1962)

18. R.W. Wood, Phys. Rev. 5, 1 (1897)

19. R.H. Fowler and L.W. Nordheim, Proc. Roy. Soc. (London) A119, 173 (1928)

20. L.W. Nordheim, Proc. Roy. Soc. (London) A121, 626 (1928)

21. R.H. Good, Jr., and E.W. Muller, Handbuch der Physik (Springer-Verlag, Berlin, 1956), Vol. 21.

22. F.M. Charbonnier and E.E. Martin, J. Appl. Phys. 33, 1897 (1962)